Summer 2018

Stability of Bimetallic Clusters in Protein Model Systems

Sean Hartnett
Bucknell University, dsh015@bucknell.edu

I, David Sean Hartnett, do grant permission for my thesis to be copied.

Stability of Bimetallic Clusters in Protein Model Systems

by

David Sean Hartnett

A Thesis

Presented to the Faculty of
Bucknell University
In Partial Fulfillment of the Requirements for the Degree of
Master of Science in Chemistry

Approved:

Adviser

Department Chairperson

August 2018

(Date: month and Year)

Acknowledgements

I would first like to thank my Advisor, Dr. Will Kerber, for his guidance and patience with me in the lab. I have become a more capable and confident chemist in his laboratory and I am extremely grateful for the chance to work with him. I was very happy for the opportunity to meet his wonderful family and talk Bucknell basketball with him when we weren't working too hard in the lab.

I would like to thank Dr. Strein and Dr. Smith, my thesis committee, for their insight into my thesis.

Time should be taken to thank all of the many hard working staff members of the Bucknell University Chemistry Department and custodial staff. My work here would not have been possible without the time and effort that they put in to making our facilities and learning experience the best available. I would like to particularly recognize Margaret Brody for coordinating the flow of supplies and chemicals in the stockroom, and Linda Godfrey for organizing any and all important functions in the department such as guest speakers and our sacred double lunch Wednesdays. I would also like to thank Dr. Brian Breczinski and Dr. Pete Findeis for the care and maintenance of our instruments such as the NMR and mass spectrometer. Also I would like to thank Pat Martino for the

coordination of the teaching labs and for putting in the extra time to run community events like the Halloween show and chemistry camp, both of which are some of my favorite memories of my time here. The aforementioned staff members are the backbone of the department and none of the work we do would be achievable without their help.

I am grateful for the contributions of the other members of my laboratory group, particularly Carson Mafrice who kept me on my toes and never allowed for a dull moment in the lab. I am also grateful for the other chemistry graduate students who were here during my time, we all kept each other sane even in the most stressful of times.

Finally, I would like to thank my family: Mom, Dad, Brook, Denis and Johanna and my girlfriend Marisa for their unwavering support and encouragement from the very beginning. I would not be where I am today without you. Thank you all for your time, energy and support.

Table of Contents

List of Figures

Chapter 1

Introduction

Chapter 3

Results and Discussion

Appendix C

Primary Metal Exchange ^{19}F-NMR Spectra

List of Tables

Chapter 3

Results and Discussion

Appendix B

Experimental Data

List of Abbreviations

1	$[Zn_2(F\text{-}HXTA)(H_2O)_3]^-$
2	$[Mg_2(F\text{-}HXTA)(H_2O)_4]^-$
°	degrees
Å	angstroms
Ac	acetate
BDNPP	bis(2,4-dinitrophenyl) phosphate
BPMP	2,6-bis[(bis(2-pyridyl-methyl)amino)methyl)]-4-methylphenol
BnTPEN	*N*-benzyl-*N,N′,N′*-tris(2-pyridylmethyl)-1,2 diaminoethane
°C	degrees Celsius
c	centi
CO	catechol oxidase
Ct.	*Chlamydia trachomatis*
D	doublet
Da	dalton
DNA	deoxyribonucleic acid
EDTA	ethylenediaminetetraacetic acid
Eq	equation
F-HXTA	(5-fluoro-2-hydroxy-1,3-xylene-α,α′-diamine-*N,N,N′,N′*-tetraacetic acid)
FloH	[2-({Bis[2-(pyridin-2-yl)ethyl]amino}methyl)-6{[bis(pyridin-2-ylmethyl)amino]methyl}-4-methylphenol]
Gk.	*Geobacillus kaustophilus*
g	grams
HXTA	*N,N′*-(2- hydroxy-5-methyl- 1,3-xylylene) bis [*N*-(carboxymethyl)glycine]

Hz	hertz
I	ionic strength
ICIMP	2-(N-carboxylmethyl)-[N-(N-methylimidazolyl-2-methyl)aminomethyl]-[6-(N-isopropylmethyl)-[N-(N-methylimidazolyl-2-methyl)]aminomethyl-4-methylphenol]
k	kilo
K	kelvin
λ	wavelength
L	liter
L-Bn	{[2-bis[(2-pyridylmethyl)aminomethyl]]-6-[benzyl-2-(pyridylmethyl)aminomethyl]-4methylphenol}
Log	logarithm
M	metal; molarity; mega
m	meter; milli
μ	micro
Me	methyl
mol	mole
$[MST]^{3-}$	*N,N′,N″*-[2,2′,2″nitrilotris(ethane-2,1-diyl)]tris(2,4,6-trimethylbenzenesulfonamido)
N4Py	*N*,*N*-bis(2-pyridylmethyl)-*N*-bis(2-pyridyl) methylamine
NMR	nuclear magnetic resonance
NTA	nitrilotriacetic acid
Ω	ohm
PAPs	purple acid phosphatases
Ph	phenyl
ppm	parts per million
Py_3tren	N,N,N-tris(2-(2-pyridylamino)ethyl)amine
RNA	ribonucleic acid

RNR	ribonucleotide reductase
s	singlet
SOD	superoxide dismutase
t	triplet
TACN	1,4,7-triazacyclononane
TMC-py	1-(pyridyl-2′-methyl)-4,8,11-trimethyl1,4,8,11-tetrazacyclotetradecane
TMTACN	1,4,7-trimethyl-1,4,7-triazacyclononane
TOF	transmitter offset frequency

Abstract

Heterobimetallic cofactors are commonly found in proteins and allow them to perform unique chemical processes that would otherwise not be possible. The interactions between these metals allow the protein to accomplish difficult chemical transformations. Previously, the thermodynamic stability of a Fe^{II}/Mn^{II} cluster in the dinucleating ligand F-HXTA (5-fluoro-2-hydroxy-1,3-xylene-α,α′-diamine-*N,N,N′,N′*-tetraacetic acid) has been investigated in our lab as a model of cluster assembly in the proteins ribonucleotide reductase (RNR) and R2-like ligand binding oxidases (R2lox). By measuring equilibrium concentrations of F-HXTA complexes via ^{19}F-NMR, it was found that the equilibrium for metal exchange between the homobimetallic Fe^{II}/Fe^{II} and Mn^{II}/Mn^{II} complexes favored the hetereobimetallic Fe^{II}/Mn^{II} product (K = 2.2) This work has been extended to see if the enhanced heterobimetallic stability is a general phenomenon or if it is specific to Fe^{II} and Mn^{II}. We investigated three new pairs of divalent metal ions: Fe^{II}/Mg^{II}, Zn^{II}/Fe^{II}, and Zn^{II}/Mg^{II} using the same methodology. Crystals of the complexes $[Mg(H_2O)_6][Mg_2(F\text{-}HXTA)(H_2O)_4]_2 \cdot 14H_2O$ and $[Zn(H_2O)_6][Zn_2(F\text{-}HXTA)(H_2O)_3]_2 \cdot 10H_2O$ were grown and characterized via x-ray crystallography ^{1}H-NMR and ^{19}F-NMR confirming the proposed structures of each complex in solution. It was found that each new metal ion pair exhibited enhanced stability for their respective heterobimetallic complexes. The metal exchange equilibria for Fe^{II}/Mg^{II}, Zn^{II}/Fe^{II}, and Zn^{II}/Mg^{II} complexes had equilibrium constants favoring the hetereobimetallic products with K_{FeMg} = 4.15(0.07), K_{ZnFe} = 4.4(0.3), and K_{ZnMg} = 5.59(0.09).

Chapter 1: INTRODUCTION

1.1 Metal Clusters in Proteins

Metallocofactors are a cluster of one or more metals that are essential to the activity of an enzyme. Proteins sometimes require metal cofactors in order to carry out certain chemical processes that the protein would otherwise be unable to perform. Sometimes these cofactors can be composed of more than one metal, and those metals may be different. The interactions between these metals allows unique chemistry within an enzyme and allows it to accomplish difficult chemical transformations.

An example of a heterobimetallic cofactor is found in [NiFe] hydrogenase.[1] Hydrogenases catalyze the oxidation of hydrogen gas to protons and electrons and can be found in archaea bacteria and selected eukaryotes, this was studied by the Hausinger group. Hydrogenases can consume excess reducing equivalents or provide electrons for energy generating pathways. NiFe hydrogenase contains at least 2 subunits, the first is 60 k-Da containing the NiFe active site and the second is a 30 k-Da subunit with one or more Fe-S clusters carrying out the electron transfer. The nickel is coordinated by 4 cysteine residues in the first subunit. Interestingly, the activity of the enzyme is limited by how buried the metal center is into the protein: the substrate must be small enough to reach the center. An example of an appropriate substrate would be H_2. These hydrogenases move energy by using H^+ as a bridging ligand; they take H_2 and break it into H^+ and H^-. The metallic core removes the electron from the H^- ion and transfers the

electron like an electron transport chain. At this point the proton transfer mechanisms are not clear.

Another example of a metal core is Fe(III)M(II) (M(II)= Fe, Zn or Mn) in purple acid phosphatases (PAPs)[2a]. PAPs are a type of enzyme classified as binuclear metallohydrolases: they require two closely spaced transition metal ions to carry out hydrolytic reactions. The two metal ions in the active site catalyze the hydrolysis of amides and esters of phosphoric acid and are linked by bridging groups, normally hydroxides. One function that PAPs perform is the metabolism of bones in the body. The Fe^{3+} forms a charge transfer complex with an invariant tyrosine ligand making the purple color. The divalent metal is Fe^{2+} in animals and Zn^{2+} or Mn^{2+} in plants; bacterial PAPs have not yet been characterized[2b]. Both plant and animal PAPs have a dimetal center coordinated to one aspartate, one tyrosine and one histidine for Fe^{3+} and two histidines and one asparagine for the divalent ion with an aspartate residue bridging the two ions. Waters coordinated to the metal atoms are present, but the exact number must be determined experimentally because the number of waters is pH dependent. Predominantly PAPs are hydrolases but they also have the capacity to oxidize lipids. PAPs play significant roles in Fe transport, the generation of reactive oxygen species as an immune response, energy metabolism, bone resorption, the uptake of phosphates and the degradation of organophosphates. Mimics of PAPs act as good drug leads due to the wide array of functions.

PAPs binding sites are nonsymmetrical, therefore metals in these binding sites reside in chemically different environments[2]. The first core metal in all of these examples

are found to act as a redox catalytic metal center, the second metal functions to help maintain the structural integrity of the core while the first metal is bound. The second metal also controls the redox potential of the first metal center and this could possibly accelerate the redox processes. Substrates bound to metals can react with another molecule either bound or not bound to metal center. There are systems with similar properties to PAPs such as Cu-Zn superoxide dismutase (SOD) and catechol oxidases (COs).

The cofactor of most interest for our study is the bimetallic core in ribonucleotide reductase (RNR)[2a]. RNR is an enzyme that reduces DNA to RNA. Class 1 RNRs contain two nonidentical dimeric subunits, R1 and R2, arranged as a R1-R2 heterodimer. Generally, in the R2 subunit of class 1 there is a diiron center, and ribonucleotide reduction is performed by an active cysteine within the R1 subunit. A tyrosyl radical in subunit R2 is formed by the reduced diiron center after oxidation with dioxygen and this initiates the reactivity of the enzyme. Class 1c of RNR is a unique case of the enzyme in which the cofactor is composed of Fe and Mn[3]. Researchers speculate that the inclusion of Mn in the cofactor is due to an extremophile adaptation to a lack of Fe available in the environment. For class 1c, the R2 subunit lacks the canonical tyrosine[4]. The Fe-Mn cofactor replaces the tyrosyl radical when the reduced $Fe^{II}Mn^{II}$ enzyme is oxidized to the $Fe^{III}Mn^{IV}$ state by O_2. For example, the proteins *Chlamydia trachomatis* (*Ct.*) RNR-R2 and RNR-R2 homologue (R2lox) from *Mycobacterium tuberculosis* lack the canonical tyrosine but possesses a Fe^{II}-Mn^{II} cofactor which replaces the tyrosyl radical when oxidized to $Fe^{III}Mn^{IV}$ with dioxygen. The manganese ion occupies the position directly

adjacent to the tyrosyl radical site in the other R2 subunits of other classes of RNR. This leads to the assumption that the high-valent Mn^{IV} species functions as a direct substitute for the tyrosyl radical in class 1c RNR.

1.2 Synthesis of Bimetallic Clusters

Systems like [NiFe] hydrogenase, PAPs and RNR have inspired chemists to synthesize heterobimetallic clusters in order to better understand the chemical environment in which these species are assembled. It is therefore important to study the electronic and magnetic interactions between metal ions, as well as the mechanism of assembly. Syntheses of these systems can be achieved selectively if there are subtle differences in the metals, usually a difference in binding affinity or differences in the substitution kinetics of the metals. Small molecules that model the binding sites of the metals are easier to work with than proteins since proteins can be denatured and are overall more complex. It is simplest to synthesize a ligand that has symmetrical binding sites for both the metals. However, success in the selective formation of the metal cluster is simpler to achieve in a ligand that is nonsymmetric with different binding sites for the metals. These scenarios are reviewed below.

1.2.1 Selectivity from Different Oxidation States

Symmetric ligands

The simplest syntheses of heterobimetallic clusters occurs when the two metals are in different oxidation states because trivalent ions tend to bind more strongly to ligands than divalent ones. For example, the Que group studied the heterobimetallic

complex $[M(III)M(II)BPMP(O_2CR)_2](BPh_4)_2$ which may be assembled from the symmetric ligand 2,6-bis[(bis(2-pyridyl-methyl)amino)methyl)]-4-methylphenol (Figure 1).[5] This ligand was mixed with a several different combinations of two metal salts. The salts were always added in the same order sequentially: first M(III) then M(II). This addition was to take advantage of M(III) being more substitutionally inert than M(II), thus M(III) is less likely to exchange coordination sites. With the addition of the more inert metal first, when bound to the ligand it will not be displaced by the labile M(II). A carboxylate salt was also added to the mixture forming carboxylate bridges between the two metals made up of acetates.

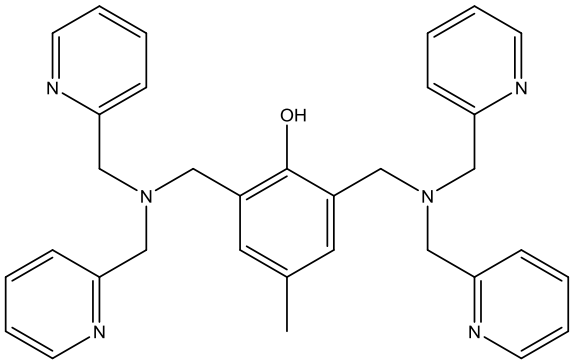

Figure 1: The symmetric dinucleating ligand 2,6-bis[(bis(2-pyridyl- methyl)amino)methyl)]-4-methylphenol (H(BPMP))

Different combinations of trivalent and divalent metal ions were used when making BPMP-dimetal complexes. The combinations are as follows: $Fe^{III}Zn^{II}$, $Fe^{III}Mn^{II}$, $Fe^{III}Cu^{II}$, $Ga^{III}Fe^{II}$, and $Fe^{III}Fe^{II}$. The triply bridged $Fe^{III}Fe^{II}$ cluster has the two carboxylate groups and a phenolate oxygen between them and the cluster was further probed in order to see its electronic and steric properties.[6] The $Fe^{III}Fe^{II}$ cluster presents

the first example of a well characterized structure of a triply bridged heterobimetallic cluster. The particular structure being characterized here has (μ-Phenoxo)bis(μ-carboxylato) bridges. Similarly, another series of bimetallic complexes were synthesized with the form: $[M^{II}M'^{III}\ BPMP(O_2CR)_2]X_2$ (M= M'= Fe, R= C_2H_5, X= BPh_4; M= M'= Fe, R= C_6H_5, X= PF_6; M= Fe, M'= Ga, R =C_2H_5, X =BPh_4; M= Zn, M'= Fe, R= CH_3, X= BPh_4; M= Zn, M'= Fe, R= C_2H_5, X= BPh_4). These complexes provide models for binuclear metal-oxo centers in proteins.

Non-symmetric Ligands:

Examples of heterobimetallic cluster formation in non-symmetric ligands are also found in the literature. Heterometallic clusters in asymmetric ligands are generally easier to prepare because one metal binding site usually has a higher affinity than the other so that difference can be exploited. The investigation of these asymmetric bimetallic clusters is relevant for understanding catalysis in metalloproteins. Different coordination numbers in the binding sites can present the possibility for open coordination sites on the metals.

A synthesis of the iron-manganese complex $[Fe^{III}Mn^{II}(LBn)(\mu\text{-}OAc)_2](ClO_4)_2$ was performed by the Latour group where the unsymmetrical dinucleating ligand HL-Bn is{[2-bis[(2-pyridylmethyl)aminomethyl]]-6-[benzyl-2-(pyridylmethyl)aminomethyl]-4methylphenol} (Figure 2).[7] This complex was studied with electron paramagnetic resonance (EPR) and was one of the first times a center of $Fe^{III}Mn^{II}$ was prepared in order to investigate the bimetallic core in systems like RNR. HL-Bn has a binding site with a high affinity for metal on the side with the two pyridines. Fe^{III} is added first and binds to

this site followed by the addition of Mn^{II}. The Fe^{III} binds to the preferred site with two pyridines and since it is more substitutionally inert than Mn^{II}, Fe^{III} does not leave that site when manganese is added. The electronic structure of the Fe(III)Mn(II) pair was found and characterized. As seen in previous examples, the Fe(III)Mn(II) core has three bridging ligands, two carboxylates and a phenolate oxygen.

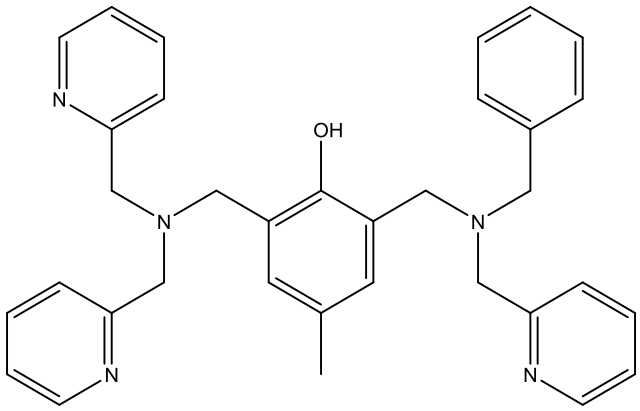

Figure 2: The non-symmetric dinucleating ligand {[2-bis[(2-pyridylmethyl)aminomethyl]]-6-[benzyl-2-(pyridylmethyl)aminomethyl]-4methylphenol (H(L-Bn))

In order to further study a metallic cluster with non-symmetric ligand binding sites we look again to models of PAPs.[8] A study by Norlander created a structural and functional model for PAP with heterodinuclear complex: $[FeMn(ICIMP)(OAc)_2Cl]$ where the ligand ICIMP is 2-(N-carboxylmethyl)-[N-(N-methylimidazolyl-2-methyl)aminomethyl]-[6-(N-isopropylmethyl)-[N-(N-methylimidazolyl-2-methyl)]aminomethyl-4-methylphenol] and the ligand is shown in Figure 3. A biomimetic hydrolysis reaction was examined at different pH levels on the substrate bis(2,4-dinitrophenyl) phosphate (BDNPP) (Figure 4). The metal ions Fe^{III} and Mn^{II} are in high-spin configurations and have distorted-octahedral geometry.

Interestingly, the substrate coordinates monodentate to the Mn^{II} ion and the bridging hydroxide between the metals becomes terminally bound to the Fe^{III} ion becoming a natural nucleophile when attacking the phosphorus center of BDNPP.

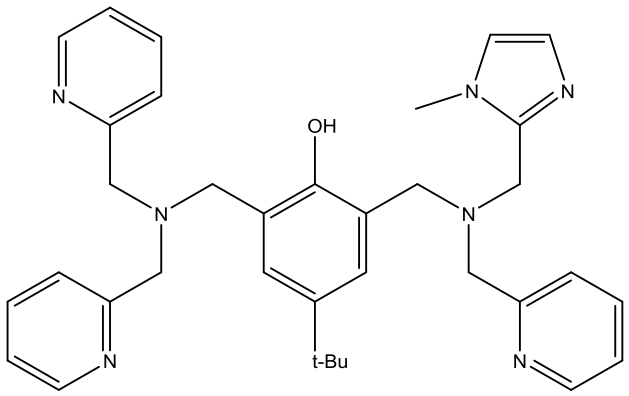

Figure 3: The non-symmetric dinucleating ligand 2-(N-carboxylmethyl)-[N-(N-methylimidazolyl-2-methyl)aminomethyl]-[6-(N-isopropylmethyl)-[N-(N-methylimidazolyl-2-methyl)]aminomethyl-4-methylphenol] (H(ICIMP))

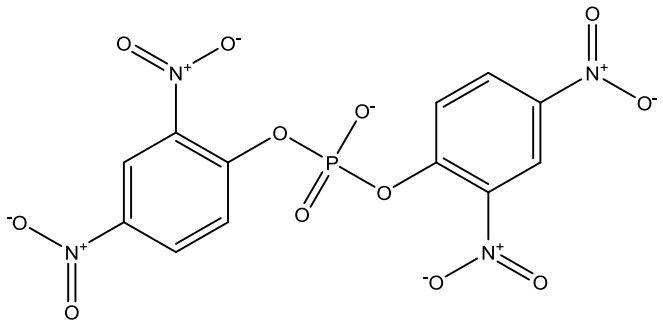

Figure 4: The hydrolysis substrate bis(2,4-dinitrophenyl) phosphate (BDNPP)

A study by Powell involving non-symmetric ligands prepared the heterodinuclear complex $[FeCu(Flo)OAc](BPh)_4$ where H(Flo) is the asymmetric ligand [2-({Bis[2-(pyridin-2-yl)ethyl]amino}methyl)-6{[bis(pyridin-2-ylmethyl)amino]methyl}-4-methylphenol] (Figure 5).[9] H(Flo) has 2 metal binding sites with one preferred over the

other, a bis(2-pyridylmethyl)amino group which is preferred over the bis(2-pyridylethyl)amino group; the groups can be seen on either side of the ligand in Figure 5. The assembly of the H(Flo) complexes are again stepwise; Fe^{III} is first added and bound to the bis(2-pyridylmethyl)amino side (left side of Figure 5) and then Cu^{II} is added which binds to the bis(2-pyridylethyl)amino side (right side of Figure 5). The unsymmetrical nature of this ligand allows site-directed $Fe^{III}Cu^{II}$ complex formation with high yield.

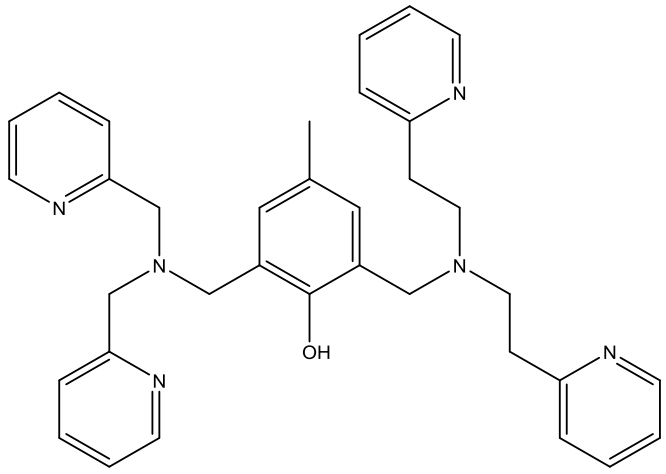

Figure 5: The non-symmetric dinucleating ligand [2-({bis[2-(pyridin-2-yl)ethyl]amino}methyl)-6{[bis(pyridin-2-ylmethyl)amino]methyl}-4-methylphenol] H(Flo). The left bis(2-pyridylmethyl)amino binding site has higher affinity than the right bis(2-pyridylethyl)amino binding site.

1.2.2 Selectivity from Substitutionally Inert Metals

Another way to get site directed bimetallic clusters is by using one kinetically inert metal like Cr(III) or Fe(III) paired with a more labile metal. The synthesis of asymmetric heterodinuclear complexes with two first-row trivalent transition metals is a good example of using substitutionally inert metals for a site directed synthesis.[10] The complex of the form $[(TACN)M'(\mu\text{-}O)(\mu\text{-}CH_3CO_2)_2M(TMTACN)](ClO_4)_2$ was prepared.

TACN is 1,4,7-triazacyclononane (R=H) and TMTACN is 1,4,7-trimethyl-1,4,7-triazacyclononane (R=Me) (Figure 6) and the core combinations ($M^{III}M'^{III}$) were $Fe^{III}Fe^{III}$, $Mn^{III}Mn^{III}$, $Fe^{III}Mn^{III}$, $Fe^{III}Cr^{III}$, $Cr^{III}Mn^{III}$, and $Cr^{III}V^{III}$. The complex $[(TACN)M'(\mu\text{-}O)(\mu\text{-}CH_3CO_2)_2M(TMTACN)](ClO_4)_2$ was synthesized in a way that is slightly different than what has been seen thus far. Separately, the ligand TMTACN is mixed with its respective metal (M) while TACN is mixed with its metal (M'). The two mixtures are then reacted with each other in water containing NaOAc to form the complex $[(TACN)M'(\mu\text{-}O)(\mu\text{-}CH_3CO_2)_2M(TMTACN)](ClO_4)_2$.The structures predicted are all confirmed by both electronic and magnetic spectroscopy.

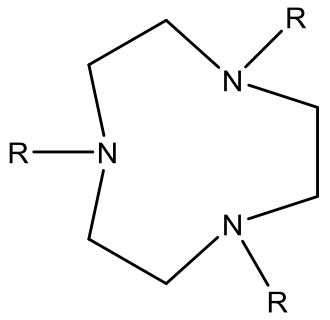

Figure 6: The general form of the ligand 1,4,7-triazacyclononane. (1) TACN: R=H (2) TMTACN: R=Me (3) MST: R= tosylate.

Another example using Cr^{III} is of the general form: $[(TMTACN)Cr(\mu\text{-}OH)(\mu\text{-}CH_3COO)_2M(TMTACN)](ClO_4)_2$ where M = Zn^{II}, Cu^{II}, Ni^{II}, Co^{II}, Fe^{II}, and Mn^{II}.[11] The metal centers Cr(III) and Fe(II) or Co(II) are linked together via a hydroxo bridge and two further acetate bridges and both metals have a distorted octahedron geometry. $[(TMTACN)Cr(\mu\text{-}OH)(\mu\text{-}CH_3COO)_2M(TMTACN)](ClO_4)_2$ is synthesized in the same

manner as the previous example; this preparation method can be used for a variety of heterodinuclear complexes with a variety of different bridging ligands.

Site directed metallic clusters can also be synthesized where Fe^{III} is the kinetically inert ion which is highly unlikely to exchange binding sites once bound.[12] The complex of the form [(TMTACN)M^{II}(μ-OH)Fe^{III}MST]OTf, was prepared where the ligand $[MST]^{3-}$ is *N,N′,N″*-[2,2′,2″nitrilotris(ethane-2,1-diyl)]tris(2,4,6-trimethylbenzenesulfonamido) is a TACN derivative (Figure 6). [(TMTACN)M^{II}(μ-OH)Fe^{III}MST]OTf has unsymmetrical metal binding sites and utilizes inert Fe^{III} for directing metal binding. Fe^{III} is combined with a divalent metal that is more labile such as Co^{II}, Ni^{II}, Cu^{II} or Zn^{II}. The clusters electronic properties can be altered systematically by inserting different transition metals using the same synthetic method as the previous two examples. The findings indicate that changing out metals does little to change the properties of [(TMTACN)M^{II}(μ-OH)Fe^{III}MST]OTf complexes. The two metal centers have different coordination environments, with the Fe^{III} centers having five-coordinate, distorted-tbp primary coordination spheres. The M^{II} center having six-coordinate, distorted octahedral primary coordination spheres.

1.2.3 Selectivity from Redox Reactions

Another way to site direct bimetallic clusters is via redox reactions. One can create a core of $Fe^{III}M^{II}$ by reducing a core of $Fe^{III}M^{III}$.[13] A way to create a stable $Fe^{III}Fe^{II}$ core in the complex [Na][Me_4N][Fe_2(HXTA)$(OAc)_2$] was found by the Munck group by using the symmetric ligand *N,N′*-(2- hydroxy-5-methyl-1,3-xylylene) bis [*N*-

(carboxymethyl)glycine] (HXTA), the structure is shown in Figure 7. The core of $Fe^{III}Fe^{III}$ in the complex $[Me_4N][Fe_2(HXTA)(OAc)_2]$ was reduced in a 50:50 HOAc buffer with β-mercaptoethanol and excess Me_4NCl to produce the $[Na][Me_4N][Fe_2(HXTA)(OAc)_2]$ complex. The core $Fe^{III}Fe^{II}$ is common in hemerythrin and the reduced forms of PAPs. $Fe^{III}Fe^{II}$ was characterized by NMR, absorption spectroscopy and magnetic experiments.

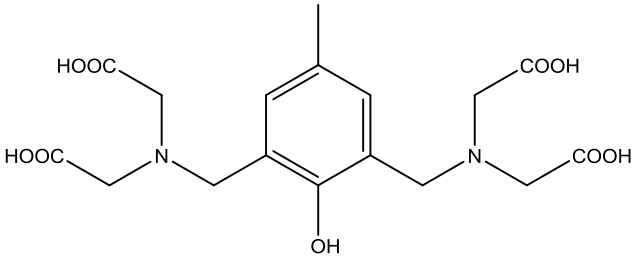

Figure 7: The symmetric dinucleating ligand N,N'-(2-hydroxy-5-methyl-1,3-xylylene) bis [N-(carboxymethyl)glycine] (HXTA)

Core assembly via metal cluster reduction was furthered by the Que group who created similar complexes with cores composed of $Fe^{III}Mn^{II}$ and $Fe^{II}Mn^{II}$, instead with the ligand HBPMP (Figure 1).[14] The species $[Fe^{II}Mn^{II}(BPMP)(O_2CCH_2CH_3)_2](BPh_4)$ is isoelectronic to $[Fe^{III}Fe^{II}(BPMP)(O_2CCH_2CH_3)_2](BPh_4)$; however, the species with the $Fe^{II}Mn^{II}$ center is much easier to probe spectroscopically because there is only one iron instead of two. The Mn^{II} is NMR silent, making the $Fe^{II}Mn^{II}$ core advantageous to investigate its individual atoms. The $[Fe^{II}Mn^{II}(BPMP)(O_2CCH_2CH_3)_2](BPh_4)$ core was created by preparing $[Fe^{III}Mn^{II}(BPMP)(O_2CCH_2CH_3)_2](BPh_4)$ and then reducing the Fe^{III} to Fe^{II} with cobaltocene, similar to the technique used by Munck**.**

A core of Fe(III)M(III) can be made by trapping M(II) with Fe(IV)O.[15] The pentadentate ligands used were: 1-(Pyridyl-2′-methyl)-4,8,11-trimethyl-1,4,8,11-tetrazacyclotetradecane (abbreviated TMC-py), *N*,*N*-bis(2-pyridylmethyl)-*N*-bis(2-pyridyl) methylamine (abbreviated N4Py) and *N*-benzyl-*N,N′,N′*-tris(2-pyridylmethyl)-1,2 diaminoethane (abbreviated BnTPEN) and are shown in Figure 8. $Fe^{IV}O$(TMC), where TMC is 1,4,8,11-tetramethylcyclam, is mixed with a separate ML solution where M=Cr^{II} or Mn^{II} and L= TMC-py, N4Py or BnTPEN, similar to the synthesis of the examples with the TACN derivatives in section 1.2.2. A bridge between the two metals is formed from the oxygen atom from the oxoiron and the oxidation states on Fe^{IV} and M^{II} change to Fe^{III} and M^{III}. High-valent mimics of the RNR 1c active site such as this allow for the investigation of O_2 activation and other factors that modulate the redox properties of the Fe-O-Mn center.

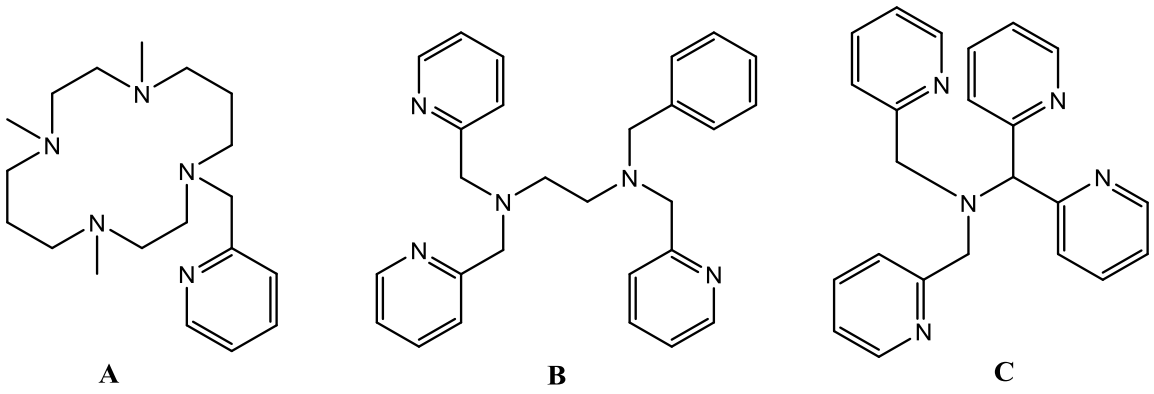

Figure 8: The ligands: A= 1-(Pyridyl-2′-methyl)-4,8,11-trimethyl1,4,8,11-tetrazacyclotetradecane (abbreviated TMC-py); B= N,N-bis(2-pyridylmethyl)-N-bis(2-pyridyl) methylamine (abbreviated N4Py); C=N-benzyl-N,N′,N′-tris(2-pyridylmethyl)-1,2 diaminoethane (abbreviated BnTPEN)

1.2.4 Selectivity for $M^{II}_a M^{II}_b$ clusters

$M^{II}_a M^{II}_b$ clusters are difficult to make selectively under kinetic control because ligand substitution rates are usually very fast.[16] The water self-exchange rate constants of transition metal ions are strongly influenced by the occupancy of the *d*-orbitals. For example, the order of reactivity for water exchange of divalent 3*d*-transition metal ions is $V^{2+} < Ni^{2+} < Co^{2+} < Fe^{2+} < Mn^{2+} < Cu^{2+}$.

It is possible to make $M^{II}_a M^{II}_b$ clusters under kinetic control if one binding site is inaccessible and cannot rapidly exchange metal ions. The Lu research group created several different combinations of $M^{II}M^{II}$ clusters metal pairings with the ligand N,N,N-tris(2-(2-pyridylamino)ethyl)amine $H_3(py_3tren)$ shown in Figure 9.[17] The metal-metal pairings are $Co^{II}Co^{II}$, $Co^{II}Fe^{II}$, $Co^{II}Mn^{II}$, $Fe^{II}Fe^{II}$, and $Fe^{II}Mn^{II}$ and the general form of their complex was $M_1M_2Cl(py_3tren)$. Adding an equivalent of $CoCl_2$ or $FeCl_2$ to the ligand $H_3(py_3tren)$ along with a solution of benzylpotassium to deprotonate the ligand gives a monometallated complex and then another equivalent of a different metal salt completes the bimetallic core of the synthesized complex. It is not possible to fill the second binding site before the first and the steric constraints for the binding site of M_1 do not allow the exchange of ligands for the metals once the second metal is added (Figure 9A).

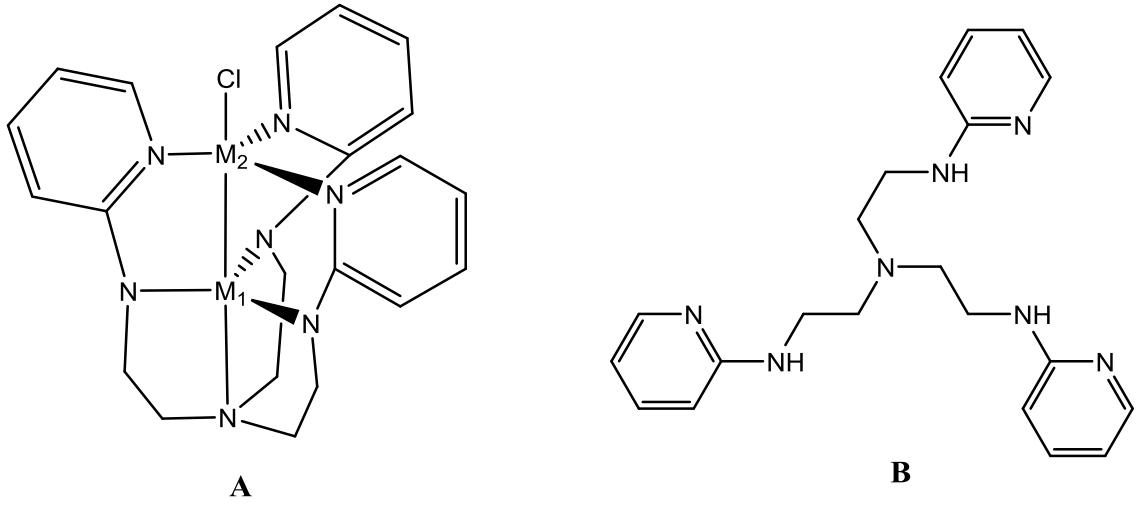

Figure 9: A: The complex $M_1M_2Cl(py_3tren)$ B: The ligand N,N,N-tris(2-(2-pyridylamino)ethyl)amine $H_3(py_3tren)$

The Latour group also used the ligand HL-Bn (Figure 2) to synthesized the complex $[Fe^{II}Mn^{II}(L\text{-}Bn)(\mu\text{-}OAc)_2](ClO_4)$**.** This complex is considered to be a biologically relevant model compound to Fe/Mn nonheme enzymes similar to RNR class 1c. This complex is nonsymmetric, and the same technique for the synthesis of $[Fe^{III}Mn^{II}(L\text{-}Bn)(\mu\text{-}OAc)_2](ClO_4)_2$used by Latour was used again for the metal cluster $Fe^{II}Mn^{II}$. Sequential addition of very carefully measured amounts of the metal was required, first the Fe^{II} and then the Mn^{II}. There was enough affinity for the Fe^{II} in the high metal affinity site that Mn^{II} ions did not replace the Fe^{II}. The addition of excess metal to each homonuclear complex did not lead to metal replacement, showing that they are not labile complexes.[7]

1.2.5 Thermodynamic Selectivity for $Fe^{II}Mn^{II}$ clusters in R2C and R2lox

Thermodynamic selectivity for a Fe(II)Mn(II) cofactor has been observed in *Chlamydia trachomatis* (Ct) R2c and the assembly mechanism has been studied *in vitro*[18]. The cofactor is formed first by the Mn^{II} ion binding to either site in the complex of Ct R2c, but once Fe^{II} is introduced the Mn^{II} is displaced to site 1. A cluster is formed anaerobically with equimolar Mn^{II} and Fe^{II} revealing Mn^{II} exclusively at site 1 with Fe^{II} in site 2. The proposed assembly is shown in Figure 10. Once O_2 is introduced, the cofactor becomes oxidized to $Mn^{IV}Fe^{III}$ and is now activated and does not undergo further substitution. When Fe^{II} is substoichometric it has specificity for site 2 and drives the selectivity.

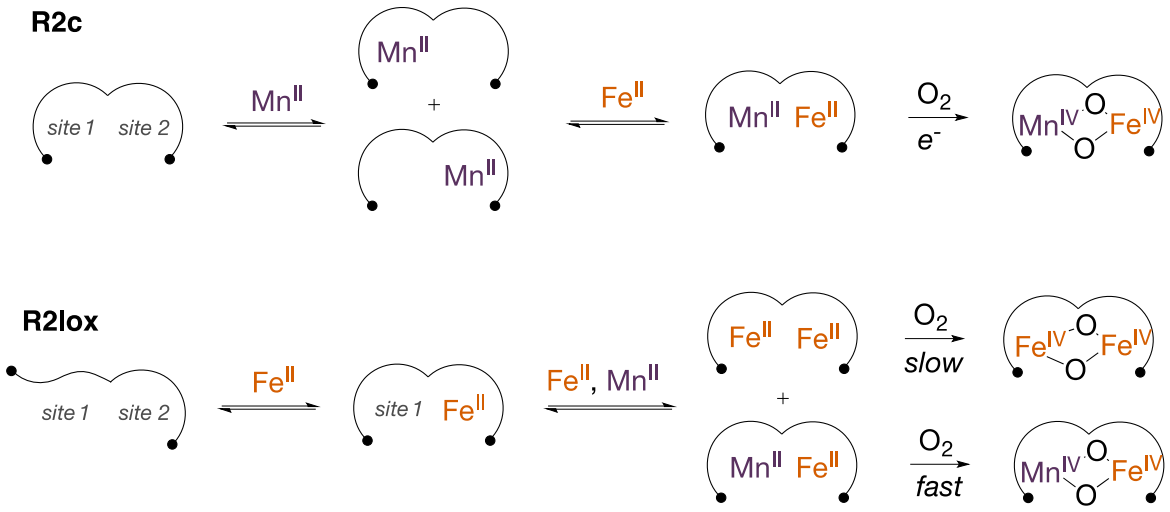

Figure 10: The proposed metallocofactor assembly mechanisms in *Ct* R2c and *Gk* R2lox.

In a study of *Gk.* R2lox we see that Mn(II) binds to R2lox only after Fe(II) is located in site 2.[19] Site 2 is specific for Fe^{II} and must be filled with Fe before Mn^{II} fills site 1. The metal ions in site 1 can exchange as long as the metal sites are reduced because of the greater lability of divalent metals. After the cofactor is assembled within the protein and O_2 is added, there is kinetic selectivity that favors oxidation of the $Mn^{II}Fe^{II}$ cofactor. R2lox activates significantly faster with oxygen with a $Mn^{II}Fe^{II}$ core than a $Fe^{II}Fe^{II}$ and the metals do not exchange after oxygen activation. The R2lox heterodinuclear cofactor of $Mn^{II}Fe^{II}$ can spontaneously assemble i*n vitro* and the protein itself can provide site-specific discrimination. These findings imply a metallochaperone to organize the metals may not be necessary in *vivo* and that the availability of metals plays a role in the assembly.

A factor that contributes to the site direction of *Ct* R2c and *Gk* R2lox (Figure 11) for assembly of the metal core is the difference in coordination sites 1 and 2.[19] An extra water ligand in site 1 and a more distorted coordination sphere in site 2 are the most distinct differences. It is speculated that the six-coordinate environment and the ability to complex with waters in the first coordination sphere might help favor Mn^{II} occupancy in both sites, but it is not clear why site 1 should be more stringent than site 2 for its selectivity of Mn^{II} over Fe^{II}. An alternate theory for the site selectivity is site 2 favors Fe^{II} binding by stabilizing the asymmetrically filled t_{2g} subshell of high-spin d^6 in a weak octahedral ligand field.

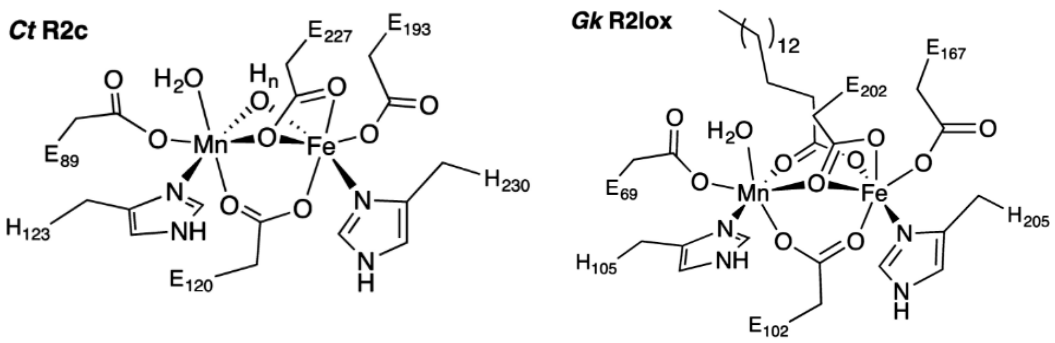

Figure 11: Schematic of the reduced active site of *C. trachomatis* R2c protein and *G. kaustophilus* R2lox homologue 1 protein.

1.3 Stability of heterobimetallic complexes of HXTA

In our lab, we have previously investigated the thermodynamics of Fe(II)/Mn(II) clusters in a model of R2c/R2lox.[20] The model compound elected for use was F-HXTA (5-fluoro-2-hydroxy-1,3-xylene-α,α′-diamine-*N,N,N′,N′*-tetraacetic acid), shown in Figure 12 along with the M_2(F-HXTA) complex.

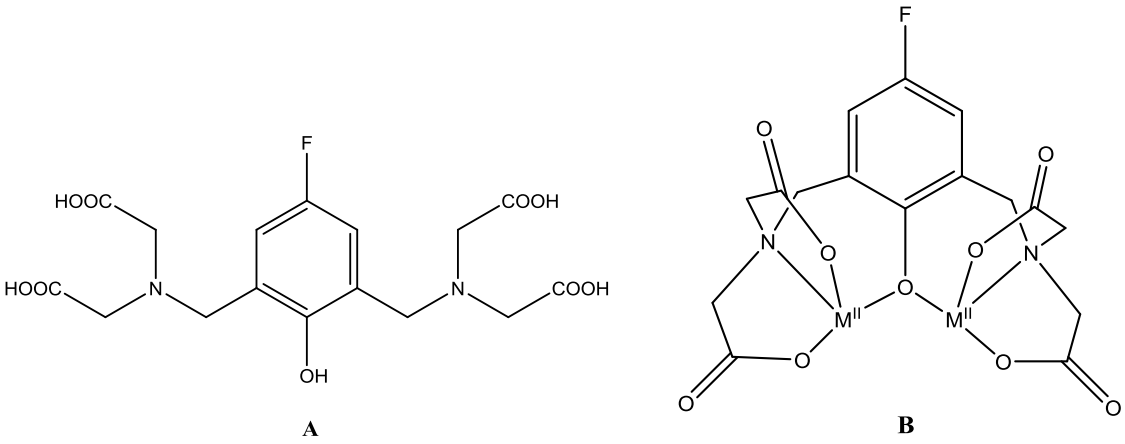

Figure 12: A: R2c/R2lox model compound H_5(F-HXTA): (5-fluoro-2-hydroxy-1,3-xylene-α,α′-diamine-N,N,N′,N′-tetraacetic acid) B: General $[M^{II}_2(\text{F-HXTA})]^-$ complex without aquo ligands.

F-HXTA is a ligand with two identical binding sites shown in Figure 12 similar to R2c/R2lox. There is a bridging oxygen atom between the two metals, and each metal is bound to two carboxylate moieties and an amine nitrogen. Homobimetallic complexes of F-HXTA were anaerobically synthesized by the addition of MCl_2 (3 equiv; M=Fe, Mn) and NaOH (5 equivalents) to H_5(F-HXTA). The complexes are shown in Figure 13. The crystal for $[Fe_2(F\text{-}HXTA)(H_2O)_4]^-$ were characterized via ^{19}F-NMR and ^{1}H-NMR, shown in Figure 14 and Figure 15 respectively. Fe^{II} is paramagnetic so the signals on the NMR experiments are broadened and shifted downfield, evident from the large spectra range in Figure 15. The $[Mn_2(F\text{-}HXTA)(H_2O)_4]^-$ crystals are NMR silent due to the slower electronic relaxation rate and the high paramagnetism of Mn^{II} which causes extreme line broadening.

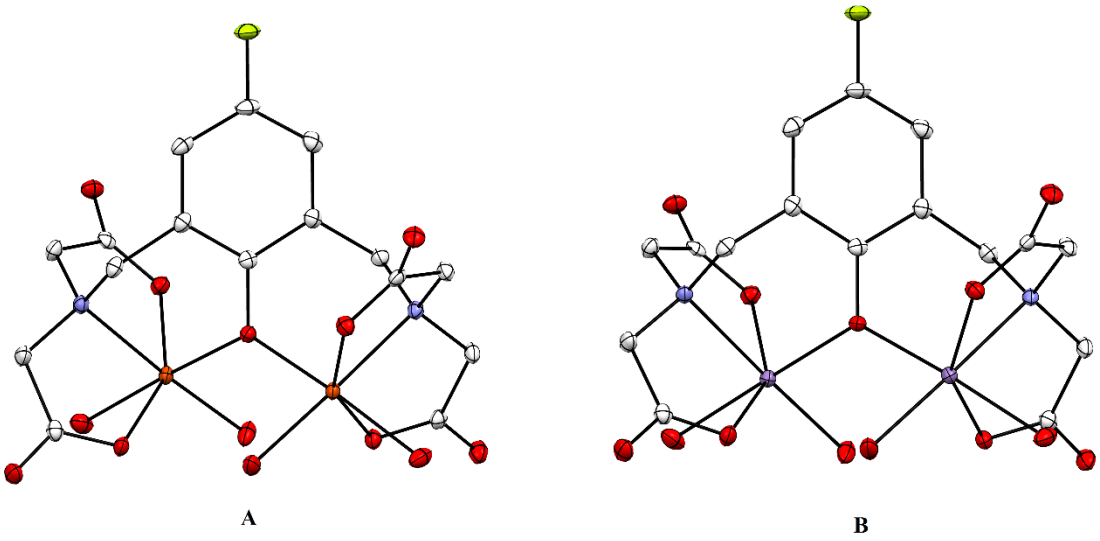

Figure 13: Displacement ellipsoid plots of $[M^{II}_2(F\text{-}HXTA)(H_2O)_4]^-$anions (A, M=Fe; B, M=Mn).The counterions are $[M(H_2O)_6]^{2+}$

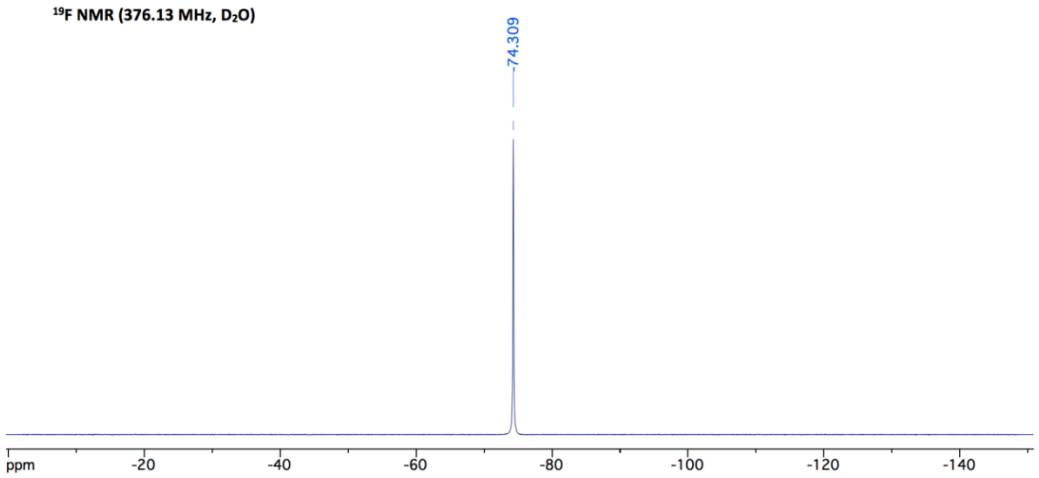

Figure 14: ^{19}F-NMR spectrum of $[Fe_2(F\text{-}HXTA)(D_2O)_4]^-$. [20]

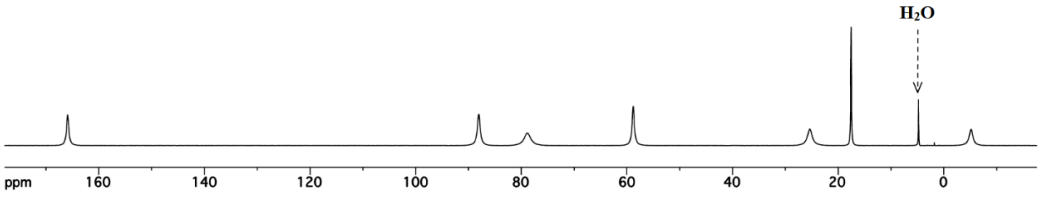

Figure 15: ^{1}H-NMR spectrum of $[Fe_2(F\text{-}HXTA)(D_2O)_4]^-$. [20]

A series of equilibrium exchange experiments were performed in order to measure the relative stability of Fe^{II}/Fe^{II}, Mn^{II}/Mn^{II} and Fe^{II}/Mn^{II} complexes in equilibrium mixtures. To a constant amount of F-HXTA an excess total amount of metal (Fe^{II}/Mn^{II}) was added in different ratios. The mixture was allowed to reach equilibrium and the concentrations of the different dimetal-HXTA complexes were measured by ^{19}F-NMR. $[Fe_2(F\text{-}HXTA)(H_2O)_4]^-$ and $[FeMn(F\text{-}HXTA)(H_2O)_4]^-$ mixtures are observable however $[Mn_2(F\text{-}HXTA)(H_2O)_4]^-$ is not, but the concentration of the latter was calculated

from F-HXTA mass balance. The overall metal replacement is shown in equation 1. Equations 2 and 3 are sequential single atom replacements. Measured values of the equilibria constants are given above the arrow.

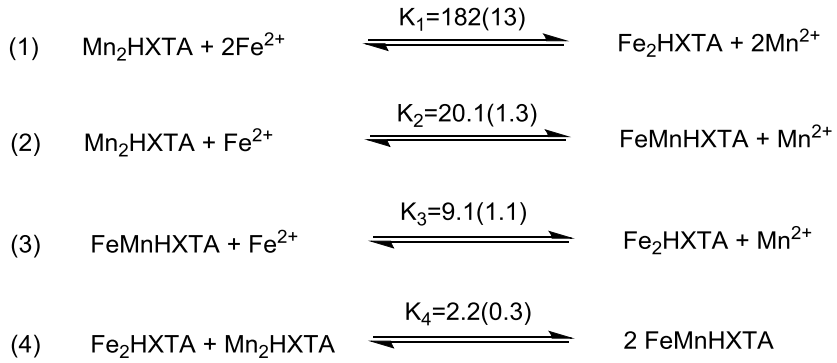

As expected from the Irving-Williams series Fe^{II} is preferred over Mn^{II} for the F-HXTA binding sites (Eq. 1);[16] however there is an unexpected stability of the mixed Fe^{II}/Mn^{II} cluster: if the metal binding sites were isolated from each other, it would be expected that the preference for replacement of Mn^{II} with Fe^{II} would be equivalent at each site. This would make the equilibrium constants in Eq 2 and 3 identical; however, they are not. The replacement of the first Mn^{II} atom (K = 20.1) is more favorable than the replacement of the second Mn^{II} atom (K = 9.1). Equation 4 shows the enhanced stability of the heterobimetallic species directly, where the K value is greater than 1 and therefore is marginally favoring the heterobimetallic products over the reactants. Note that $K_4=K_2/K_3$ There is not an obvious reason for enhanced stability of the heterobimetallic species but it is suspected to be due to the bridging oxygen atom.[20]

The concentrations of each species formed from the equilibrium between Mn^{II}, Fe^{II} and F-HXTA is shown graphically in Figure 16. The smooth curves are the calculated

concentrations of each species based on the exchange equilibria between the metal and F-HXTA (K_1-K_3) and the points are the experimental concentrations. It should be noted that where the two homobimetallic species curves intersect, the heterobimetallic curve is slightly higher indicating this relative enhanced stability (K_2>K_3). If the enhanced stability were not present, then all three curves would intersect (K_2=K_3).

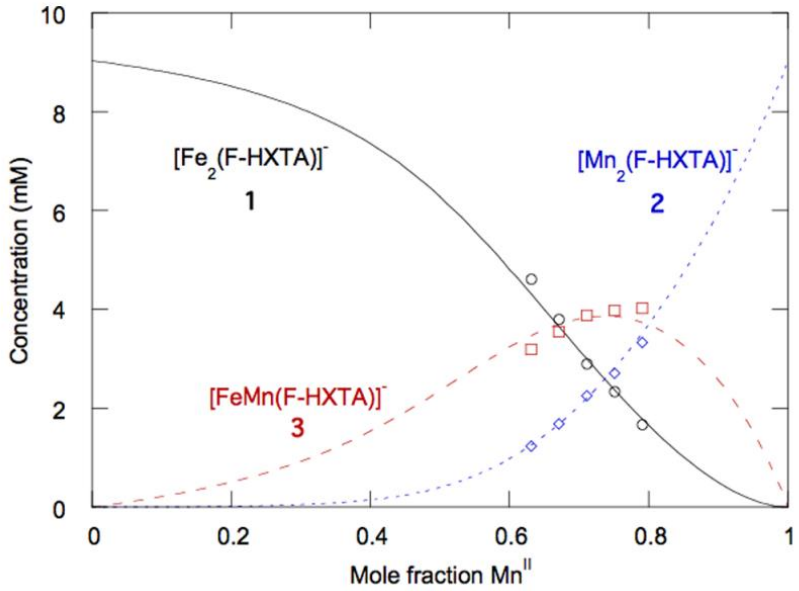

Figure 16: Concentrations of the bimetallic species of HXTA as a function of the Fe^{II}/Mn^{II} ratio.[20]

As an extension to the study with Fe^{II} and Mn^{II} binding to F-HXTA, the work moving forward by our lab sought to answer the question of whether or not the relative enhanced stability of F-HXTA clusters is a general phenomenon or if it is specific to Fe^{II} and Mn^{II}. In order to do so, two more metals were introduced: Zn^{II} and Mg^{II}. They were chosen because they are both divalent metals that are similar in size to both Fe^{II} and Mn^{II}. The same equilibrium experiments were performed in three different combinations:

Zn^{II}/Mg^{II}, Zn^{II}/Fe^{II} and Fe^{II}/Mg^{II} with the same ligand F-HXTA in order to see if the phenomenon of relative enhanced stability of the heterobimetallic mixture is still present.

1.4 References

[1] Boer, J. L.; Mulrooney, S. B.; Hausinger, R. P. *Archives of Biochemistry and Biophysics* **2014**, *544*, 142–152.

[2] (a) Schenk, G.; Mitić, N.; Gahan, L. R.; Ollis, D. L.; Mcgeary, R. P.; Guddat, L. W. *Accounts of Chemical Research* **2012**, *45*(9), 1593–1603. (b) Schenk, G.; Elliott, T. W.; Leung, E.; Carrington, L. E.; Mitić, N.; Gahan, L. R.; Guddat, L. W. *BMC Structural Biology* **2008**, *8*(1), 6. (c) Cotruvo, J. A.; Stubbe, J. *Annual Review of Biochemistry* **2011**, *80*(1), 733–767.

[3] Jiang, W.; Yun, D.; Saleh, L.; Barr, E. W.; Xing, G.; Hoffart, L. M.; Maslak, M. A.; Krebs, C.; Bollinger, J. M. *Science* **2007**, 316, 1188− 1191.

[4] Högbom, M.; Stenmark, P.; Voevodskaya, N.; McClarty, G. *Science* **2004**, 305, 245−248.

[5] Borovik, A. S.; Que, L. J.; Papaefthymiou, V.; Muenck, E.; Taylor, L. F.; Anderson, O. P. *Journal of the American Chemical Society* **1988**, *19*(28).

[6] Borovik, A. S.; Papaefthymiou, V.; Taylor, L. F.; Anderson, O. P.; Que, L. *Journal of the American Chemical Society* **1989**, *111*(16), 6183–6195.

[7] Carboni, M.; Clémancey, M.; Molton, F.; Pécaut, J.; Lebrun, C.; Dubois, L.; Blondin, G.; Latour, J.-M. *Inorganic Chemistry* **2012**, *51*(19), 10447–10460.

[8] Das, B.; Daver, H.; Singh, A.; Singh, R.; Haukka, M.; Demeshko, S.; Meyer, F.; Lisensky, G.; Jarenmark, M.; Himo, F.; Nordlander, E. *European Journal of Inorganic Chemistry* **2014**, *2014*(13), 2204–2212.

[9] Heims, F.; Mereacre, V.; Ciancetta, A.; Mebs, S.; Powell, A. K.; Greco, C.; Ray, K. *European Journal of Inorganic Chemistry* **2012**, *2012*(29), 4565–4569.

[10] Hotzelmann, R.; Wieghardt, K.; Floerke, U.; Haupt, H. J.; Weatherburn, D. C.; Bonvoisin, J.; Blondin, G.; Girerd, J. J. *Journal of the American Chemical Society* **1992**, *114*(5), 1681–1696.

[11] Chaudhuri, P.; Winter, M.; Kueppers, H.-J.; Wieghardt, K.; Nuber, B.; Weiss, J. *Inorganic Chemistry* **1987**, *26*, 3302-3310

[12] Sano, Y.; Lau, N.; Weitz, A. C.; Ziller, J. W.; Hendrich, M. P.; Borovik, A. S. *Inorganic Chemistry* **2017**, *56*(22), 14118–14128.

[13] Borovik, A. S.; Murch, B. P.; Que, L. J.; Papaefthymiou, V.; Munck, E. *Journal of the American Chemical Society* **1987**, *109*(10) 7190-7191.

[14] Holman, T. R.; Wang, Z.; Hendrich, M. P.; Que, L. *Inorganic Chemistry* **1995**, *34*(1), 134–139.

[15] Zhou, A; Crossland, P.M; Draksharapu, A; Jasniewski, A. J; Kleespies, S,T; Que Jr., L. *Journal of Biological Inorganic Chemistry* **2018**, 23, 155–165

[16] Helm, L.; Merbach, A. E. *Chemical Reviews* **2005**, *105*, 1923-1959

[17] Tereniak, S. J.; Carlson, R. K.; Clouston, L. J.; Young, V. G.; Bill, E.; Maurice, R.; Chen, Y.-S.; Kim, H. J.; Gagliardi, L.; Lu, C. C. *Journal of the American Chemical Society* **2013**, *136*(5), 1842–1855.

[18] Dassama, L. M. K.; Krebs, C.; Bollinger, J. M.; Rosenzweig, A. C.; Boal, A. K. *Biochemistry* **2013**, *52*(37), 6424–6436.

[19] Griese, J. J.; Roos, K.; Cox, N.; Shafaat, H. S.; Branca, R. M. M.; Lehtio, J.; Graslund, A.; Lubitz, W.; Siegbahn, P. E. M.; Hogbom, M. *Proceedings of the National Academy of Sciences* **2013**, *110*(43), 17189–17194.

[20] Kerber, W. D.; Goheen, J. T.; Perez, K. A.; Siegler, M. A. *Inorganic Chemistry* **2015**, *55*(2), 848–857.

Chapter 2: EXPERIMENTAL

2.1 Experimental Procedures

General. Aqueous solutions were made in Type I ultra-pure water with a resistivity of at least 18 $M\Omega cm^{-1}$. $Fe(ClO_4)_2 \cdot 4H_2O$, $Mg(ClO_4)_2 \cdot 6H_2O$ were obtained from Strem Chemicals and $Zn(ClO_4)_2 \cdot 6H_2O$ was obtained from Alfa Aesar and stored in a desiccator. 4-Flourophenol was sublimed under vacuum. *N*-Methylmorpholine was distilled from sodium metal under $N_2(g)$. Air sensitive samples were prepared in a COY Laboratories anaerobic chamber containing <1% O_2 using freeze-pump-thaw degassed solvents. H_5(F-HXTA)•XH_2O was prepared according to the procedure previously described by Kerber et. al.[1] Target concentrations of H_5(F-HXTA)•XH_2O are higher than the actual concentrations due to unknown waters of hydration in the crystal structure. ***Caution!*** *Although no difficulties were encountered in this work, organic perchlorates are potentially explosive. They should be prepared in small quantities and handled with care.*

$[Zn(H_2O)_6][Zn_2(F\text{-}HXTA)(H_2O)_3]_2 \cdot 10H_2O$. A 147.3 mg portion of H_5(F-HXTA) (0.366 mmols) was dissolved in 6.000 mL of a 0.207 M solution of NaOH solution (1.242 mmols). A 311.1 mg portion of $Zn(NO_3)_2 \cdot 6H_2O$ (1.198 mmols) was dissolved in this solution and the pH was raised to 6.94 with the 0.207 M NaOH solution at which point a white precipitate formed. After syringe filtration with a 0.45 μm nylon filter, the solution was capped and stored at 5°C. Colorless crystals suitable for X-ray structure determination formed after 3 weeks, this procedure yielded 0.1115g of crystals for a

19.16% yield. ^{1}H-NMR (D_2O, 400 MHz): δ 6.75 (d, 2H, $^{3}J_{HF}$=9.0 Hz), δ 3.469 (br, 4H), δ 3.216 (s, 8H). (^{19}F-NMR (D_2O, 376 MHz): δ -133.06 (t, 1F, $^{3}J_{HF}$=8.91 Hz).

$[Mg(H_2O)_6][Mg_2(F\text{-}HXTA)(H_2O)_4]_2 \cdot 14H_2O$. A 120.0 mg portion of H_5(F-HXTA) (0.298 mmol) was dissolved in 3.300 mL of a 0.245M solution of NaOH (0.809 mmol). A 220.5 mg portion of $Mg(NO_3)_2 \cdot 6H_2O$ (0.897 mmol) was dissolved in this solution and the pH was adjusted to 8.31 by addition of 0.245M NaOH and left open in the laboratory for evaporation. After 10 weeks the solution was filtered with a 0.45 μm nylon syringe and was capped and placed in a 5°C refrigerator. One week later crystals formed yielding 0.0601 g (7.72%). ^{1}H-NMR (D_2O, 400 MHz): δ 6.760 (d, 2H, $^{3}J_{HF}$=9.1 Hz), δ 3.720 (d, 2H), δ 3.384 (d, 2H), δ 3.241 (d, 2H), δ 3.139 (d, 2H), δ 3.021 (d, 2H), δ 2.942 (d, 2H). ^{19}FNMR (D_2O, 376 MHz): δ -134.10 (t, 1F, $^{3}J_{HF}$=9.01 Hz)

Standardization of $Zn(ClO_4)_2$ and $Mg(ClO_4)_2$. Using an Eriochrome Black T indicator, along with an ammonia/ammonium buffer, 0.2M $M(ClO_4)_2$, solutions were standardized by titration according to a published procedure.[2] The titrant was standard 0.05M EDTA from Alfa Aesar, yielding $[Zn(ClO_4)_2]$ = 0.1975 M and $[Mg(ClO_4)_2]$ = 0.1906 M.

Metal Titration Experiments. A 10.00 mL solution of Na_3H_2(F-HXTA) (0.1000 M) was made by adding 0.0402 g (0.0001 mols) of H_5(F-HXTA) and 3 equivalents of NaOH (0.0003 mols) to a 10 mL volumetric flask. A ^{19}F-NMR was taken of this solution. Increments of 0.5 equivalents of metal solutions ($M(ClO_4)_2$ M= Mg^{II}, Zn^{II}) were added to

this Na_3H_2(F-HXTA) solution. ^{19}F-NMR spectra were taken until 2.5 equivalents of metal compared to Na_3H_2(F-HXTA) was added.

Metal Exchange Experiments. Solutions were prepared by diluting aliquots of aqueous stock solutions to the final target concentrations. Calibrated automatic pipettes and volumetric flasks were used throughout. Because H_5(F-HXTA) is insoluble in water, stock solutions were prepared as Na_3H_2(F-HXTA) by adding 3 equivalents of NaOH. Samples were prepared in an anaerobic chamber and sealed in J-Young style NMR tubes for analysis. Sample pH measured in H_2O/D_2O mixture was corrected for isotopic composition using the formula $pH_{corr}=pH_{meas}-n(0.073 \times pH_{meas} - 0.42)$ where n is the deuterium mole fraction of the sample.[3] Target concentrations for the species in solution were as follows: Na_3H_2(F-HXTA) 0.010 M, NTA 0.005 M, total metal 0.040 M, *N*-methylmorpholine 0.042 M, 4-fluorophenol 0.005 M. F-HXTA concentrations were calculated to be 90% of the target range because unknown waters of hydration add mass in the crystal structure. The pH was targeted to be around 7.5 and the D_2O content 10%. These numbers were for the Zn/Mg and Mg/Fe combinations of metals; 70% lower concentrations were used for all materials in solution for Zn/Fe due to lower solubility of F-HXTA complexes.

Representative Procedure. To a 5.00 mL volumetric flask containing 10% of D_2O, was added 1.520 mL of Na_2H_3(F-HXTA) (0.0330 M, 0.050 mmol), 0.498 mL of NTA (0.0502M, 0.025 mmol), 0.430 mL of $Zn_2(ClO_4)_2$ (0.1975 M; 0.085 mmol), 0.604 mL of $Mg_2(ClO_4)_2$ (0.1906 M; 0.115 mmol), 0.126 mL of 4-fluorophenol (0.1980 M; 0.025 mmol), and 0.230 mL of *N*-methylmorpholine (0.9823 M; 0.226 mmol). The flask was

diluted to the mark with H_2O. The pH was measured and an aliquot was sealed in an NMR tube and equilibrated at 25℃ for 8 hours prior to analysis.

NMR Spectroscopy. Spectra were acquired on a Varian 400 MHz DirectDrive spectrometer equipped with a 5 mm ASW PFG probe. Data were processed in iNMR. Chemical shifts are reported relative to solvent resonances for ^{1}H and relative to sodium hexafluorophosphate for ^{19}F-NMR of the homobimetallic crystallizations and 4-fluorphenol for the metal exchange experiments. T_1 measurements were made with a calibrated 90° pulse using a standard inversion-recovery pulse sequence.

Equilibrium Measurements. Initially for each metal combination, the largest T1 value was found, which always corresponded to the 4-fluorphenol peak. The recycle time used was 7x that T1 value. A 90° pulse was calibrated for each acquisition of the experiment. For the combinations including Fe, it was necessary to use two acquisitions with different sweep widths changing the TOF due to the wide dispersion of peaks in the spectra. This allowed all peaks of interest to be measured with a 90° pulse relative to the internal standard. A total of 1024 to 2000 transients were collected for quantitative experiments based on the signal to noise ratio of each sample. The FID was 9058 points for the Mg/Zn combination and was around 37,500 points for the other two metal combinations. The probe temperature was set to 25°C and 10 Hz of exponential line broadening was used during analysis.

Speciation Modeling. Concentration curves for the bimetallic species were calculated in HYSS2008[4] at the following initial conditions: $[M_a^{II}]$ = 0-40 mM; $[M_b^{II}]$ = 40-0 mM; [F-

HXTA] = 8.4 mM; [NTA] = 5 mM; [ClO_4^-] = 80 mM. Except for the Fe/Zn combination which was cut by 70% from these concentrations because it is slightly more insoluble than the other mixtures. The model used for this calculation consisted of the formation constants (β) for each bimetallic species. $\beta_{1\text{-}3}$ were calculated from $K_{1\text{-}3}$ by choosing an arbitrarily large value for β_1 (10^{20}) such that essentially no F-HXTA was present and then calculating the relative values of β_2 and β_3 from the equilibrium equations.

2.2 References

[1] Kerber, W. D.; Goheen, J. T.; Perez, K. A.; Siegler, M. A. *Inorganic Chemistry* **2015**, *55*(2), 848-857.

[2] Mendham, J. et.al. M. J. K. *Vogels textbook of quantitative chemical analysis.*, 5th ed.; Pearson: New Delhi, **2009**, 324-329

[3] Krężel, A.; Bal, W. *J. Inorg. Biochem.* **2004**, 98, 161−166

[4] (a) Alderighi, L.; Gans, P.; Ienco, A.; Peters, D.; Sabatini, A.; Vacca, A. *Coord. Chem. Rev*. **1999**, 184, 311−318. (b) Hyperquad Simulation and Speciation (HySS2009), Protonic Software, 2009; http://www.hyperquad.co.uk/hyss.htm (accessed July 24th, 2018).

Chapter 3: RESULTS AND DISCUSSION

3.1 Preparation and Characterization of Homobimetallic Complexes

Dizinc(II) and dimagnesium(II) complexes of the ligand H_5(F-HXTA) (5-fluoro-2-hydroxyl-1,3-xylene-α,α'-diamine-N,N,N',N'-tetraacetic acid) were prepared and isolated in order to structurally characterize the metal complexes. A previous study has characterized the crystal structures for the diiron and dimanganese complexes of H_5(F-HXTA).[1] Addition of excess $M(NO_3)_2$ (3 equiv; M= Mg, Zn) and NaOH (5 equiv) to H_5(F-HXTA) gave neutral to slightly basic (pH 7-8) solutions from which the complex anions $[Zn_2(F\text{-}HXTA)(H_2O)_3]^-$ (**1**) and $[Mg_2(F\text{-}HXTA)(H_2O)_4]^-$ (**2**) crystallized after a period of weeks to months $[Zn(H_2O)_6][\mathbf{1}]_2 \bullet 10H_2O$ and $[Mg(H_2O)_6][\mathbf{2}]_2 \bullet 14H_2O$, as determined by X-ray crystallography. The dimagnesium(II) species was more difficult to crystallize because it is much more soluble than the dizinc(II) species. Recrystallization of $[Zn(H_2O)_6][\mathbf{1}]_2 \bullet 10H_2O$ using a seed crystal gave an isolated yield of 19 %. Seeding was ineffective for $[Mg(H_2O)_6][\mathbf{2}]_2 \bullet 14H_2O$ and a lower isolated yield of 8% was obtained.

X-ray structures of $[Zn^{II}_2(F\text{-}HXTA)(H_2O)_3]^-$ and $[Mg^{II}_2(F\text{-}HXTA)(H_2O)_4]^-$ are given in Figure 1 and the results of X-ray structural determination are reported in Table 1 and Table 2. (Crystallographic data is found in Table 1 and selected bond lengths and angles are in Table 2.) The most obvious difference between the two is that both Mg sites in **2** are 6-coordinate however Zn2 at site 2 (Zn2) is 5-coordinate in **1**, with one fewer water molecule attached. Zn1 has a distorted octahedral configuration with angles that range from 79.16° to 101.82°. The Zn atom is displaced by the mean square plane

(defined by N1, O1W, O2W and O5) by 0.061 Å. The carboxylate ligands are *trans* across the square plane and also substantially deviate from linearity with the O1-Zn1-O3 angle found to be 158.61°. Since Zn2 is 5-coordinate and has only one aquo ligand, the structural parameter τ_5 may be used to define the geometry of Zn2 with the limiting square pyramidal and trigonal bypyramidal structures represented by $\tau_5 = 0$ and 1 respectively[2]. Complex **2** has $\tau_5 = 0.448$ indicating an intermediate geometry slightly biased towards a square pyramid. Zn2 is displaced from the mean square plane defined by N2, O6, O3W, and O8 by 0.371 Å, and the angles between apical O5 and the atoms in the square plane range from 93.78° to 109.78°.

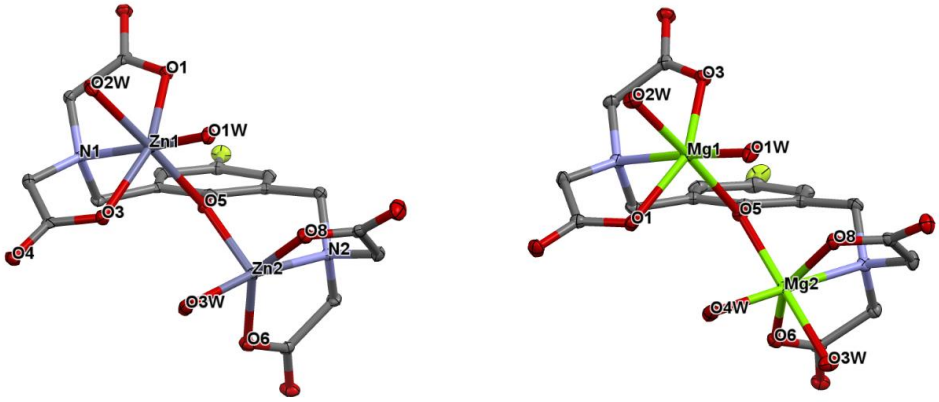

Figure 1. X-ray structures of $[Zn^{II}_2(F\text{-}HXTA)(H_2O)_3]^-$ (**1**) and $[Mg^{II}_2(F\text{-}HXTA)(H_2O)_4]^-$ (**2**). Hydrogen atoms omitted for clarity.

Complex **2** was found to have approximate C_2 symmetry, similar to previous structures of Fe(II) and Mn(II) with this ligand.[1] The metal-ligand angles in the distorted octahedron of **2** range from 76.42° to 103.94°. The Mg atoms are displaced from the mean square plane (defined by N1, O1W, O2W, and O5 and N2, O3W, O4W and O5) by 0.070 Å and 0.009 Å. The carboxylate ligands are *trans* across the square plane and

deviate substantially from linearity, with angles of 152.97° for O1-Mg1-O3 and 153.52° for O6-Mg2-O8.

Table 1: Crystallographic data for $[Zn(H_2O)_6][1]_2 \bullet 10H_2O$ and $[Mg(H_2O)_6][2]_2 \bullet 14H_2O$.

	$[Zn(H_2O)_6][\mathbf{1}]_2 \bullet 10H_2O$	$[Mg(H_2O)_6][\mathbf{2}]_2 \bullet 14H_2O$
Crystal data		
Empirical formula	$C_{32}H_{72}F_2N_4O_{40}Zn_5$	$C_{32}H_{84}F_2Mg_5N_4O_{46}$
Formula weight	1517.78	1420.58
Crystal system	Triclinic	Triclinic
Space group	*P*-1	*P*-1
a [Å]	10.5309 (3)	10.8336(3)
b [Å]	10.8052 (3)	11.3855(3)
c [Å]	13.7649 (4)	13.3069(4)
α (°)	102.549 (2)	92.844(2)
β (°)	109.982 (3)	113.681(3)
γ (°)	105.130 (3)	90.617(2)
V (Å^3)	1337.44(7)	1500.45(8)
Z	1	1
T (K)	110(2)	110(2)
Crystal size (mm)	0.26 × 0.18 × 0.06	0.28 × 0.24 × 0.22
μ (mm^{-1})	2.33	1.78
Data collection		
T_{min}, T_{max}	0.629, 1.000	0.714, 0.778
Measd reflections	21754	8695
Unique reflections	6140	8695

Obsd reflns [$I>2\sigma(I)$]	5576	7952
R_{int}	0.023	0.021
$(\sin\theta/\lambda)_{max}$ ($Å^{-1}$)	0.650	0.616
Refinement		
$R[F^2 > 2\sigma(F^2)]$	0.022	0.031
$wR(F^2)$	0.053	0.091
S	1.04	1.07
Parameters (Restraints)	442 (33)	488 (42)
$\Delta\rho_{max}$, $\Delta\rho_{min}$ (e $Å^{-3}$)	0.41, -0.30	0.38, -0.25

Table 2: Selected bond lengths and angles for $[Zn_2(F\text{-}HXTA)(H_2O)_3]^-$ (**1**) and $[Mg_2(F\text{-}HXTA)(H_2O)_4]^-$ (**2**)

	$[Zn_2(F\text{-}HXTA)(H_2O)_3]^-$ (**1**)	$[Mg_2(F\text{-}HXTA)(H_2O)_4]^-$ (**2**)
Bond lengths (Å)		
M1-N1	2.1504(13)	2.2042(12)
M2-N2	2.1588(14)	2.2156(12)
M1-O5	2.0755(11)	2.0761(10)
M2-O5	2.0035(11)	2.0724(10)
M1-O1	2.0653(11)	2.1345(11)
M2-O6	2.0442(12)	2.0528(10)
M1-O3	2.1002(12)	2.0674(11)
M2-O8	2.0235(12)	2.0928(11)
M1-O1W	2.0257(12)	2.0175(11)
M1-O2W	2.2029(12)	2.1119(11)
M2-O3W	2.0338(12)	2.1179(11)
M2-O4W	N/A	2.0127(11)

Bond angles (°)		
M1-O5-M2	129.31(5)	129.57(5)
N1-M1-O5	92.33(5)	91.00(4)
N1-M1-O2W	88.37(5)	91.04(4)
O1W-M1-O5	93.81(5)	87.63(4)
O1W-M1-O2W	85.29(5)	90.12(4)
O1-M1-O3	158.61(4)	152.97(4)
N2-M2-O5	93.78(5)	91.00(4)
N2-M2-O3W	169.82(5)	90.42(4)
O4W-M2-O5	N/A	89.48(4)
O3W-M2-O4W	N/A	89.19(5)
O6-M2-O8	142.93(5)	153.52(4)
O5-M2-O6	109.78(5)	98.34(4)
O5-M2-O8	103.61(5)	93.62(4)

Elemental analysis (C,H,N) was performed on the crystals of $[Zn(H_2O)_6][\mathbf{1}]_2 \cdot 10H_2O$ and $[Mg(H_2O)_6][\mathbf{2}]_2 \cdot 14H_2O$ as another method of characterization of the isolated complexes. The samples were dried under vacuum before analysis and as a result, some of the waters of hydration were lost from the crystal lattice. The results suggest $[Zn(H_2O)_6][\mathbf{1}]_2 \cdot 10H_2O$ crystals lost a total of 14 water molecules and the $[Mg(H_2O)_6][\mathbf{2}]_2 \cdot 14H_2O$ crystals lost 10 water molecules. It is unclear which molecules of water were lost from the crystals, but the mostly likely candidates are the waters of

crystallization. The theoretical composition of the formulas $Zn_5(F\text{-}HXTA)_2(H_2O)_8$ and $Mg_5(F\text{-}HXTA)_2(H_2O)_{18}$ gives C, H, N compositions within 0.4% of the experimental analysis values we observed. Previous homobimetallic species with Fe and Mn both lost 22 molecules of water when dried for the elemental analysis.[1]

Figure 2 shows the ^{19}F-NMR spectrum of $[Mg_2(F\text{-}HXTA)(H_2O)_4]^-$ (**2**) after dissolving the isolated crystals in D_2O, which has a triplet peak at -134.10 ppm ($^3J_{HF}$=9.01 Hz). Figure 4 is the ^{19}F-NMR spectrum of the $[Zn_2(F\text{-}HXTA)(H_2O)_3]^-$ (**1**) crystals with a triplet peak at -133.06 ppm ($^3J_{HF}$=9.1 Hz). These spectra are what was expected for their respective compounds; a single peak per complex but split into a triplet peak with the F coupling to the aryl H's. Figure 3 is the ^{1}H-NMR of $[Mg_2(F\text{-}HXTA)(H_2O)_4]^-$ (**2**). The complex anion in $[Mg(H_2O)_6][\mathbf{2}]_2 \bullet 14H_2O$ has C_2 symmetry and 7 unique sets of F-HXTA protons: the two equivalent aryl protons, two distinct benzylic protons, and then four ditinct protons on each arm of the amines. When dissolved in D_2O, the ^{1}H-NMR spectrum shows 7 resonances indicating the C2 symmetry observed in the crystal structure is maintained in solution. A clear aromatic doublet at 6.75 ppm ($^3J_{HF}$=9.1 Hz) with an integration of 2 is observed; it is split into a doublet due to the aryl H coupling with the F. A series of 6 doublets corresponding to the different sets of hydrogens on the F-HXTA ligand is also present. The doublets are distinct diastereotopic methylene peaks, because the two hydrogens on each carbon are not equivalent and therefore split each other with a large coupling constant (J_{HH}=12-18 Hz). This conclusion is supported by an integration of 2 for each doublet; diastereotopic methylene peaks were also previously observed for the $[Fe_2(F\text{-}HXTA)(H_2O)_4]^-$ complex.[1]

Figure 5 shows the ^{1}H-NMR spectrum of $[Zn_2(F\text{-}HXTA)(H_2O)_3]^-$ crystals and this is generally less sharp than the $[Mg_2(F\text{-}HXTA)(H_2O)_4]^-$ spectrum. The aromatic peak at 6.79 ppm is clear with an integration of 2 but the diastereotopic methylenes that were apparent in the $[Mg_2(F\text{-}HXTA)(H_2O)_4]^-$ spectrum have collapsed together into two peaks around the same area. The ^{1}H-NMR spectrum of $[Zn(H_2O)_6][\mathbf{1}]_2 \bullet 10H_2O$ crystals dissolved in D_2O shows only 3 broad resonances indicating rapid inter conversion of the C_2 enantiomers on the NMR timescale. The most likely mechanism is loss of coordinated water molecules and flattening of the complex anion into an intermediate with C_s symmetry.

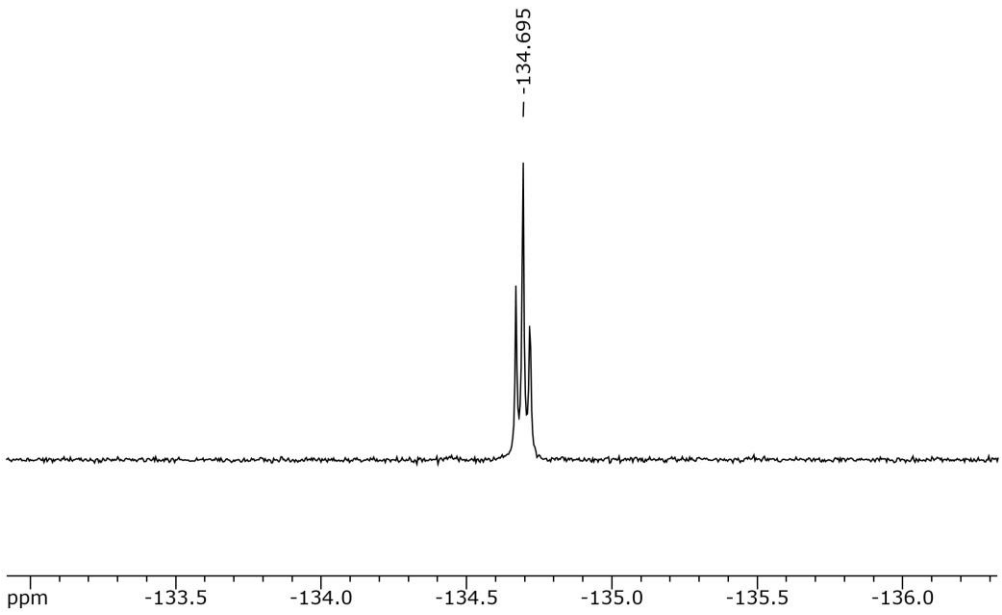

Figure 2: ^{19}F-NMR of $[Mg(H_2O)_6][\mathbf{2}]_2 \bullet 12H_2O$ in D_2O referenced to C_6F_6.

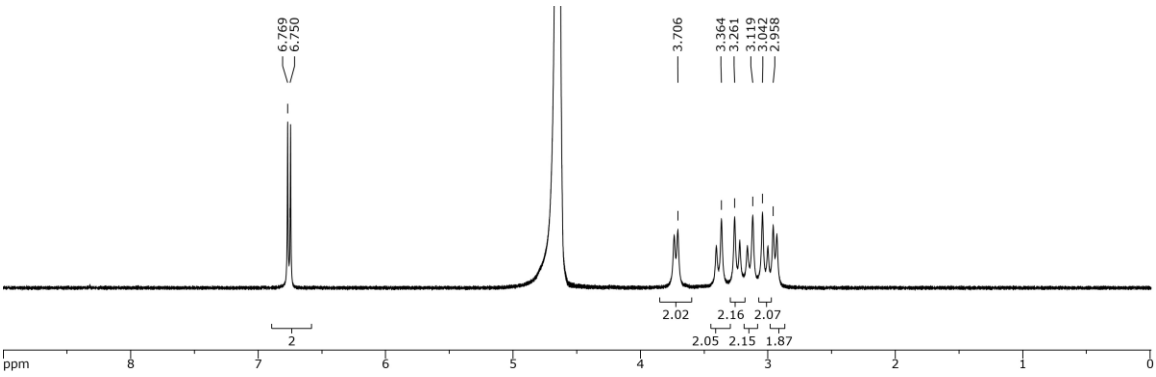

Figure 3: ^{1}H-NMR of $[Mg(H_2O)_6][\mathbf{2}]_2 \cdot 12H_2O$ in D_2O.

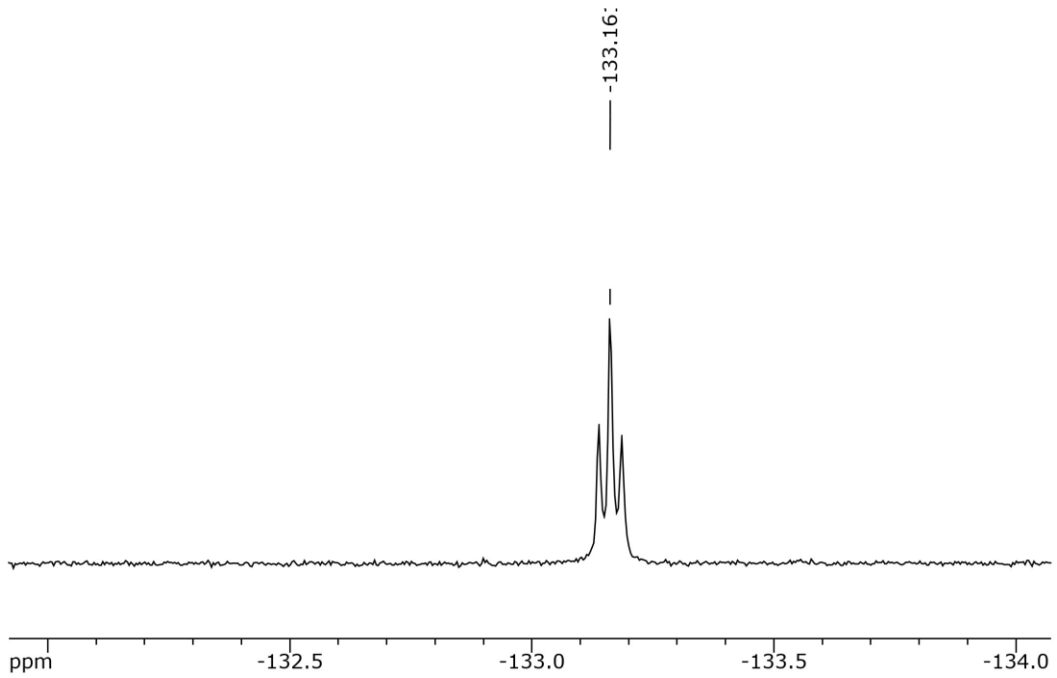

Figure 4: ^{19}F-NMR of $[Zn(H_2O)_6][\mathbf{1}]_2 \cdot 2H_2O$ in D_2O referenced to $NaPF_6$.

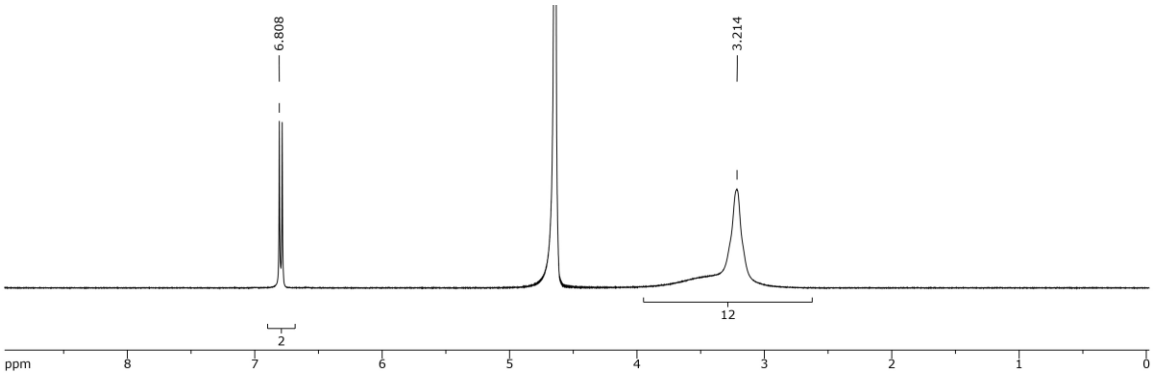

Figure 5: ^{1}H-NMR of $[Zn(H_2O)_6][1]_2 \bullet 2H_2O$ in D_2O.

3.2 Designing Metal Exchange Experiments

Our previous Fe^{II}/Mn^{II} exchange experiments with F-HXTA were performed by measuring the amounts of the different bimetallic-HXTA complexes in equilibrium after adding different ratios of the two metal salts. We proposed to repeat these experiments with pairs from the group: Fe^{2+}, Mg^{2+} and Zn^{2+}. The purpose of the exchange experiments is to investigate the relative stabilities of the different F-HXTA species formed. The total amount of the two metals added, regardless of the ratio, was in excess of the amount of F-HXTA (greater than two equivalents). Under these conditions, F-HXTA is saturated with metal and an equilibrium is established between the two homobimetallic F-HXTA species and a heterobimetallic F-HXTA species, as shown in Eqs 1 – 3. Equation 1 is the net overall reaction from one homobimetallic species to another, and equation 2 and equation 3 are the single step metal replacements that sum to equation 1. In order to measure the equilibrium constants, ^{19}F-NMR was used with an internal standard (4-fluorophenol) of known concentration to measure against the

concentrations of all three bimetallic-HXTA complexes.

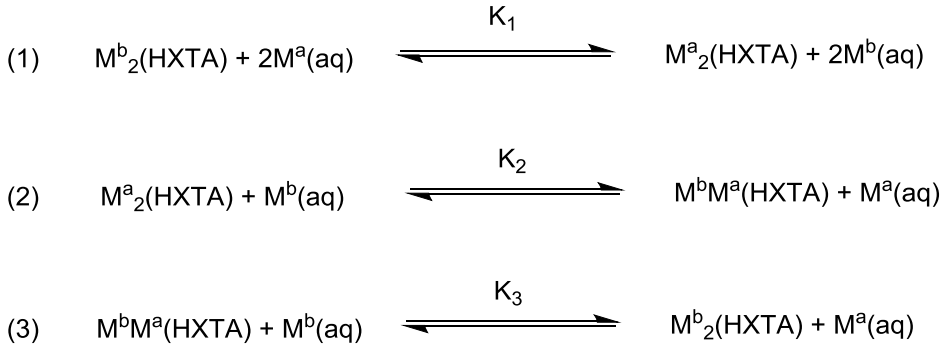

Before comprehensive equilibrium experiments could be conducted, it was important to first perform three control experiments: the first was to determine how long it takes mixtures of metal and F-HXTA to reach equilibrium, the second was to confirm all coordination sites are occupied under the conditions of interest, and the third was to make sure all species are present at measurable concentrations. In order to accomplish the first objective, a series of ^{19}F-NMR spectra were taken of the Zn^{2+}/Mg^{2+} exchange at different time intervals. The first was when the mixture was initially made, then 4.5 and 24 hours later. During the time between the initial solution being made and the NMR measurements, the mixture was kept in a water bath at a constant temperature of 25°C. Peak areas were compared to each other to see how long it took for concentrations of each F-HXTA species in the solution to reach a constant value. The integrated ^{19}F-NMR spectra at each time interval can be found in Figure 6. As expected, each spectrum had similar integrals for each peak and therefore reaches equilibrium rapidly enough that essentially no wait time is required. However, for consistency the time between solution preparation and beginning of the NMR acquisition was chosen to be 6.5 hours.

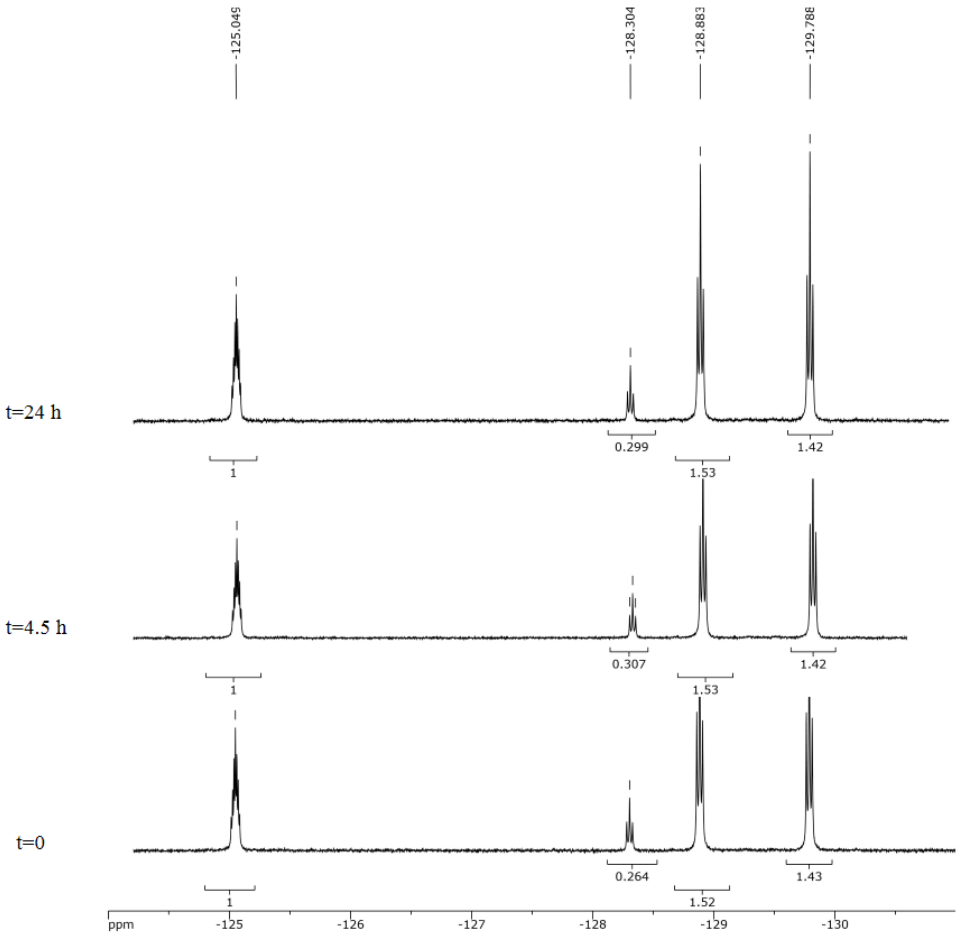

Figure 6: Time interval NMR spectra, bottom to top: initial, 4.5 hours, 24 hours. Peaks: 4-fluorphenol (-125.05 ppm), Zn_2HXTA (-128.30 ppm), ZnMgHXTA(-128.88 ppm), Mg_2HXTA(-129.79 ppm)

It was also important prior to the equilibrium experiment to determine if under the conditions of the experiment that F-HXTA was fully saturated with metal so all the coordination sites are occupied. In order to do so, a series of experiments were performed in which the concentration of F-HXTA was held constant and the amount of $M(ClO_4)_2$ ($M=Mg^{II}$, Zn^{II}) was added in increments of 0.5 molar equivalents with respect to F-HXTA. The range of equivalents added were from 0.0:1 to 2.5:1, Metal:F-HXTA. The mixtures were monitored via ^{19}F-NMR and the results can be seen in Figure 7 and Figure

8 for Zn^{II} and Mg^{II} respectively. A similar experiment with Fe^{II} and F-HXTA was performed previously.[1]

Figure 7 and Figure 8 show a similar trend: In the initial spectrum A, only F-HXTA is present without any metal added and that is the largest peak shown in the spectrum. After the first 0.5 M equivalent of metal is added, two peaks upfield from that initial F-HXTA peak begin to form and those are from mononucleated M-(F-HXTA) and dinucleated M_2(F-HXTA), seen in spectrum B. As each new equivalent of metal is added to the mixture, the initial F-HXTA peak and the M(F-HXTA) peak decrease in intensity as the M_2(F-HXTA) peak increases in intensity. At the exchange equilibrium ratio of 2.0:1 metal:F-HXTA, the initial F-HXTA peak and the M(F-HXTA) peak are insignificant intensities and therefore not factors in the exchange experiment. In both Figure 7 and Figure 8, there is a small peak up field from the rest of the F-HXTA and complex peaks. That is due to the slow degradation of the F-HXTA which can happen over time while the compound is in solution.

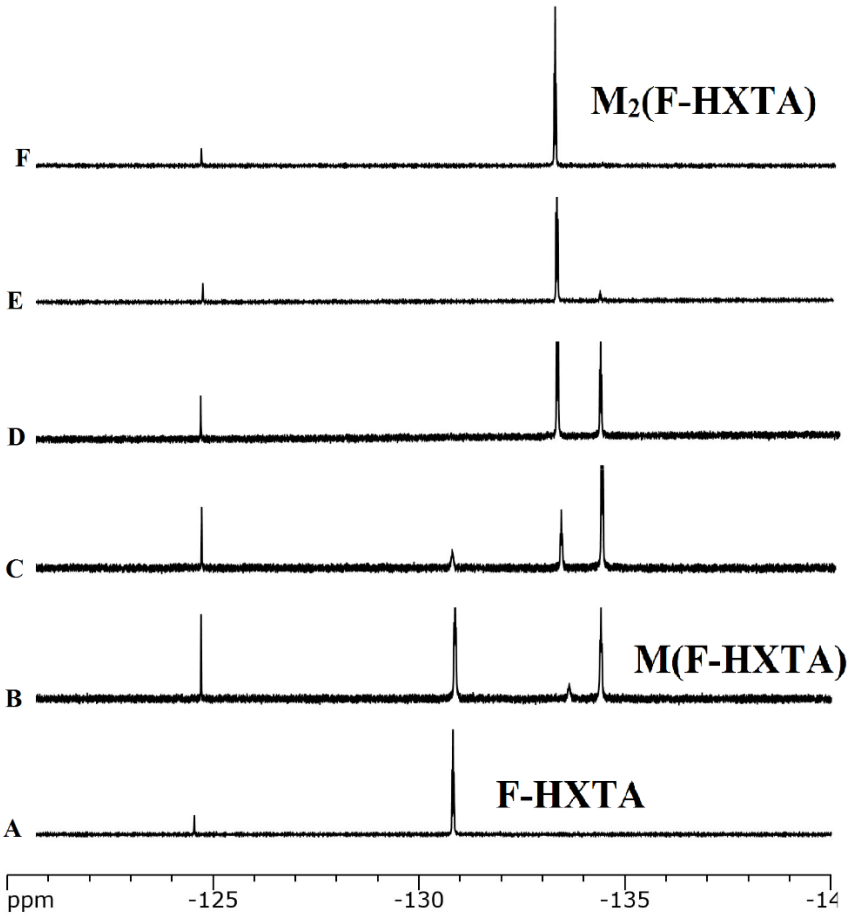

Figure 7: Incremental addition of $Zn(ClO_4)_2$ to F-HXTA: **A**= 0.0 equivalents of $Zn(ClO_4)_2$; **B**= 0.5 equivalents of $Zn(ClO_4)_2$; **C**= 1.0 equivalents of $Zn(ClO_4)_2$; **D**= 1.5 equivalents of $Zn(ClO_4)_2$; **E**= 2.0 equivalents of $Zn(ClO_4)_2$; **F**= 2.5 equivalents of $Zn(ClO_4)_2$, The equivalence is with a respect to the F-HXTA concentration.

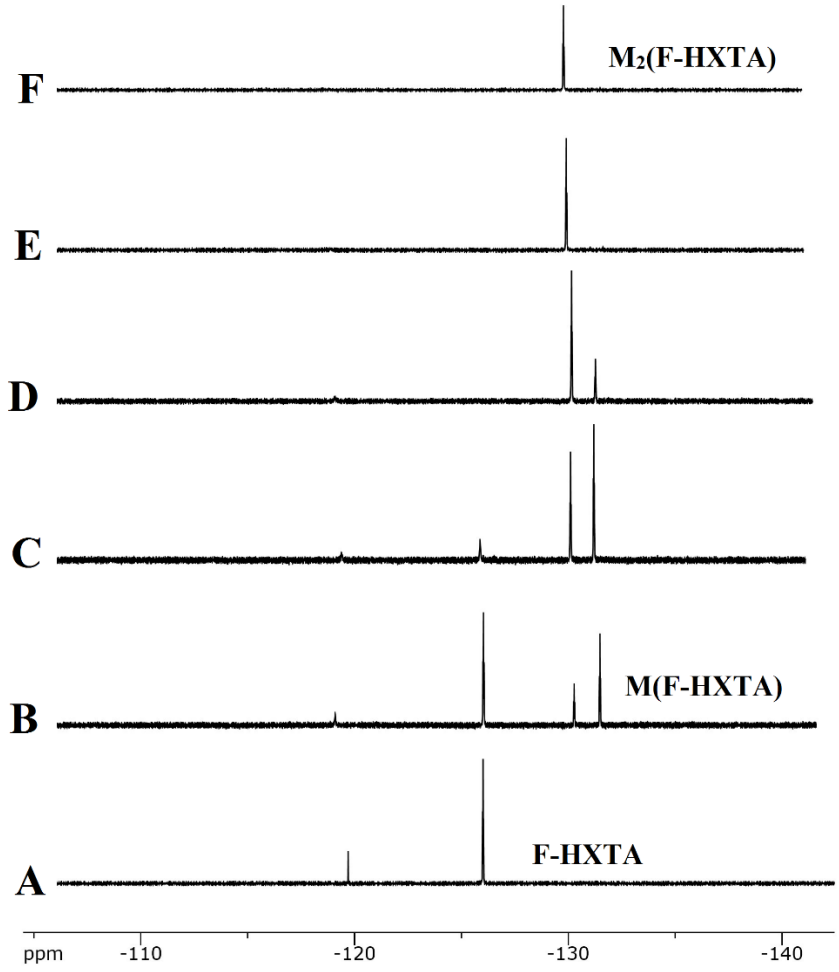

Figure 8: Incremental addition of $Mg(ClO_4)_2$ to F-HXTA: A= 0.0 equivalents of $Mg(ClO_4)_2$; B= 0.5 equivalents of $Mg(ClO_4)_2$; C= 1.0 equivalents of $Mg(ClO_4)_2$; D= 1.5 equivalents of $Mg(ClO_4)_2$; E= 2.0 equivalents of $Mg(ClO_4)_2$; F= 2.5 equivalents of $Mg(ClO4)_2$, The equivalence is with a respect to the F-HXTA concentration.

Equations 1-3 are representative of the metal exchange equilibria for each of the experimental metal combinations Zn^{2+}, Mg^{2+} and Fe^{2+}. The experimental approach for measuring K_{1-3} described above will only work if all species are present in reasonable amounts i.e. K_{1-3} are neither too large nor too small. In order to get a good idea of what the formation constants between F-HXTA and these metals might look like, we found it

helpful to examine metal complexes of the similarly structured, but mononucleating ethylenediaminetetraacetic acid (H_4EDTA) ligand. Equations 4-6 illustrate the formation constants (β) of the metals of concern with EDTA on a logarithmic scale.[3] A formation constant is an equilibrium constant for the formation of a complex between a free metal ion and a ligand. β values are typically very large between a metal and a chelating ligand; therefore, it is convenient to deal with these values on a logarithmic scale.

(4) $EDTA^{4-} + Zn^{2+} \rightleftharpoons ZnEDTA^{2-}$ $\log(\beta)=16.26$

(5) $EDTA^{4-} + Mg^{2+} \rightleftharpoons MgEDTA^{2-}$ $\log(\beta)=8.69$

(6) $EDTA^{4-} + Fe^{2+} \rightleftharpoons FeEDTA^{2-}$ $\log(\beta)=14.2$

(7) $MgEDTA^{2-} + Zn^{2+} \rightleftharpoons ZnEDTA^{2-} + Mg^{2+}$ $K_7=74.13$

(8) $MgEDTA^{2-} + Fe^{2+} \rightleftharpoons FeEDTA^{2-} + Mg^{2+}$ $K_8=42.66$

(9) $FeEDTA^{2-} + Zn^{2+} \rightleftharpoons ZnEDTA^{2-} + Fe^{2+}$ $K_9=14.12$

Since EDTA's structure is similar to that of F-HXTA, it can be inferred that both ligands will have similar relative affinities for Mg/Zn, Mg/Fe and Zn/Fe. The metal affinities for EDTA are illustrated in equations 7-9, and these equations are considered analogous to equation 1 for F-HXTA. These numbers are significantly larger than 1 and thus all favor the products. We therefore expect that for F-HXTA the formations constants of each metal are too different to accurately measure the concentrations of all

M_2(F-HXTA) complexes simultaneously. One metal binds much more favorably than the other in a mixture of two metals and F-HXTA. Therefore, the concentration of one of the metal species will approach zero thus making equilibrium constants impossible to calculate by the method outlined above. Preliminary experiments using F-HXTA and Zn/Mg mixtures showed this to be the case. The solution to be able to perform equilibrium calculations for this system is to introduce a leveling agent into the system. A leveling agent is a molecule that has relative binding affinity to the ligand of interest, in this case F-HXTA. The leveling agent will bias the system towards a more even distribution of the different dimetal-HXTA complexes that can all be measured via ^{19}F-NMR.

Initially, EDTA was used as the leveling agent. EDTA is commercially available in high purity and has a similar molecular structure to F-HXTA so seemed to be the most obvious choice. However after several trials it was determined that EDTA would not sufficiently differentiate the different metal species. The concentration of the $[Mg(EDTA)]^{2-}$ complex was still too low to calculate the equilibrium constants of interest. The next leveling agent tested was nitrilotriacetic acid (NTA). As was the case with EDTA, the formation constants (β) of the metals of interest with NTA are well established and thus reliably accurate.[4] After preliminary trials with NTA, we found that the equilibrium values were close enough that they could be simultaneously calculated with ^{19}F-NMR. It was settled that NTA would be an effective leveling agent to allow us to observe the equilibria.

The two ligands partition the stronger binding metal which shifts the equilibrium constants towards 1 so the constant becomes measurable for our experiment. The amount of NTA needed to satisfy this equilibrium shift had to be more than the amount of the high affinity metal not complexed to HXTA, so that there were measurable amounts of both M^a(NTA) and M^b(NTA) present in equations 10-12 (See Appendix B Tables 1, 5 and 9). It is assumed that the remainder of the high affinity metal not bound to F-HXTA is bound to NTA and the remainder of the NTA binds the low affinity metal.

The mixture of Zn^{II}/Mg^{II} will be used for the following example: The concentrations of all F-HXTA complexes are measured by ^{19}F-NMR. The amount of the Zn(NTA) complex is known because the remaining Zn^{II} not bound to F-HXTA is assumed to preferentially complex with NTA because $\beta_{ZnNTA} >> \beta_{MgNTA}$ and $[NTA]_{total} > [Zn]_{free}$, where $[Zn]_{free}$ is the concentration of Zn not bound to F-HXTA. Since the total amount of Zn^{II} added to the mixture is known, the amount of Zn(NTA) can be calculated by subtracting the F-HXTA bound Zn^{II} concentration from the total Zn^{II} added. The amount of total NTA added was also known, so the Mg(NTA) concentration could also be found by subtracting the Zn(NTA) concentration from the total NTA concentration. It is assumed that all NTA is bound because of the high formation constants with each of the metals being used (equations 13-15). With these concentrations known, it is possible to calculate $K_{1\text{-}3}$'.

(10) $M^a{}_2(HXTA) + 2M^b(NTA) \overset{K_1'}{\rightleftharpoons} M^b{}_2(HXTA) + 2M^a(NTA)$

(11) $M^a{}_2(HXTA) + M^b(NTA) \overset{K_2'}{\rightleftharpoons} M^bM^a(HXTA) + M^a(NTA)$

(12) $M^bM^a(HXTA) + M^b(NTA) \overset{K_3'}{\rightleftharpoons} M^b{}_2(HXTA) + M^a(NTA)$

Addition of NTA allowed us to measure equilibrium constants for F-HXTA competition with M(NTA) (Eqs 10-12) *via* the ^{19}F-NMR technique described above; however, the equilibria that we are interested in are between F-HXTA with the free metals, not metal-NTA complexes. In order to convert the measured equilibrium values ($K_{1\text{-}3}$') containing NTA in the equilibrium back to $K_{1\text{-}3}$ which contain free metal ions, we can use the known formation constants (β) between each metal and NTA. Equations 13-15 illustrates each of these equilibria.[4] Again these values are reported on the logarithmic scale.

(13) $Zn^{2+} + NTA^{3-} \overset{\log(\beta)=10.67}{\rightleftharpoons} ZnNTA^-$

(14) $Mg^{2+} + NTA^{3-} \overset{\log(\beta)=5.41}{\rightleftharpoons} MgNTA^-$

(15) $Fe^{2+} + NTA^{3-} \overset{\log(\beta)=8.83}{\rightleftharpoons} FeNTA^-$

The known values of β_{ZnNTA} and β_{MgNTA} were used to convert K' into K, which is shown in equations 16-18. By doing this conversion it gives us a way to measure the exchange equilibrium concentrations via ^{19}F-NMR and using the leveling agent NTA.

$$(16)\quad K_1 = \frac{K_1' * (\beta_{ZnNTA})^2}{(\beta_{MgNTA})^2}$$

$$(17)\quad K_2 = \frac{K_2' * (\beta_{ZnNTA})}{(\beta_{MgNTA})}$$

$$(18)\quad K_3 = \frac{K_3' * (\beta_{ZnNTA})}{(\beta_{MgNTA})}$$

3.3 Results from the Metal Exchange Experiments

The metal exchange experiment was performed by preparing solutions of Na_2H_3(F-HXTA) with four total equivalents of two metals in different ratios from stock solutions of $Zn(ClO_4)_2$, $Mg(ClO_4)_2$ and $Fe(ClO_4)_2$. These mixtures were buffered at pH 7.5 with *N*-methylmorpholine and ^{19}F-NMR data was taken using 4-fluorophenol as an internal standard to measure the concentrations of M_2(F-HXTA) complexes. By using the measured concentrations of bimetallic F-HXTA complexes, it is possible to calculate the free metal and M(NTA) complex concentrations. The net ionic strength of each mixture was maintained at 0.106 M, 0.110 M and 0.033 M for the Fe/Mg, Zn/Mg, and Zn/Fe mixtures respectively. The ionic strength of the Zn/Fe mixture is about 3 times lower than the other two mixtures, which is due to this metal pair being significantly less soluble

than the others. It would not be possible to obtain accurate concentrations of each species via ^{19}F-NMR with a significant amount of precipitate in the NMR tube. The precipitate problem was solved by decreasing the concentrations of each species in the mixture by a factor of 3. The concentration of each metal-(F-HXTA) complex is therefore much lower for this combination than the other two involving Mg.

Another obstacle that was encountered during the experimentation was the paramagnetic metal ion Fe^{2+} in the NMR. Paramagnetism broadens the peaks of each of the metal-(F-HXTA) complexes turning them from a triplet to singlet, which is apparent in Figures 9-36 in Appendix C. In addition to peak broadening, the paramagnetic Fe_2(F-HXTA) peak in the ^{19}F-NMR was shifted significantly more downfield than the homobimetallic species of Mg and Zn. The heterobimetallic species involving the Fe as expected showed up in between the two homobimetallic peaks. These spectra can be seen in Figures 9-36 in Appendix C.

There are two spectra per experiment for Fe^{II}/Zn^{II} and Fe^{II}/Mg^{II} experiments because the peaks are so significantly spaced out that a 90° pulse could note be calibrated for all peaks in a spectrum. When the transmitter offset (TOF) is centered between two distant signals in a given NMR spectrum it is possible to get an accurate 90° pulse width for each. It was determined that two spectra would be sufficient to properly integrate every species peak compared to the internal standard in a given experiment. Both spectra were done in separate trials, with their own pulse widths calibrated and TOF measured to account for the large space between peaks. TOF_1 is between the Fe_2(F-HXTA) peak and

the close clusters of diamagnetic peaks and TOF_2 is between FeM(F-HXTA) and the diamagnetic peaks (M=Mg or Zn).

It was found that there was a relative enhanced stability of each of the heterobimetallic species as observed previously. This means that although both site 1 and site 2 of the F-HXTA ligand are equivalent, the replacement of two atoms of the same metal with two atoms of another metal are not equivalent. This inequality is apparent because in none of the metal combinations does $K_2=K_3$. Physically, if $K_2=K_3$ were true it would mean that the replacement of the first metal creating a heterobimetallic species (equation 24) would be thermodynamically equivalent to replacement of the second metal creating the second homobimetallic species equation 25. Thermodynamic equivalence would be the case if the two sites were completely isolated from each other rather than share the bridging oxygen atom. Equations 19-22 summarize the enhanced stability of each of the metal combinations, including Fe and Mn from previous works.[1]

(19) $Zn_2HXTA + Mg_2HXTA \underset{}{\overset{K_{ex}=5.59(0.09)}{\rightleftharpoons}} 2\ ZnMgHXTA$

(20) $Zn_2HXTA + Fe_2HXTA \underset{}{\overset{K_{ex}=4.4(0.3)}{\rightleftharpoons}} 2\ ZnFeHXTA$

(21) $Fe_2HXTA + Mg_2HXTA \underset{}{\overset{K_{ex}=4.15(0.07)}{\rightleftharpoons}} 2\ FeMgHXTA$

(22) $Fe_2HXTA + Mn_2HXTA \underset{}{\overset{K_{ex}=2.2(0.3)}{\rightleftharpoons}} 2\ FeMnHXTA$

(23) $M^b{}_2(HXTA) + 2M^a(aq) \underset{}{\overset{K_1}{\rightleftharpoons}} M^a{}_2(HXTA) + 2M^b(aq)$

(24) $M^a{}_2(HXTA) + M^b(aq) \overset{K_2}{\rightleftharpoons} M^bM^a(HXTA) + M^a(aq)$

(25) $M^bM^a(HXTA) + M^b(aq) \overset{K_3}{\rightleftharpoons} M^b{}_2(HXTA) + M^a(aq)$

Each one of the equilibrium values for equations 19-22 are equivalent to $\frac{K_2}{K_3}$. We denote this constant K exchange (K_{ex}) so therefore: $K_{ex} = \frac{K_2}{K_3}$. Table 3 gives the different metal combination $K_{1\text{-}3}$ values as well as their respective K_{ex}, they are all larger than 1 indicating that the heterobimetallic species are more stable. The individual stability constants $\beta_{1\text{-}3}$ must be large because there are no clear M^{II} (F-HXTA) mononucleated ligands present in this mixture. An interesting observation was that the K_{ex} of each of the new metal combinations were greater than the K_{ex} of Fe/Mn, the metals present in the original study of the protein RNR class 1c. The greater K_{ex} for the non-protein metal mixtures indicates that the heterobimetallic species of the new metal combinations are even more relatively stable compared to the original mixture.

Table 3: Comprehensive summary of average $K_{1\text{-}3}$ and K_{ex} values with uncertainties, where $K_{ex}=K_2/K_3$, for each metal ion pair

M^a	M^b	K_1	K_2	K_3	K_{ex}
Mg(II)	Zn(II)	$(1.4\pm0.8)*10^{11}$	$(8\pm2)*10^5$	$(1.5\pm0.4)*10^5$	5.59(0.09)
Fe(II)	Zn(II)	$(7\pm4)*10^2$	50(20)	11(5)	4.4(0.3)
Mg(II)	Fe(II)	$(2.6\pm0.8)*10^7$	$(1.0\pm0.2)*10^4$	$(2.5\pm0.4)*10^3$	4.15(0.07)
Mn(II)	Fe(II)	182(13)	20.1 (1.3)	9.1 (1.1)	2.2(0.3)

The speciation of each mixture as a function of the ratios of the metal species in the presence of the leveling agent NTA are shown in Figures 9-11. The curves are the theoretical models of the speciation done in the program HySS while the points along each of the curves are the experimental values recorded from the NMR experiments. Remarkably, at the point where the homobimetallic species are equal, the heterobimetallic species concentration is considerably greater in the mixture which indicates an enhanced stability of this mixed species. If the replacement of the two metals were equivalent thermodynamically, then all three of the curves would intersect at that point. The observation that the heterobimetallic peak at the intersection of the two homobimetallic curves is higher was consistent through each of the mixtures as shown below in the speciation charts shown in Figures 9-11. The mixture containing Zn and Fe in Figure 11 has a noticeably larger deviation from the predicted trend lines than the other two mixtures. This is due to the lower concentration of all reacting species compared to the other two mixtures.

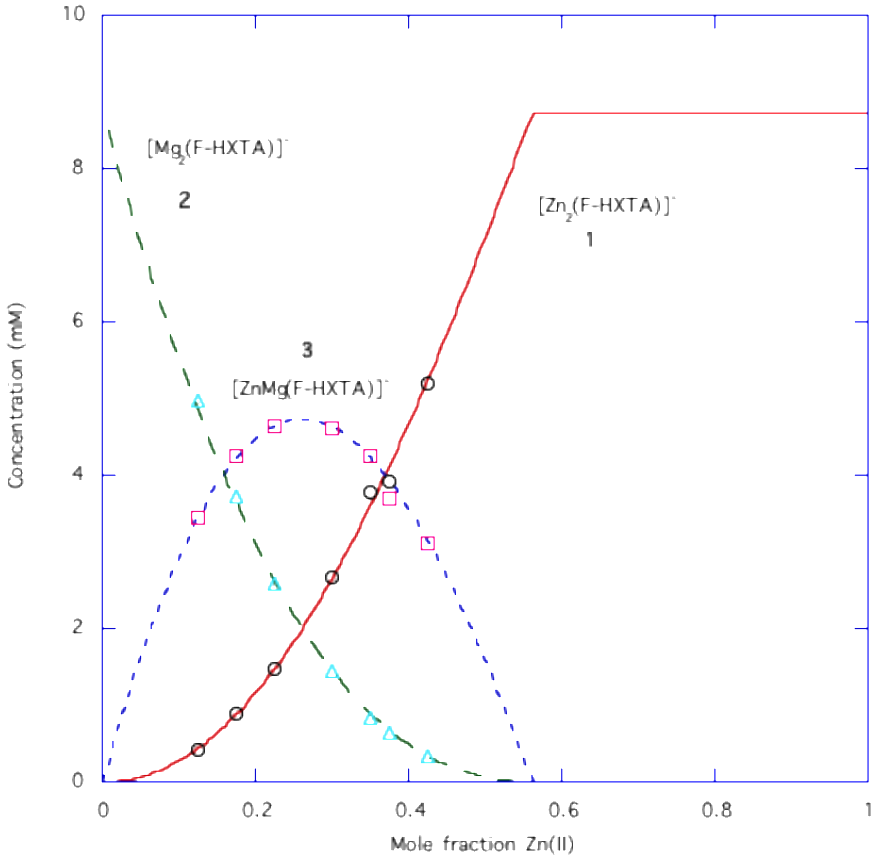

Figure 9: concentrations of Mg_2HXTA, Zn_2HXTA and ZnMgHXTA as a function of Mg^{II}/Zn^{II} ratio. [F-HXTA]=8.73 mM; $[M(ClO_4)_2]$total=40.1 mM; pH=7.61 [NTA]=5 mM; [4-fluorophenol]= 4.99 mM; Ionic strength= 0.110 at 25°C.

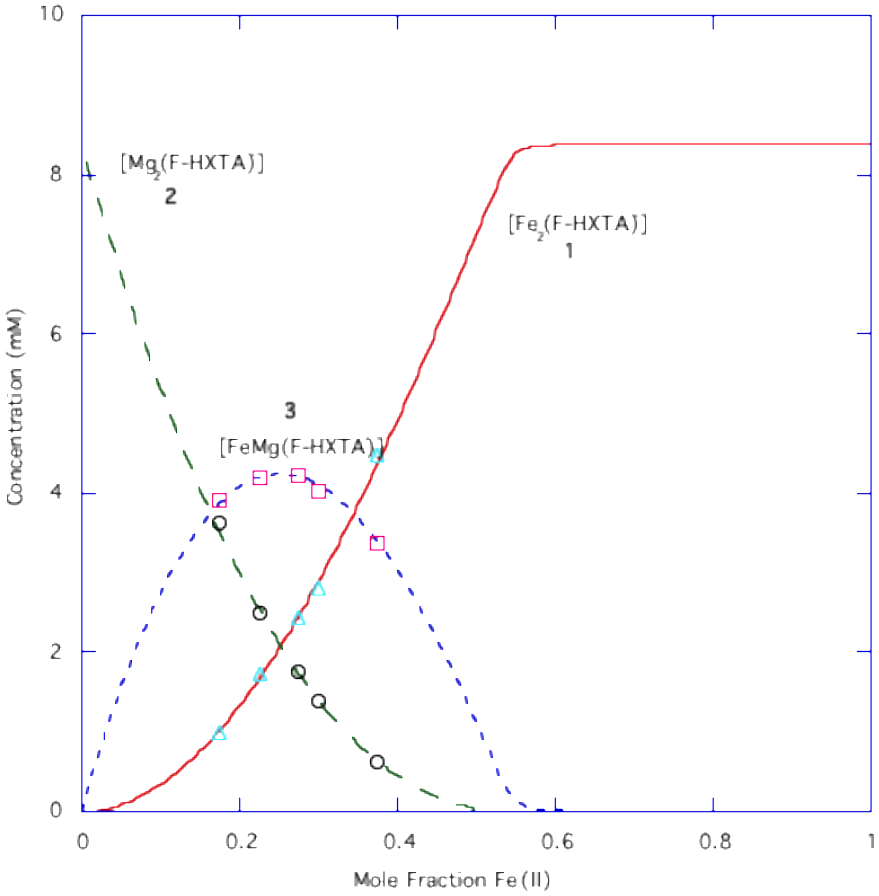

Figure 10: concentrations of Fe_2HXTA, Mg_2HXTA and FeMgHXTA as a function of Mg^{II}/Fe^{II} ratio. [F-HXTA]=8.40 mM; $[M(ClO_4)_2]$total=40.0 mM; pH=7.50 [NTA]=5 mM; [4-fluorophenol]= 4.99 mM; Ionic strength= 0.106 at 25°C.

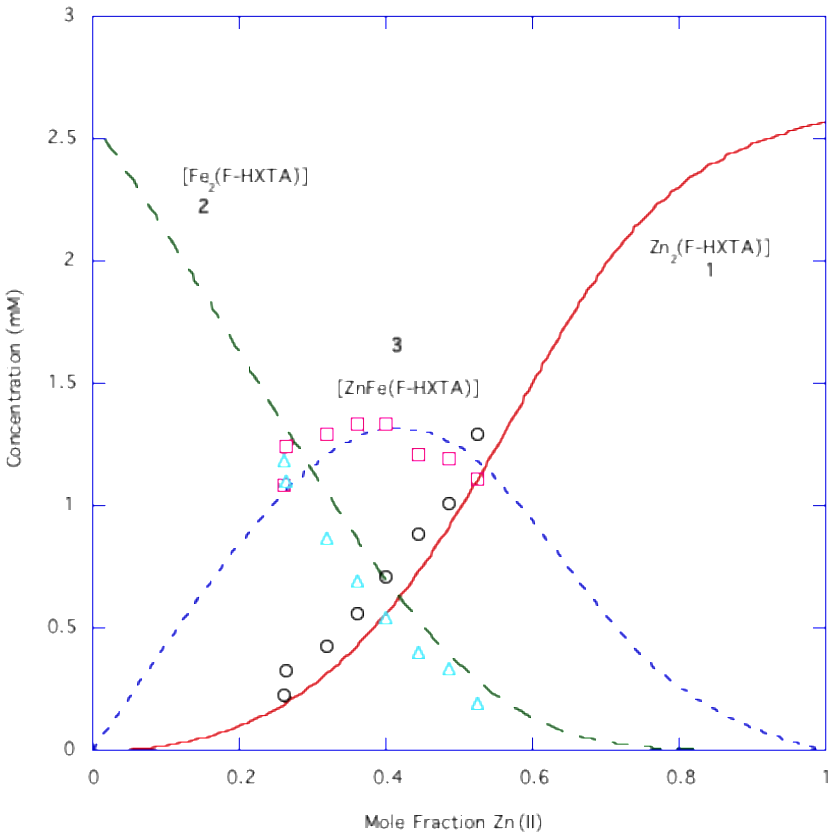

Figure 11: concentrations of Fe_2HXTA, Zn_2HXTA and ZnFeHXTA as a function of Fe^{II}/Zn^{II} ratio. [F-HXTA]=2.57 mM; [$M(ClO_4)_2$]total=12.0 mM; pH=7.01 [NTA]=3.01 mM; [4-fluorophenol]= 1.50 mM; Ionic strength= 0.033 at 25°C.

The major result of these experiments was the enhanced stability of the heterobimetallic species, and not just in the Fe/Mn mixture but in all of the metal mixtures. The result indicates that the factor causing the observed relative enhanced stability is not dependent on the metals in the binding sites but rather the binding site of F-HXTA itself. The next step of this study is now to synthesize a new model ligand that has a slightly different binding site than F-HXTA perhaps with two isolated metal sites to see if the replacements are now equivalent. Or the binding site could be made asymmetrical to see how this effects the exchange experiments.

3.4 References

---

[1] Kerber, W. D.; Goheen, J. T.; Perez, K. A.; Siegler, M. A. *Inorganic Chemistry* **2015**, *55*(2), 848-857.

[2] Addison, A. W.; Rao, N. T.; Reedijk, J.; van Rijn, J.; Verschoor, G. C. J. Chem. Soc. Dalton Trans., 1984, 1349-1356.

[3] Anderegg, G. *Critical evaluation of equilibrium constants in solution*; Pergamon: Oxford, 1977.

[4] Schwarzenbach, G.; Anderegg, G.; Schneider, W.; Senn, H. *Helvetica*, **1955**, 1147-1170

Appendix A: Crystal Structure of $[Zn(H_2O)_6][1]_2 \cdot 10H_2O$ and $[Mg(H_2O)_6][2]_2 \cdot 14H_2O$

$[Zn(H_2O)_6][1]_2 \cdot 10H_2O$

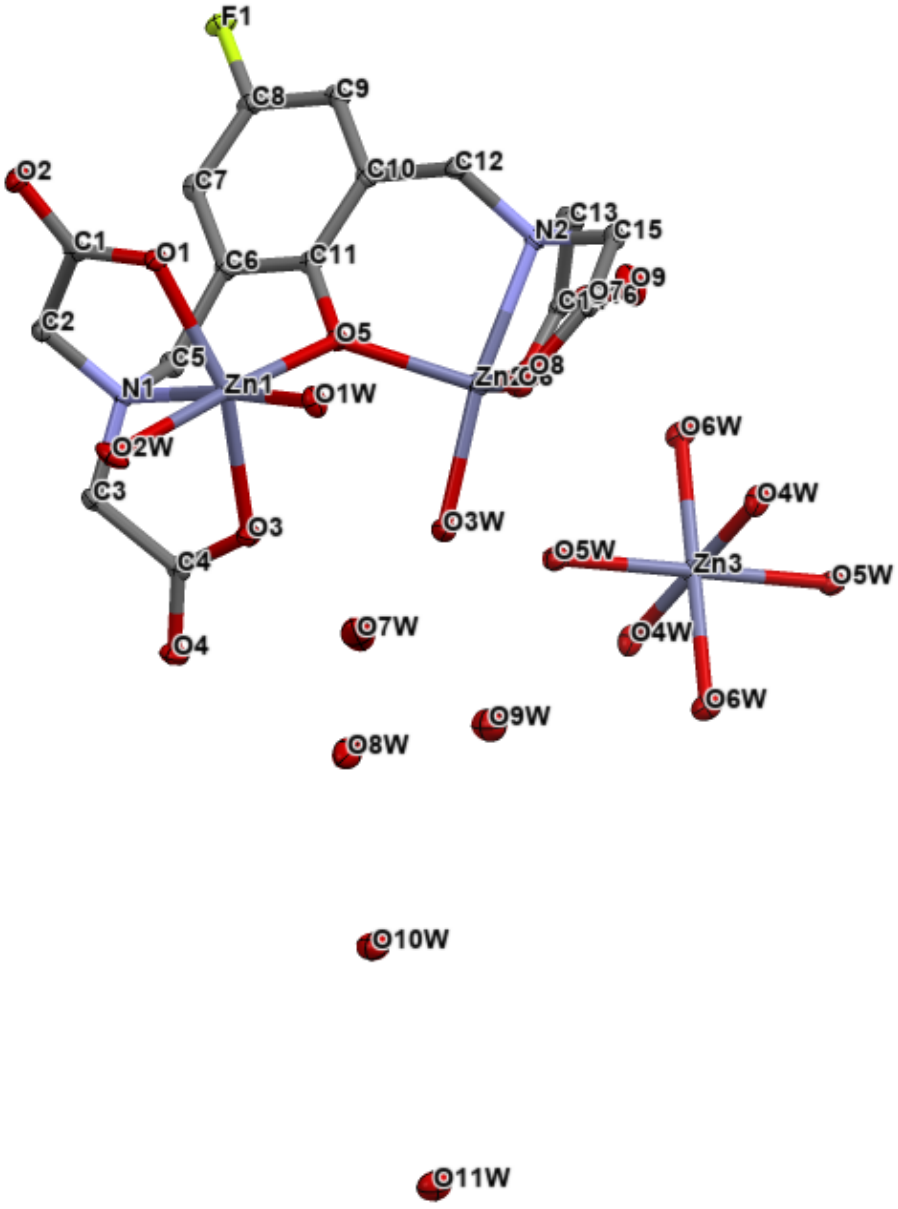

Bond Lengths (Å):

Zn(1) –O(1)W……2.0257(12)
Zn(1)-O(1)……..2.0653(11)
Zn(1)-O(5)……..2.0755(11)
Zn(1)-O(3)……..2.1002(12)
Zn(1)-N(1)……..2.1504(13)
Zn(1)-O(2)W……..2.2029(12)
Zn(2)-O(5)……..2.0035(11)
Zn(2)-O(8)……..2.0235(12)
Zn(2)-O(3)W……..2.0338(12)
Zn(2)-O(6)……..2.0442(12)
Zn(2)-N(2)……..2.1588(14)
C(1)-O(2)……1.2532(19)
C(1)-O(1)……1.2715(19)
C(1)-C(2)……1.521(2)
C(2)-N(1)……1.473(2)
C(2)-H(2)A……0.9900
C(2)-H(2)B……0.9900
C(3)-N(1)……1.474(2)
C(3)-C(4)……1.527(2)
C(3)-H(3)A……0.9900
C(3)-H(3)B……0.9900
C(4)-O(4)……1.239(2)
C(4)-O(3)……1.280(2)
C(5)-N(1)……1.486(2)
C(5)-C(6)……1.506(2)
C(5)-H(5)A……0.9900
C(5)-H(5)B……0.9900
C(6)-C(7)……1.399(2)
C(6)-C(11)……..1.403(2)
C(7)-C(8)……1.379(2)
C(7)-H(7)……0.9500
C(8)-F(1)……1.3663(18)
C(8)-C(9)……1.375(2)
C(9)-C(10)……..1.396(2)
C(9)-H(9)……0.9500
C(10)-C(11)……1.404(2)
C(10)-C(12)……1.504(2)
C(11)-O(5)……..1.3574(19)
C(12)-N(2)……..1.493(2)
C(12)-H(12)A……0.9900
C(12)-H(12)B……0.9900
C(13)-N(2)……..1.473(2)
C(13)-C(14)……1.520(2)
C(13)-H(13)A……0.9900
C(13)-H(13)B……0.9900
C(14)-O(7)……..1.250(2)
C(14)-O(6)……..1.271(2)
C(15)-N(2)……...1.473(2)
C(15)-C(16)……1.527(2)
C(15)-H(15)A……..0.9900
C(15)-H(15)B……..0.9900
C(16)-O(9)……...1.247(2)
C(16)-O(8)……...1.270(2)
O(1)W-H(1)W(1)…….0.846(18)
O(1)W-H(1)W(2)…….0.827(18)
O(2)W-H(2)W(1)…….0.785(18)
O(2)W-H(2)W(2)…….0.828(18)
O(3)W-H(3)W(1)…….0.819(18)
O(3)W-H(3)W(2)…….0.822(18)
Zn(3)-O(6)W……2.0714(12)
Zn(3)-O(6)W……2.0714(12)
Zn(3)-O(5)W……2.0923(12)
Zn(3)-O(5)W……2.0924(12)
Zn(3)-O(4)W……2.1062(13)
Zn(3)-O(4)W……2.1062(13)
O(4)W-H(4)W(1)…….0.828(18)
O(4)W-H(4)W(2)…….0.802(18)
O(5)W-H(5)W(1)…….0.811(18)
O(5)W-H(5)W(2)…….0.818(18)
O(6)W-H(6)W(1)…….0.801(18)
O(6)W-H(6)W(2)…….0.827(18)
O(7)W-H(7)W(1)…….0.827(19)
O(7)W-H(7)W(2)…….0.81(2)
O(8)W-H(8)W(1)…….0.841(19)
O(8)W-H(8)W(2)…….0.815(19)
O(9)W-H(9)W(1)…….0.869(19)
O(9)W-H(9)W(2)…….0.803(19)
O(10)W-H(101)……....0.831(18)
O(10)W-H(102)……0.819(18)
O(11)W-H(111) ……...0.809(19)
O(11)W-H(112)……....0.812(18)

Bond Angles (°):

O(1)W-Zn(1)-O(1)……101.82(5)
O(1)W-Zn(1)-O(5)……93.81(5)
O(1)-Zn(1)-O(5)……97.81(4)
O(1)W-Zn(1)-O(3)……97.08(5)
O(1)-Zn(1)-O(3)……158.61(4)
O(5)-Zn(1)-O(3)……90.78(4)
O(1)W-Zn(1)-N(1)……172.85(5)
O(1)-Zn(1)-N(1)……80.94(5)
O(5)-Zn(1)-N(1)……92.33(5)
O(3)-Zn(1)-N(1)……79.16(5)
O(1)W-Zn(1)-O(2)W……85.29(5)
O(1)-Zn(1)-O(2)W……85.44(5)
O(5)-Zn(1)-O(2)W……176.74(5)
O(3)-Zn(1)-O(2)W……86.22(5)
N(1)-Zn(1)-O(2)W……88.37(5)
O(5)-Zn(2)-O(8)……103.61(5)
O(5)-Zn(2)-O(3)W……95.17(5)
O(8)-Zn(2)-O(3)W……101.08(5)
O(5)-Zn(2)-O(6)……109.78(5)
O(8)-Zn(2)-O(6)……142.93(5)
O(3)W-Zn(2)-O(6)……91.66(5)
O(5)-Zn(2)-N(2)……93.78(5)
O(8)-Zn(2)-N(2)……81.46(5)
O(3)W-Zn(2)-N(2)……169.82(5)
O(6)-Zn(2)-N(2)……80.74(5)
O(2)-C(1)-O(1)……123.45(16)
O(2)-C(1)-C(2)……117.54(14)
O(1)-C(1)-C(2)……118.93(14)
N(1)-C(2)-C(1)……112.64(13)
N(1)-C(2)-H(2)A……109.1
C(1)-C(2)-H(2)A……109.1
N(1)-C(2)-H(2)B……109.1
C(1)-C(2)-H(2)B……109.1
H(2)A-C(2)-H(2)B……107.8
N(1)-C(3)-C(4)……111.28(13)
N(1)-C(3)-H(3)A……109.4
C(4)-C(3)-H(3)A……109.4
N(1)-C(3)-H(3)B……109.4
C(4)-C(3)-H(3)B……109.4
H(3)A-C(3)-H(3)B……108.0
O(4)-C(4)-O(3)……123.87(15)
O(4)-C(4)-C(3)……118.08(15)
O(3)-C(4)-C(3)……118.04(14)
N(1)-C(5)-C(6)……114.65(13)
N(1)-C(5)-H(5)A……108.6
C(6)-C(5)-H(5)A……108.6
N(1)-C(5)-H(5)B……108.6
C(6)-C(5)-H(5)B……108.6
H(5)A-C(5)-H(5)B……107.6
C(7)-C(6)-C(11)……119.92(15)
C(7)-C(6)-C(5)……120.77(15)
C(11)-C(6)-C(5)……119.12(14)
C(8)-C(7)-C(6)……118.60(15)
C(8)-C(7)-H(7)……120.7
C(6)-C(7)-H(7)……120.7
F(1)-C(8)-C(9)……118.61(15)
F(1)-C(8)-C(7)……118.60(15)
C(9)-C(8)-C(7)……122.79(15)
C(8)-C(9)-C(10)……119.06(15)
C(8)-C(9)-H(9)……120.5
C(10)-C(9)-H(9)……120.5
C(9)-C(10)-C(11)……119.65(15)
C(9)-C(10)-C(12)……120.39(15)
C(11)-C(10)-C(12)……119.91(14)
O(5)-C(11)-C(6)……119.44(14)
O(5)-C(11)-C(10)……120.62(15)
C(6)-C(11)-C(10)……119.94(15)
N(2)-C(12)-C(10)……112.19(13)
N(2)-C(12)-H(12A)……109.2
C(10)-C(12)-H(12A)……109.2
N(2)-C(12)-H(12B)……109.2
C(10)-C(12)-H(12B)……109.2
H(12A)-C(12)-H(12B)……107.9
N(2)-C(13)-C(14)……113.11(13)
N(2)-C(13)-H(13A)……109.0
C(14)-C(13)-H(13A)……109.0
N(2)-C(13)-H(13B)……109.0
C(14)-C(13)-H(13B)……109.0
H(13A)-C(13)-H(13B)……107.8
O(7)-C(14)-O(6)……124.24(16)
O(7)-C(14)-C(13)……116.84(14)
O(6)-C(14)-C(13)……118.91(14)
N(2)-C(15)-C(16)……111.45(13)
N(2)-C(15)-H(15A)……109.3
C(16)-C(15)-H(15A)……109.3
N(2)-C(15)-H(15B)……109.3
C(16)-C(15)-H(15B)……109.3
H(15A)-C(15)-H(15B)……108.0
O(9)-C(16)-O(8)……123.48(16)
O(9)-C(16)-C(15)……118.27(16)
O(8)-C(16)-C(15)……118.23(15)
C(2)-N(1)-C(3)……114.72(12)
C(2)-N(1)-C(5)……111.81(12)
C(3)-N(1)-C(5)……108.10(12)
C(2)-N(1)-Zn(1)……106.13(10)
C(3)-N(1)-Zn(1)……106.47(9)
C(5)-N(1)-Zn(1)……109.38(9)
C(13)-N(2)-C(15)……113.29(13)
C(13)-N(2)-C(12)……112.07(13)
C(15)-N(2)-C(12)……109.64(13)
C(13)-N(2)-Zn(2)……109.56(10)
C(15)-N(2)-Zn(2)……103.51(10)

C(12)-N(2)-Zn(2)……108.33(10)
C(1)-O(1)-Zn(1)……..114.73(10)
C(4)-O(3)-Zn(1)……..114.67(10)
C(11)-O(5)-Zn(2)……116.83(9)
C(11)-O(5)-Zn(1)……113.82(9)
Zn(2)-O(5)-Zn(1)……129.31(5)
C(14)-O(6)-Zn(2)……117.62(11)
C(16)-O(8)-Zn(2)……114.81(11)
Zn(1)-O(1)W-H(1)W(1)……..117.5(14)
Zn(1)-O(1)W-H(1)W(2)……..125.5(15)
H(1)W(1)-O(1)W-H(1)W(2)……...104.7(19)
Zn(1)-O(2)W-H(2)W(1)……..126.3(16)
Zn(1)-O(2)W-H(2)W(2)……..118.8(15)
H(2)W(1)-O(2)W-H(2)W(2)……...111(2)
Zn(2)-O(3)W-H(3)W(1)……..127.4(15)
Zn(2)-O(3)W-H(3)W(2)……..114.0(15)
H(3)W(1)-O(3)W-H(3)W(2)……...107.6(19)
O(6)W-Zn(3)-O(6)W……...180.0
O(6)W-Zn(3)-O(5)W……...92.24(5)
O(6)W-Zn(3)-O(5)W……...87.76(5)
O(6)W-Zn(3)-O(5)W……...87.76(5)
O(6)W-Zn(3)-O(5)W……...92.24(5)
O(5)W-Zn(3)-O(5)W……..180.00(8)
O(6)W-Zn(3)-O(4)W……...91.69(5)
O(6)W-Zn(3)-O(4)W……...88.31(5)
O(5)W-Zn(3)-O(4)W……...90.73(5)
O(5)W-Zn(3)-O(4)W……...89.27(5)
O(6)W-Zn(3)-O(4)W……...88.31(5)
O(6)W-Zn(3)-O(4)W……...91.69(5)
O(5)W-Zn(3)-O(4)W……...89.27(5)
O(5)W-Zn(3)-O(4)W……...90.73(5)
O(4)W-Zn(3)-O(4)W……..180.0
Zn(3)-O(4)W-H(4)W(1)……..117.5(15)
Zn(3)-O(4)W-H(4)W(2)……..118.6(16)
H(4)W(1)-O(4)W-H(4)W(2)……...105(2)
Zn(3)-O(5)W-H(5)W(1)……..119.5(15)
Zn(3)-O(5)W-H(5)W(2)……..116.4(15)
H(5)W(1)-O(5)W-H(5)W(2)……...108(2)
Zn(3)-O(6)W-H(6)W(1)……..115.6(15)
Zn(3)-O(6)W-H(6)W(2)……..114.6(15)
H(6)W(1)-O(6)W-H(6)W(2)……...108.9(19)
H(7)W(1)-O(7)W-H(7)W(2)……...109(2)
H(8)W(1)-O(8)W-H(8)W(2)……...107(2)
H(9)W(1)-O(9)W-H(9)W(2)……...106(2)
H(101)-O(10)W-H(102)……..103.2(19)
H(111)-O(11)W-H(112)……..108(2)

Torsion Angles (°):

O(2)-C(1)-C(2)-N(1)……..166.80(13)
O(1)-C(1)-C(2)-N(1)……..-16.5(2)
N(1)-C(3)-C(4)-O(4)……..-161.42(14)
N(1)-C(3)-C(4)-O(3)……...19.8(2)
N(1)-C(5)-C(6)-C(7)……...-115.75(17)
N(1)-C(5)-C(6)-C(11)…….69.18(19)
C(11)-C(6)-C(7)-C(8)…….1.3(2)
C(5)-C(6)-C(7)-C(8)……...-173.73(15)
C(6)-C(7)-C(8)-F(1)…….-179.12(14)
C(6)-C(7)-C(8)-C(9)……...0.5(3)
F(1)-C(8)-C(9)-C(10)…….177.70(14)
C(7)-C(8)-C(9)-C(10)…….-2.0(3)
C(8)-C(9)-C(10)-C(11)……...1.5(2)
C(8)-C(9)-C(10)-C(12)……...-175.80(15)
C(7)-C(6)-C(11)-O(5)…….177.79(15)
C(5)-C(6)-C(11)-O(5)…….-7.1(2)
C(7)-C(6)-C(11)-C(10)……...-1.7(2)
C(5)-C(6)-C(11)-C(10)……...173.40(15)
C(9)-C(10)-C(11)-O(5)……...-179.21(15)
C(12)-C(10)-C(11)-O(5)…….-1.9(2)
C(9)-C(10)-C(11)-C(6)……...0.3(2)
C(12)-C(10)-C(11)-C(6)…….177.61(15)
C(9)-C(10)-C(12)-N(2)……...-117.05(16)
C(11)-C(10)-C(12)-N(2)…….65.65(19)
N(2)-C(13)-C(14)-O(7)……...-178.29(14)
N(2)-C(13)-C(14)-O(6)……...2.8(2)
N(2)-C(15)-C(16)-O(9)……...-156.40(15)
N(2)-C(15)-C(16)-O(8)……...24.8(2)
C(1)-C(2)-N(1)-C(3)……...143.33(13)
C(1)-C(2)-N(1)-C(5)……-93.12(15)
C(1)-C(2)-N(1)-Zn(1)……...26.07(14)
C(4)-C(3)-N(1)-C(2)…….-149.65(13)
C(4)-C(3)-N(1)-C(5)…….84.84(15)
C(4)-C(3)-N(1)-Zn(1)……...-32.59(15)
C(6)-C(5)-N(1)-C(2)…….65.35(17)
C(6)-C(5)-N(1)-C(3)…….-167.44(13)
C(6)-C(5)-N(1)-Zn(1)……-51.90(15)
C(14)-C(13)-N(2)-C(15)……...113.39(16)
C(14)-C(13)-N(2)-C(12)……. -121.90(15)
C(14)-C(13)-N(2)-Zn(2)……...-1.62(16)
C(16)-C(15)-N(2)-C(13)……...-151.78(14)
C(16)-C(15)-N(2)-C(12)……...82.21(16)
C(16)-C(15)-N(2)-Zn(2)……...-33.21(15)
C(10)-C(12)-N(2)-C(13)……...61.35(17)
C(10)-C(12)-N(2)-C(15)……...-171.95(13)
C(10)-C(12)-N(2)-Zn(2)……-59.64(14)
O(2)-C(1)-O(1)-Zn(1)……172.68(12)
C(2)-C(1)-O(1)-Zn(1)……-3.77(17)
O(4)-C(4)-O(3)-Zn(1)……-173.49(12)
C(3)-C(4)-O(3)-Zn(1)……5.16(17)
C(6)-C(11)-O(5)-Zn(2)……..130.13(13)
C(10)-C(11)-O(5)-Zn(2)……-50.37(18)
C(6)-C(11)-O(5)-Zn(1)……..-51.88(17)
C(10)-C(11)-O(5)-Zn(1)……127.63(13)
O(7)-C(14)-O(6)-Zn(2)……..178.62(12)
C(13)-C(14)-O(6)-Zn(2)……-2.60(19)
O(9)-C(16)-O(8)-Zn(2)……..-178.67(13)
C(15)-C(16)-O(8)-Zn(2)…….0.07(18)

$[Mg(H_2O)_6][2]_2 \cdot 14H_2O$

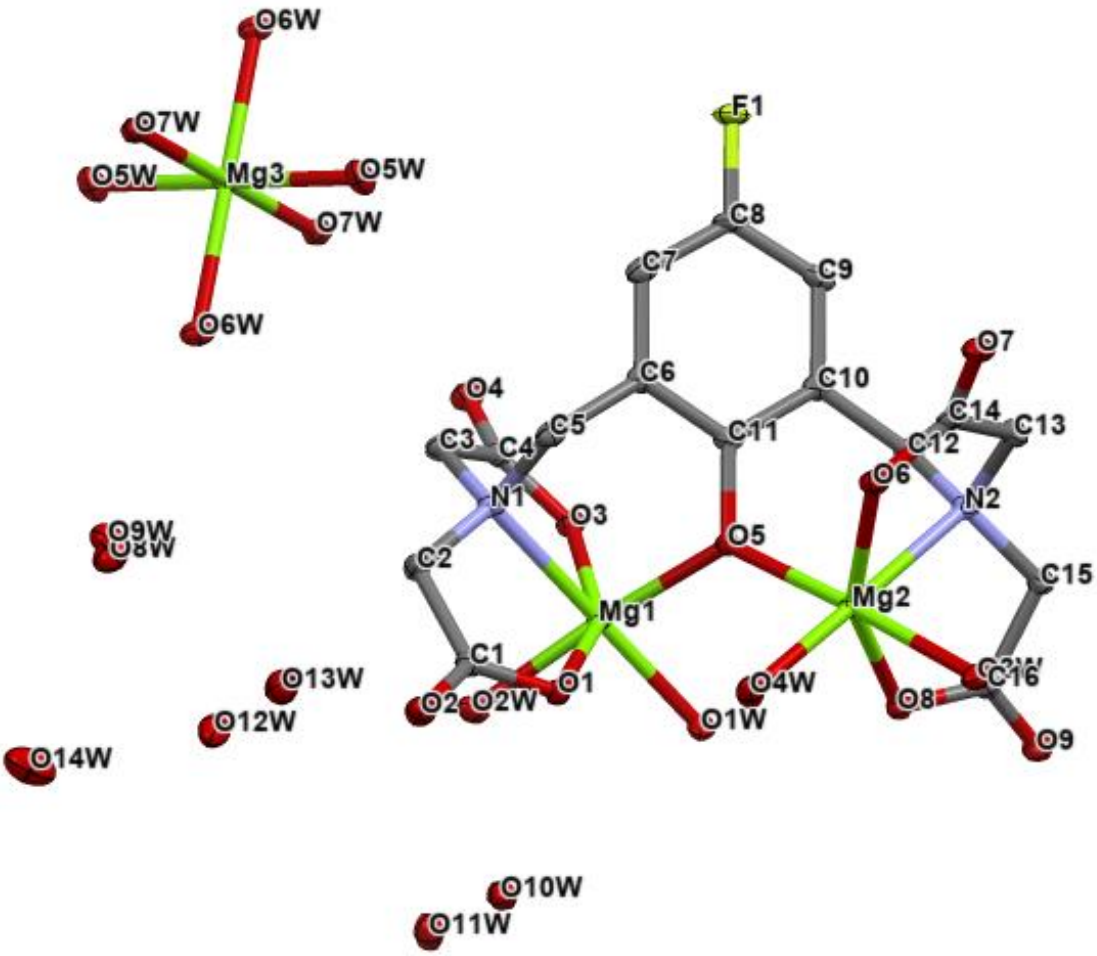

Bond Lengths (Å):

Mg(1)-O(1)W	2.0175(11)
Mg(1)-O(3)	2.0674(11)
Mg(1)-O(5)	2.0761(10)
Mg(1)-O(2)W	2.1119(11)
Mg(1)-O(1)	2.1345(11)
Mg(1)-N(1)	2.2042(12)
O(1)W-H(1)W(1)	0.864(19)
O(1)W-H(1)W(2)	0.807(19)
O(2)W-H(2)W(1)	0.844(19)
O(2)W-H(2)W(2)	0.833(19)
Mg(2)-O(4)W	2.0127(11)
Mg(2)-O(6)	2.0528(10)
Mg(2)-O(5)	2.0724(10)
Mg(2)-O(8)	2.0928(11)
Mg(2)-O(3)W	2.1179(11)
Mg(2)-N(2)	2.2156(12)
O(3)W-H(3)W(1)	0.796(19)
O(3)W-H(3)W(2)	0.809(19)
O(4)W-H(4)W(1)	0.844(19)
O(4)W-H(4)W(2)	0.867(19)
C(1)-O(2)	1.2485(18)
C(1)-O(1)	1.2715(17)
C(1)-C(2)	1.5250(18)
C(2)-N(1)	1.4727(17)
C(2)-H(2)A	0.9900
C(2)-H(2)B	0.9900
C(3)-N(1)	1.4739(17)
C(3)-C(4)	1.5281(19)
C(3)-H(3)A	0.9900
C(3)-H(3)B	0.9900
C(4)-O(4)	1.2503(18)
C(4)-O(3)	1.2704(17)
C(5)-N(1)	1.4896(16)
C(5)-C(6)	1.5060(18)
C(5)-H(5)A	0.9900
C(5)-H(5)B	0.9900
C(6)-C(7)	1.394(2)
C(6)-C(11)	1.407(2)
C(7)-C(8)	1.380(2)
C(7)-H(7)	0.9500
C(8)-F(1)	1.3714(16)
C(8)-C(9)	1.376(2)
C(9)-C(10)	1.3977(19)
C(9)-H(9)	0.9500
C(10)-C(11)	1.4068(19)
C(10)-C(12)	1.5040(19)
C(11)-O(5)	1.3467(16)
C(12)-N(2)	1.4831(17)
C(12)-H(12)A	0.9900
C(12)-H(12)B	0.9900
C(13)-N(2)	1.4719(16)
C(13)-C(14)	1.5226(19)
C(13)-H(13)A	0.9900
C(13)-H(13)B	0.9900
C(14)O(7)	1.2505(17)
C(14)-O(6)	1.2708(17)
C(15)-N(2)	1.4734(17)
C(15)-C(16)	1.5258(18)
C(15)-H(15)A	0.9900
C(15)-H(15)B	0.9900
C(16)-O(9)	1.2469(17)
C(16)-O(8)	1.2723(17)
Mg(3)-O(5)W	2.0403(10)
Mg(3)-O(5)W	2.0403(10)
Mg(3)-O(6)W	2.0429(10)
Mg(3)-O(6)W	2.0429(10)
Mg(3)-O(7)W	2.1413(10)
Mg(3)-O(7)W	2.1413(10)
O(5)W-H(5)W(1)	0.828(19)
O(5)W-H(5)W(2)	0.832(19)
O(6)W-H(6)W(1)	0.812(19)
O(6)W-H(6)W(2)	0.881(19)
O(7)W-H(7)W(1)	0.810(19)
O(7)W-H(7)W(2)	0.841(18)
O(8)W-H(8)W(1)	0.88(2)
O(8)W-H(8)W(2)	0.84(2)
O(9)W-H(9)W(1)	0.820(19)
O(9)W-H(9)W(2)	0.856(19)
O(10)W-H(0)W(3)	0.838(19)
O(10)W-H(0)W(4)	0.817(19)
O(11)W-H(1)W(3)	0.83(2)
O(11)W-H(1)W(4)	0.78(2)
O(12)W-H(2)W(3)	0.85(2)
O(12)W-H(2)W(4)	0.82(2)
O(13)W-H(3)W(3)	0.83(2)
O(13)W-H(3)W(4)	0.86(2)
O(14)W-H(4)W(3)	0.84(2)
O(14)W-H(4)W(4)	0.87(2)

Bond Angles (°):

O1W-Mg1-O3……103.29(5)
O(1)W-Mg(1)-O(5)……87.63(4)
O(3)-Mg(1)-O(5)……100.42(4)
O(1)W-Mg(1-O(2)W……..90.12(4)
O(3)-Mg(1)-O(2)W……84.97(4)
O(5)-Mg(1)-O(2)W……174.51(5)
O(1)W-Mg(1)-O(1)……100.84(4)
O(3)-Mg(1)-O(1)……152.97(4)
O(5)-Mg(1)-O(1)……92.54(4)
O(2)W-Mg(1)-O(1)……82.97(4)
O(1)W-Mg(1)-N(1)……177.15(5)
O(3)-Mg(1)-N(1)……79.42(4)
O(5)-Mg(1)-N(1)……91.00(4)
O(2)W-Mg(1)-N(1)……91.04(4)
O(1)-Mg(1)-N(1)……76.72(4)
Mg(1)-O(1)W-H(1)W(1)……122.4(13)
Mg(1)-O(1)W-H(1)W(2)……127.2(14)
H1W1-O1W-H1W2……105.1(18)
Mg(1)-O(2)W-H(2)W(1)……122.8(14)
Mg(1)-O(2)W-H(2)W(2)……128.9(14)
H(2)W(1)-O(2)W-H(2)W(2)……..106.6(19)
O(4)W-Mg(2)-O(6)……99.72(5)
O(4)W-Mg(2)-O(5)……89.48(4)
O(6)-Mg(2)-O(5)……98.34(4)
O(4)W-Mg(2)-O(8)……103.94(5)
O(6)-Mg(2)-O(8)……153.52(4)
O(5)-Mg(2)-O(8)……93.62(4)
O(4)W-Mg(2)-O(3)W……89.19(5)
O(6)-Mg(2)-O(3)W……84.57(4)
O(5)-Mg(2)-O(3)W……176.97(4)
O(8)-Mg(2)-O(3)W……84.06(4)
O(4)W-Mg(2)-N(2)……178.24(5)
O(6)-Mg(2)-N(2)……78.53(4)
O(5)-Mg(2)-N(2)……91.00(4)
O(8)-Mg(2)-N(2)……77.72(4)
O(3)W-Mg(2)-N(2)……...90.42(4)
Mg(2)-O(3)W-H(3)W(1)……127.4(15)
Mg(2)-O(3)W-H(3)W(2)……123.3(14)
H(3)W(1)-O(3)W-H(3)W(2)……109(2)
Mg(2)-O(4)W-H(4)W(1)……128.8(14)
Mg(2)-O(4)W-H(4)W(2)……121.1(14)
H(4)W(1)-O(4)W-H(4)W(2)……104.7(18)
O(2)-C(1)-O(1)……124.69(13)
O(2)-C(1)-C(2)……117.15(12)
O(1)-C(1)-C(2)……118.07(12)
N(1)-C(2)-C(1)……111.43(11)
N(1)-C(2)-H(2)A……109.3
C(1)-C(2)-H(2)A……109.3
N(1)-C(2)-H(2)B……109.3
C(1)-C(2)-H(2)B……109.3
H(2)A-C(2)-H(2)B……108.0
N(1)-C(3)-C(4) ……113.15(11)
N(1)-C(3)-H(3)A……108.9
C(4)-C(3)-H(3)A……108.9
N(1)-C(3)-H(3)B……108.9
C(4)-C(3)-H(3)B……...108.9
H(3)A-C(3)-H(3)B……...107.8
O(4)-C(4)-O(3)……125.48(13)
O(4)-C(4)-C(3)……116.25(12)
O(3)-C(4)-C(3)……118.20(12)
N(1)-C(5)-C(6)……113.68(11)
N(1)-C(5)-H(5)A……108.8
C(6)-C(5)-H(5)A……108.8
N(1)-C(5)-H(5)B……108.8
C(6)-C(5)-H(5)B……108.8
H(5)A-C(5)-H(5)B……107.7
C(7)-C(6)-C(11)……120.17(13)
C(7)-C(6)-C(5)……120.72(12)
C(11)-C(6)-C(5)……118.94(12)
C(8)-C(7)-C(6)……118.86(13)
C(8)-C(7)-H(7)……120.6
C(6)-C(7)-H(7)……120.6
F(1)-C(8)-C(9)……118.73(13)
F(1)-C(8)-C(7)……118.61(13)
C(9)-C(8)-C(7)……122.66(13)
C(8)-C(9)-C(10)……118.92(13)
C(8)-C(9)-H(9)……120.5
C(10)-C(9)-H(9)……120.5
C(9)-C(10)-C(11)……120.04(13)
C(9)-C(10)-C(12)……120.79(12)
C(11)-C(10)-C(12)……119.09(12)
O(5)-C(11)-C(10)……120.32(12)
O(5)-C(11)-C(6)……120.34(12)
C(10)-C(11)-C(6)……119.33(12)
N(2)-C(12)-C(10)……113.13(11)
N(2)-C(12)-H(12)A……109.0
C(10)-C(12)-H(12)A……109.0
N(2)-C(12)-H(12)B……109.0
C(10)-C(12)-H(12)B……109.0
H(12)A-C(12)-H(12)B……107.8
N(2)-C(13)-C(14)……112.51(11)
N(2)-C(13)-H(13)A……109.1
C(14)-C(13)-H(13)A……109.1
N(2)-C(13)-H(13)B……109.1
C(14)-C(13)-H(13)B……109.1
H(13)A-C(13)-H(13)B……107.8
O(7)-C(14)-O(6)……124.44(13)
O(7)-C(14)-C(13)……117.40(12)
O(6)-C(14)-C(13)……118.09(11)
N(2)-C(15)-C(16)……111.39(11)
N(2)-C(15)-H(15)A……109.3
C(16)-C(15)-H(15)A……109.3
N(2)-C(150-H(15)B……109.3
C(16)-C(15)-H(15)B……109.3
H(15)A-C(15)-H(15)B……108.0
O(9)-C(16)-O(8)……124.51(12)
O(9)-C(16)-C(15)……116.91(12)
O(8)-C(16)-C(15)……118.49(12)
C(2)-N(1)-C(3)……113.21(10)
C(2)-N(1)-C(5)……108.43(11)
C(3)-N(1)-C(5)……111.42(10)
C(2)-N(1)-Mg(1)……106.22(8)

C(3)-N1-Mg(1)……107.94(8)
C(5)-N1-Mg(1)……109.45(8)
C(13)-N2-C(15)……113.54(11)
C(13)-N2-C(12)……111.54(10)
C(15)-N(2)-C(12)……109.00(11)
C(13)-N(2)-Mg(2)……108.09(8)
C(15)-N(2)-Mg(2)……105.32(8)
C(12)-N(2)-Mg(2)……109.10(8)
C(1)-O(1)-Mg(1)……115.01(9)
C(4)-O(3)-Mg(1)……118.12(9)
C(11)-O(5)-Mg(2)……114.60(8)
C(11)-O(5)-Mg(1)……115.76(8)
Mg(2)-O(5)-Mg(1)……129.57(5)
C(14)-O(6)-Mg(2)……118.85(9)
C(16)-O(8)-Mg(2)……115.44(8)
O(5)W-Mg(3)-O(5)W……180.0
O(5)W-Mg(3)-O(6)W……88.47(4)
O(5)W-Mg(3)-O(6)W……91.53(4)
O(5)W-Mg(3)-O(6)W……91.53(4)
O(5)W-Mg(3)-O(6)W……88.47(4)
O(6)W-Mg(3)-O(6)W……180.0
O(5)W-Mg(3)-O(7)W……89.42(4)
O(5)W-Mg(3)-O(7)W……90.58(4)
O(6)W-Mg(3)-O(7)W……89.12(4)
O(6)W-Mg(3)-O(7)W……90.88(4)
O(5)W-Mg(3)-O(7)W……90.58(4)
O(5)W-Mg(3)-O(7)W……89.42(4)
O(6)W-Mg(3)-O(7)W……90.88(4)
O(6)W-Mg(3)-O(7)W……89.12(4)
O(7)W-Mg(3)-O(7)W……180.0
Mg(3)-O(5)W-H(5)W(1)……122.9(14)
Mg(3)-O(5)W-H(5)W(2)……126.8(14)
H(5)W(1)-O(5)W-H(5)W(2)……108.6(19)
Mg(3)-O(6)W-H(6)W(1)……120.4(14)
Mg(3)-O(6)W-H(6)W(2)……120.6(13)
H(6)W(1)-O(6)W-H(6)W(2)……105.8(18)
Mg(3)-O(7)W-H(7)W(1)……116.9(14)
Mg(3)-O(7)W-H(7)W(2)……119.6(14)
H(7)W(1)-O(7)W-H(7)W(2)……105.2(18)
H(8)W(1)-O(8)W-H(8)W(2)……103.2(19)
H(9)W(1)-O(9)W-H(9)W(2)……104.2(19)
H(0)W(3)-O(10)W-H(0)W(4)……104.9(19)
H(1)W(3)-O(11)W-H(1)W(4)……105(2)
H(2)W(3)-O(12)W-H(2)W(4)……103(2)
H(3)W(3)-O(13)W-H(3)W(4)……106(2)
H(4)W(3)-O(14)W-H(4)W(4)……105(2)

Torsion Angle (°):

O2-C1-C2-N1……167.97(12)
O1-C1-C2-N1……-15.28(17)
N1-C3-C4-O4……-170.44(11)
N1-C3-C4-O3……12.37(17)
N1-C5-C6-C7……116.26(14)
N1-C5-C6-C11……-68.53(16)
C11-C6-C7-C8……-1.6(2)
C5-C6-C7-C8……173.57(13)
C6-C7-C8-F1……-179.21(12)
C6-C7-C8-C9……0.3(2)
F1-C8-C9-C10……-179.42(12)
C7-C8-C9-C10……1.1(2)
C8-C9-C10-C11……-1.2(2)
C8-C9-C10-C12……175.48(12)
C9-C10-C11-O5……-179.20(12)
C12-C10-C11-O5……4.10(19)
C9-C10-C11-C6……-0.1(2)
C12-C10-C11-C6……-176.78(12)
C7-C6-C11-O5……-179.41(12)
C5-C6-C11-O5……5.34(19)
C7-C6-C11-C10……1.5(2)
C5-C6-C11-C10……-173.77(12)
C9-C10-C12-N2……114.48(14)
C11-C10-C12-N2……-68.85(15)
N2-C13-C14-O7……-172.46(11)
N2-C13-C14-O6……10.57(17)
N2-C15-C16-O9……166.88(12)
N2-C15-C16-O8……-16.31(18)
C1-C2-N1-C3……151.51(11)
C1-C2-N1-C5……-84.31(13)
C1-C2-N1-Mg1……33.24(12)
C4-C3-N1-C2……-135.74(11)
C4-C3-N1-C5……101.74(13)
C4-C3-N1-Mg1……-18.46(12)
C6-C5-N1-C2……170.83(11)
C6-C5-N1-C3……-63.93(14)
C6-C5-N1-Mg1……55.37(12)
C14-C13-N2-C15……-135.80(12)
C14-C13-N2-C12……100.57(13)
C14-C13-N2-Mg2……-19.36(13)
C16-C15-N2-C13……150.27(12)
C16-C15-N2-C12……-84.73(13)
C16-C15-N2-Mg2……32.21(13)
C10-C12-N2-C13……-63.56(14)
C10-C12-N2-C15……170.29(10)
C10-C12-N2-Mg2……55.77(12)
O2-C1-O1-Mg1……163.45(11)
C2-C1-O1-Mg1……-13.03(14)
O4-C4-O3-Mg1……-175.12(10)
C3-C4-O3-Mg1……1.79(15)
C10-C11-O5-Mg2……54.19(15)
C6-C11-O5-Mg2……-124.91(11)
C10-C11-O5-Mg1……-128.45(11)
C6-C11-O5-Mg1……52.45(15)
O7-C14-O6-Mg2……-170.97(10)
C13-C14-O6-Mg2……5.77(15)
O9-C16-O8-Mg2……165.27(11)
C15-C16-O8-Mg2……-11.28(16)

Appendix B: EXPERIMENTAL DATA

Zn(II)/Mg(II) Competition Experiments

Table 1. Initial conditions for Zn(II)/Mg(II) competition.[1]

entry	Na_3H_2(HXTA) (mM)	$Zn(ClO_4)_2$ (mM)	$Mg(ClO_4)_2$ (mM)	Na_2H(NTA) (mM)	[4-FP] (mM)	pH[2]
A	10.05 ± 0.06	10.03 ± 0.07	30.00 ± 0.24	5.00 ± 0.03	4.99 ± 0.03	7.58
B	10.05 ± 0.06	16.99 ± 0.12	23.02 ± 0.18	5.00 ± 0.03	4.99 ± 0.03	7.58
C	10.05 ± 0.06	15.01 ± 0.11	25.01 ± 0.20	5.00 ± 0.03	4.99 ± 0.03	7.60
D	10.05 ± 0.06	6.99 ± 0.05	33.01 ± 0.26	5.00 ± 0.03	4.99 ± 0.03	7.61
E	10.05 ± 0.06	12.01 ± 0.09	28.02 ± 0.22	5.00 ± 0.03	4.99 ± 0.03	7.62
F	10.05 ± 0.06	5.02 ± 0.04	34.99 ± 0.28	5.00 ± 0.03	4.99 ± 0.03	7.64
G	10.05 ± 0.06	9.01 ± 0.07	30.99 ± 0.25	5.00 ± 0.03	4.99 ± 0.03	7.61
H	10.05 ± 0.06	14.02 ± 0.10	26.00 ± 0.21	5.00 ± 0.03	4.99 ± 0.03	7.60

(1) Uncertainties from glassware/pipette tolerances; T = 25.0°C; Ionic strength held constant at *I* = 0.110 M (2) Buffered by 45.19 mM *N*-methylmorpholine; pH corrected for 10% v/v D_2O content.

Table 2. ^{19}F NMR data for Zn(II)/Mg(II) competition.

entry	$[Zn_2(HXTA)]^-$		$[Mg_2(HXTA)]^-$		$[ZnMg(HXTA)]^-$		4-fluorophenol	
	δ (ppm)	Integral	δ (ppm)	Integral	δ (ppm)	Integral	δ (ppm)	Integral
A	-120.14	0.394	-122.03	0.438	-121.18	0.976	-117.56	1
B	-120.63	1.040	-122.02	0.068	-121.18	0.622	-117.56	1
C	-120.63	0.784	-122.02	0.127	-121.18	0.741	-117.56	1
D	-120.64	0.176	-122.02	0.745	-121.18	0.851	-117.55	1
E	-120.64	0.536	-122.02	0.289	-121.18	0.927	-117.55	1
F	-120.64	0.084	-122.03	0.995	-121.19	0.690	-117.56	1
G	-120.64	0.293	-122.02	0.516	-121.18	0.928	-117.55	1
H	-120.64	0.757	-122.03	0.168	-121.18	0.851	-117.56	1

Table 3. Equilibrium concentrations for Zn(II)/Mg(II) competition.

entry	$[Zn_2(HXTA)]^-$ (mM)[1]	$[Mg_2(HXTA)]^-$ (mM)[1]	$[ZnMg(HXTA)]^-$ (mM)[2]	$[Zn(NTA)]^-$ (mM)[2]	$[Mg(NTA)]^-$ (mM)[2]
A	1.97 ± 0.03	2.19 ± 0.10	4.87 ± 0.07	1.23 ± 0.12	3.77 ±0.32
B	5.19 ± 0.08	0.34 ± 0.11	3.10 ± 0.05	3.50 ± 0.21	1.50 ± 0.29
C	3.91 ±0.06	0.63 ± 0.10	3.70 ± 0.06	3.49 ± 0.17	1.51 ± 0.29
D	0.88 ± 0.01	3.72 ± 0.09	4.25 ± 0.07	0.99 ± 0.09	4.01 ± 0.33
E	2.67 ±0.04	1.44 ± 0.10	4.63 ± 0.07	2.03 ± 0.14	2.97 ± 0.31
F	0.42 ± 0.01	4.96 ± 0.08	3.44 ± 0.05	0.73 ± 0.07	4.26 ± 0.33
G	1.46 ± 0.02	2.57 ± 0.10	4.63 ± 0.07	1.45 ± 0.11	3.55 ± 0.32
H	3.78 ± 0.06	0.84 ± 0.11	4.25 ± 0.07	2.22 ± 0.17	2.78 ± 0.30

(1) Measured vs 4-FP; (2) Calculated from mass balance equations.

Table 4. Equilibrium constants for Zn(II)/Mg(II) competition.[1]

entry	K_1 ($\beta_{ZnZn}^2/\beta_{MgMg}^2$)	K_2 ($\beta_{ZnMg}/\beta_{MgMg}$)	K_3 ($\beta_{ZnZn}/\beta_{ZnMg}$)
A	$2.79 \cdot 10^{11}$	$1.24 \cdot 10^{6}$	$2.25 \cdot 10^{5}$
B	$9.29 \cdot 10^{10}$	$7.15 \cdot 10^{5}$	$1.30 \cdot 10^{5}$
C	$3.83 \cdot 10^{10}$	$4.59 \cdot 10^{5}$	$8.33 \cdot 10^{4}$
D	$1.29 \cdot 10^{11}$	$8.43 \cdot 10^{5}$	$1.53 \cdot 10^{5}$
E	$1.31 \cdot 10^{11}$	$8.51 \cdot 10^{5}$	$1.53 \cdot 10^{5}$
F	$9.44 \cdot 10^{10}$	$7.33 \cdot 10^{5}$	$1.29 \cdot 10^{5}$
G	$1.12 \cdot 10^{11}$	$8.00 \cdot 10^{5}$	$1.40 \cdot 10^{5}$
H	$2.33 \cdot 10^{11}$	$1.15 \cdot 10^{6}$	$2.02 \cdot 10^{5}$
Avg.	$1.39 \cdot 10^{11}$	$8.49 \cdot 10^{5}$	$1.52 \cdot 10^{5}$
St. Dev.	$7.89 \cdot 10^{10}$	$2.48 \cdot 10^{5}$	$4.42 \cdot 10^{4}$

(1) Calculated from concentration data in Table 3

Fe(II)/Mg(II) Competition Experiments

Table 5. Initial conditions for Fe(II)/Mg(II) competition.[1]

entry	$Na_3H_2(HXTA)$ (mM)	$Fe(ClO_4)_2$ (mM)	$Mg(ClO_4)_2$ (mM)	$Na_2H(NTA)$ (mM)	[4-FP] (mM)	pH[2]
A	10.34 ± 0.06	10.99 ± 0.09	29.01 ± 0.21	5.00 ± 0.03	4.99 ± 0.03	7.44
B	10.03 ± 0.06	15.01 ± 0.12	25.01 ± 0.18	5.00 ± 0.03	4.99 ± 0.03	7.57
C	10.03 ± 0.06	6.99 ± 0.05	33.01 ±0.24	5.00 ± 0.03	4.99 ± 0.03	7.55
D	10.03 ± 0.06	12.01 ± 0.09	27.98 ± 0.21	5.00 ± 0.03	4.99 ± 0.03	7.55
E	10.03 ± 0.06	9.03 ± 0.07	30.99 ± 0.23	5.00 ± 0.03	4.99 ± 0.03	7.38
F	10.03 ± 0.06	4.99 ± 0.04	35.03 ± 0.26	5.00 ± 0.03	4.99 ± 0.03	7.38

(1) Uncertainties from glassware/pipette tolerances; T = 25.0°C; Ionic strength held constant at I = 0.1075 M (2) Buffered by 41.84 mM *N*-methylmorpholine; pH corrected for 10% v/v D_2O content.

Table 6. ^{19}F NMR data for Fe(II)/Mg(II) competition.

entry	$[Fe_2(HXTA)]^-$		$[Mg_2(HXTA)]^-$		$[FeMg(HXTA)]^-$		4-fluorophenol	
	δ (ppm)	Integral	δ (ppm)	Integral	δ (ppm)	Integral	δ (ppm)	Integral
A	-69.05	0.486	-122.04	0.352	-94.45	0.846	-117.53	1
B	-69.71	0.897	-122.02	0.123	-94.77	0.676	-117.48	1
C	-69.71	0.200	-122.02	0.726	-94.78	0.786	-117.52	1
D	-69.71	0.564	-122.02	0.277	-94.78	0.805	-117.49	1
E	-69.71	0.345	-122.02	0.503	-94.78	0.840	-117.50	1
F	-69.71	0.103	-122.02	0.932	-94.78	0.627	-117.53	1

Table 7. Equilibrium concentrations for Fe(II)/Mg(II) competition.

entry	$[Fe_2(HXTA)]^-$ (mM)[1]	$[Mg_2(HXTA)]^-$ (mM)[1]	$[FeMg(HXTA)]^-$ (mM)[2]	$[Fe(NTA)]^-$ (mM)[2]	$[Mg(NTA)]^-$ (mM)[2]
A	2.42 ± 0.09	1.76 ± 0.03	4.22 ± 0.06	1.92 ± 0.22	3.08 ± 0.23
B	4.48 ± 0.08	0.61 ± 0.01	3.37 ± 0.05	2.67 ± 0.21	2.33 ± 0.19
C	1.00 ± 0.10	3.62 ± 0.06	3.92 ± 0.06	1.07 ± 0.22	3.93 ± 0.27
D	2.81 ± 0.09	1.38 ±0.02	4.02 ± 0.06	2.37 ± 0.21	2.63 ± 0.22
E	1.72 ± 0.10	2.51 ± 0.04	4.19 ± 0.06	1.40 ± 0.22	3.60 ± 0.25
F	0.51 ± 0.11	4.65 ± 0.07	3.13 ± 0.05	0.83 ± 0.22	4.17 ± 0.30

(1) Measured vs 4-FP; (2) Calculated from mass balance equations.

Table 8. Equilibrium constants for Fe(II)/Mg(II) competition.[1]

entry	K_1 ($\beta_{FeFe}^2/\beta_{MgMg}^2$)	K_2 ($\beta_{FeMg}/\beta_{MgMg}$)	K_3 ($\beta_{FeFe}/\beta_{FeMg}$)
A	$2.45 \cdot 10^7$	$1.01 \cdot 10^4$	$2.42 \cdot 10^3$
B	$3.83 \cdot 10^7$	$1.26 \cdot 10^4$	$3.04 \cdot 10^3$
C	$2.57 \cdot 10^7$	$1.05 \cdot 10^4$	$2.46 \cdot 10^3$
D	$1.74 \cdot 10^7$	$8.51 \cdot 10^3$	$2.05 \cdot 10^3$
E	$3.17 \cdot 10^7$	$1.14 \cdot 10^4$	$2.79 \cdot 10^3$
F	$1.93 \cdot 10^7$	$8.90 \cdot 10^3$	$2.17 \cdot 10^3$
Avg.	$2.62 \cdot 10^7$	$1.03 \cdot 10^4$	$2.49 \cdot 10^3$
St. Dev.	$7.78 \cdot 10^6$	$1.52 \cdot 10^3$	$3.73 \cdot 10^2$

(1) Calculated from concentration data in Table 7

Zn(II)/Fe(II) Competition Experiments

Table 9. Initial conditions for Zn(II)/Fe(II) competition.[1]

entry	$Na_3H_2(HXTA)$ (mM)	$Zn(ClO_4)_2$ (mM)	$Fe(ClO_4)_2$ (mM)	$Na_2H(NTA)$ (mM)	[4-FP] (mM)	pH[2]
A	3.00 ± 0.04	4.50 ± 0.03	7.50 ± 0.06	3.01 ±0.02	1.50 ± 0.01	7.02
B	3.00 ± 0.04	6.00 ± 0.04	6.01 ± 0.05	3.01 ±0.02	1.50 ± 0.01	7.01
C	3.00 ± 0.04	5.49 ± 0.04	6.52 ± 0.05	3.01 ±0.02	1.50 ± 0.01	7.14
D	3.00 ± 0.04	3.99 ± 0.03	8.01 ± 0.06	3.01 ±0.02	1.50 ± 0.01	7.04
E	3.00 ± 0.04	5.02 ± 0.04	6.99 ± 0.05	3.01 ±0.02	1.50 ± 0.01	7.01
F	3.00 ± 0.04	6.52 ± 0.05	5.50 ± 0.04	3.01 ±0.02	1.50 ± 0.01	6.97
G	3.00 ± 0.04	3.48 ± 0.03	8.52 ± 0.07	3.01 ±0.02	1.50 ± 0.01	6.97
H	3.00 ± 0.04	3.00 ± 0.02	8.99 ± 0.07	3.01 ±0.02	1.50 ± 0.01	7.01

(1) Uncertainties from glassware/pipette tolerances; T = 25.0°C; Ionic strength held constant at I = 0.0330 M (2) Buffered by 12.55 mM *N*-methylmorpholine; pH corrected for 10% v/v D_2O content.

Table 10. ^{19}F NMR data for Zn(II)/Fe(II) competition.

entry	$[Zn_2(HXTA)]^-$		$[Fe_2(HXTA)]^-$		$[ZnFe(HXTA)]^-$		4-fluorophenol	
	δ (ppm)	**Integral**	**δ (ppm)**	**Integral**	**δ (ppm)**	**Integral**	**δ (ppm)**	**Integral**
A	-120.62	0.375	-69.72	0.441	-93.91	0.912	-117.54	1
B	-120.63	0.668	-69.73	0.222	-93.91	0.794	-117.54	1
C	-120.63	0.590	-69.72	0.268	-93.90	0.803	-117.54	1
D	-120.63	0.282	-69.73	0.577	-93.91	0.856	-117.53	1
E	-120.63	0.469	-69.72	0.361	-93.91	0.886	-117.54	1
F	-120.63	0.859	-69.72	0.130	-93.90	0.737	-117.54	1
G	-120.61	0.216	-69.72	0.733	-93.90	0.824	-117.54	1
H	-120.62	0.152	-69.72	0.718	-93.90	0.789	-117.54	1

Table 11. Equilibrium concentrations for Zn(II)/Fe(II) competition.

entry	$[Zn_2(HXTA)]^-$ (mM)[1]	$[Fe_2(HXTA)]^-$ (mM)[1]	$[ZnFe(HXTA)]^-$ (mM)[2]	$[Zn(NTA)]^-$ (mM)[2]	$[Fe(NTA)]^-$ (mM)[2]
A	0.56 ± 0.01	0.69 ± 0.05	1.33 ± 0.02	2.05 ± 0.04	0.96 ± 0.11
B	1.01 ± 0.02	0.33 ± 0.05	1.19 ± 0.02	2.80 ± 0.04	0.21 ± 0.11
C	0.89 ± 0.01	0.40 ±0.05	1.21 ± 0.02	2.51 ± 0.05	0.50 ± 0.11
D	0.42 ± 0.01	0.87 ± 0.05	1.29 ± 0.02	1.85 ± 0.04	1.16 ± 0.11
E	0.71 ± 0.01	0.54 ± 0.05	1.33 ± 0.02	2.27 ± 0.05	0.74 ± 0.11
F	1.29 ± 0.02	0.20 ± 0.05	1.11 ± 0.02	2.82 ± 0.06	0.19 ± 0.11
G	0.33 ± 0.01	1.10 ± 0.05	1.24 ± 0.02	1.59 ± 0.03	1.42 ± 0.11
H	0.23 ± 0.01	1.19 ± 0.04	1.08 ± 0.02	1.46 ± 0.03	1.54 ± 0.12

(1) Measured vs 4-FP; (2) Calculated from mass balance equations.

Table 12. Equilibrium constants for Zn(II)/Fe(II) competition.[1]

entry	K_1 ($\beta_{ZnZn}^2/\beta_{FeFe}^2$)	K_2 ($\beta_{ZnFe}/\beta_{FeFe}$)	K_3 ($\beta_{ZnZn}/\beta_{ZnFe}$)
A	$8.56\cdot10^2$	$6.23\cdot10^1$	$1.37\cdot10^1$
B	$8.07\cdot10^1$	$1.85\cdot10^1$	$4.36\cdot10^0$
C	$4.22\cdot10^2$	$4.15\cdot10^1$	$1.02\cdot10^1$
D	$9.10\cdot10^2$	$6.40\cdot10^1$	$1.42\cdot10^1$
E	$6.54\cdot10^2$	$5.51\cdot10^1$	$1.19\cdot10^1$
F	$1.36\cdot10^2$	$2.57\cdot10^1$	$5.29\cdot10^0$
G	$1.13\cdot10^3$	$6.97\cdot10^1$	$1.63\cdot10^1$
H	$1.03\cdot10^3$	$6.64\cdot10^1$	$1.54\cdot10^1$
Avg.	$6.52\cdot10^2$	$5.04\cdot10^1$	$1.14\cdot10^1$
St. Dev.	$4.01\cdot10^2$	$1.96\cdot10^1$	$4.51\cdot10^0$

(1) Calculated from concentration data in Table 11

Appendix C: PRIMARY METAL EXCHANGE ^{19}F-NMR SPECTRA

Zn^{II} and Mg^{II} Exchange Experiments

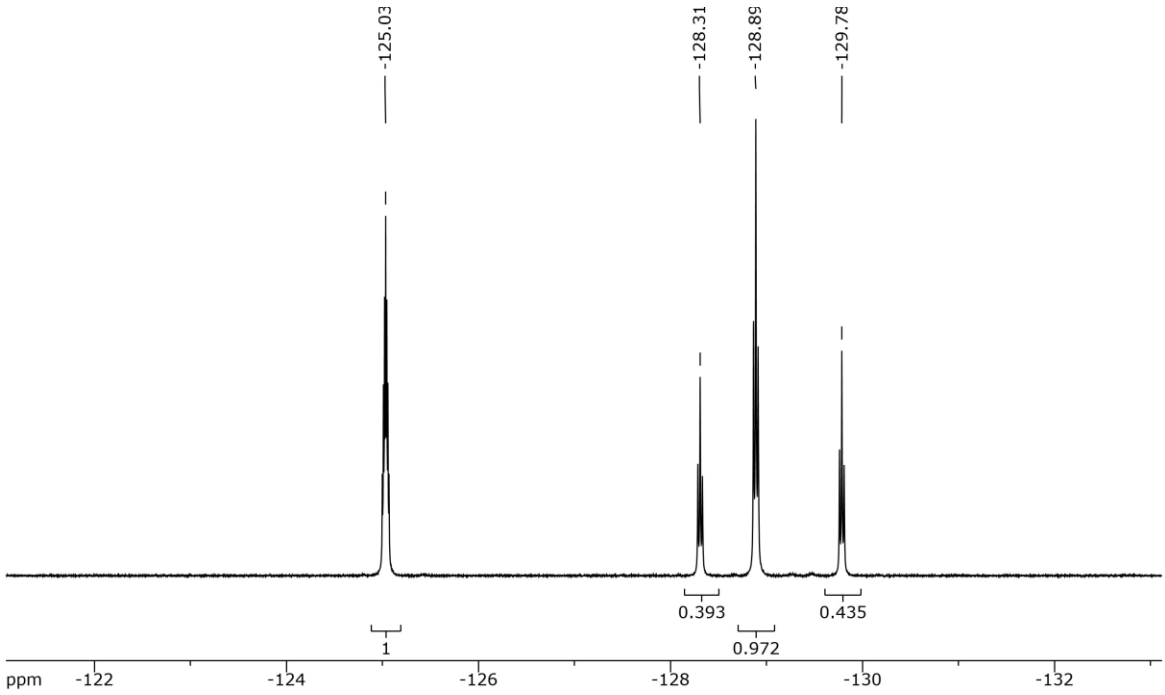

Figure 1: Zn(II)/Mg(II) exchange for entry A in Table 2.

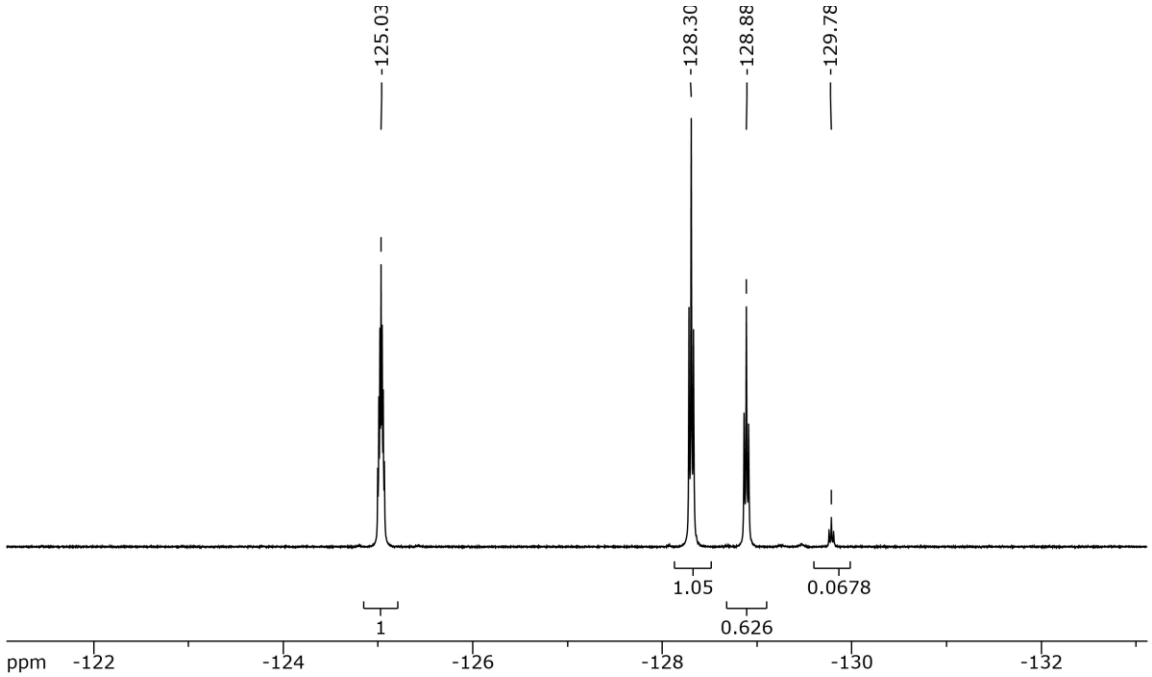

Figure 2: Zn(II)/Mg(II) exchange for entry B in Table 2.

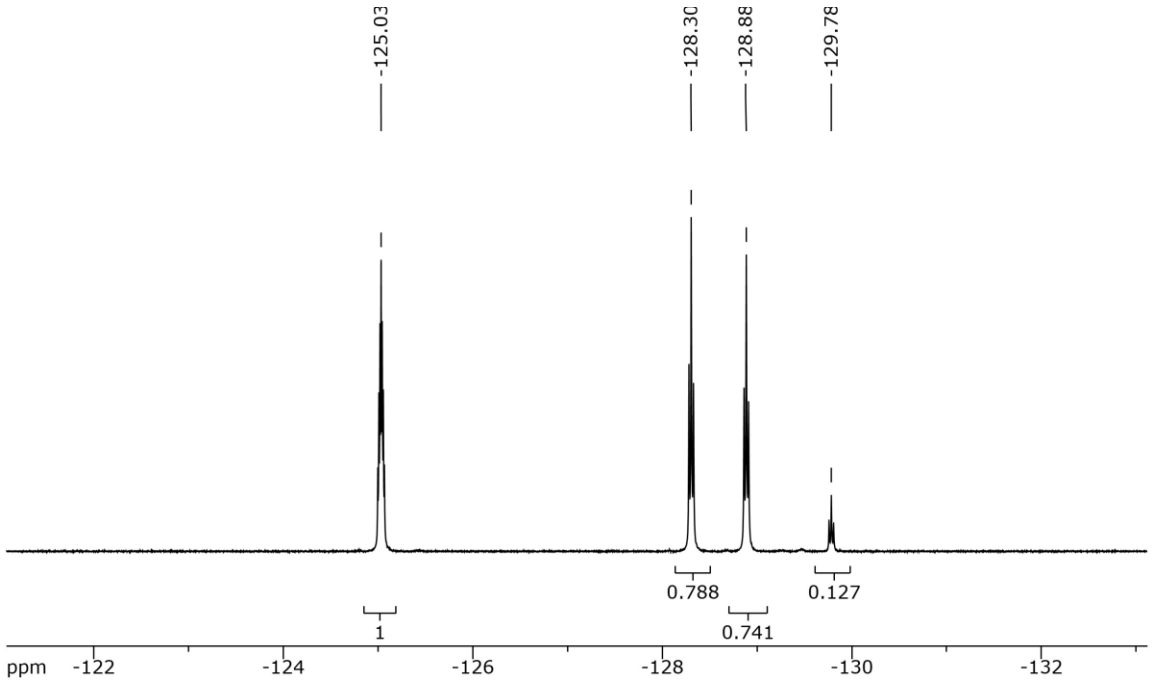

Figure 3: Zn(II)/Mg(II) exchange for entry C in Table 2

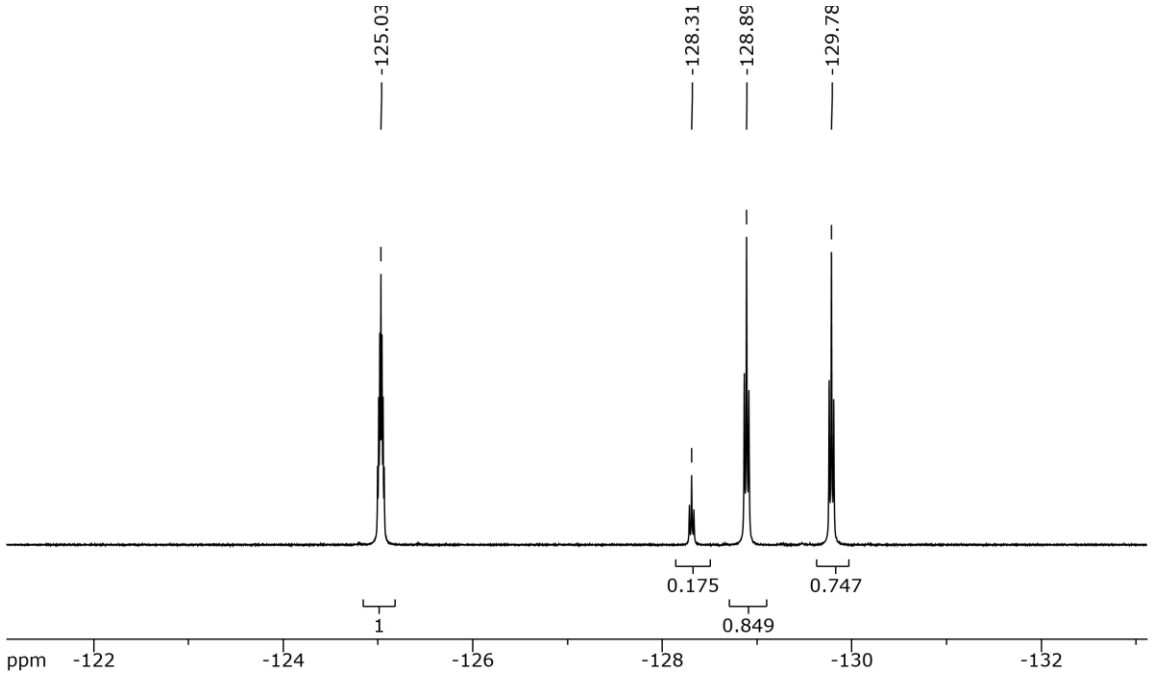

Figure 4: Zn(II)/Mg(II) exchange for entry D in Table 2

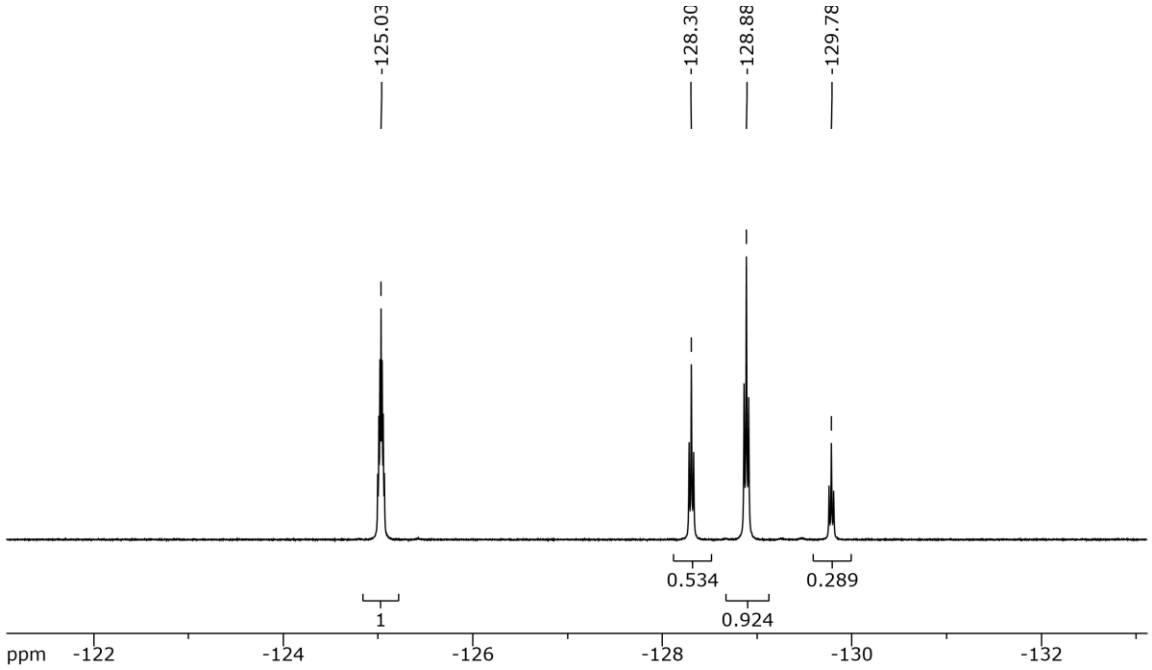

Figure 5: Zn(II)/Mg(II) exchange for entry E in Table 2

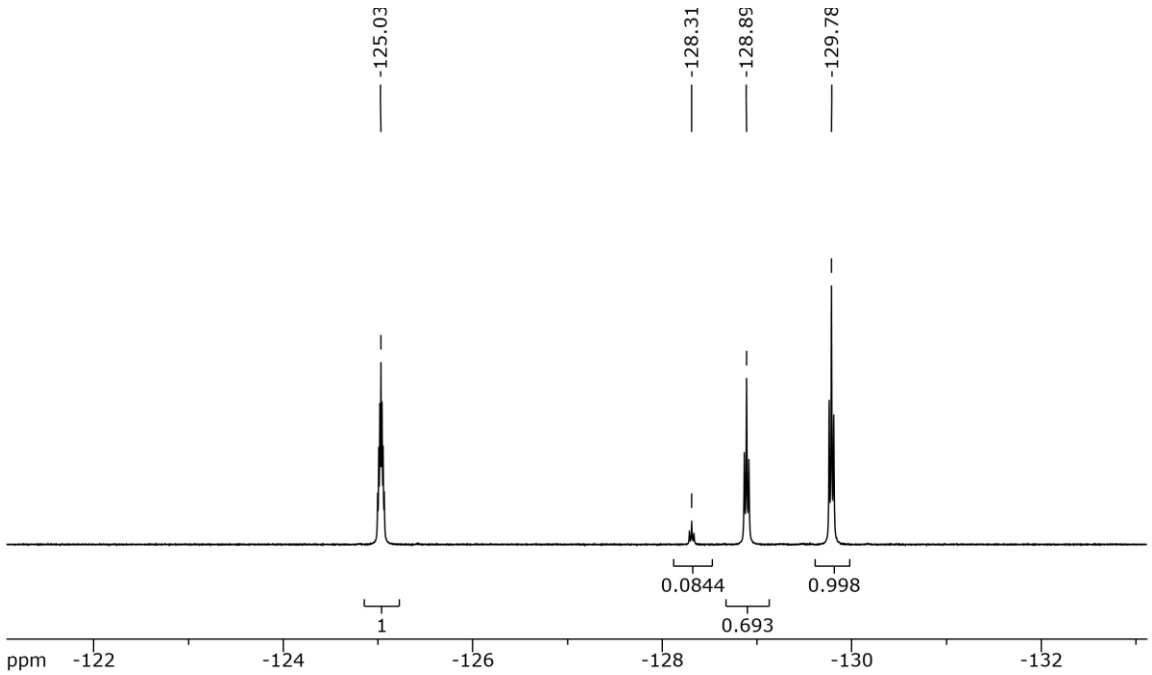

Figure 6: Zn(II)/Mg(II) exchange for entry F in Table 2

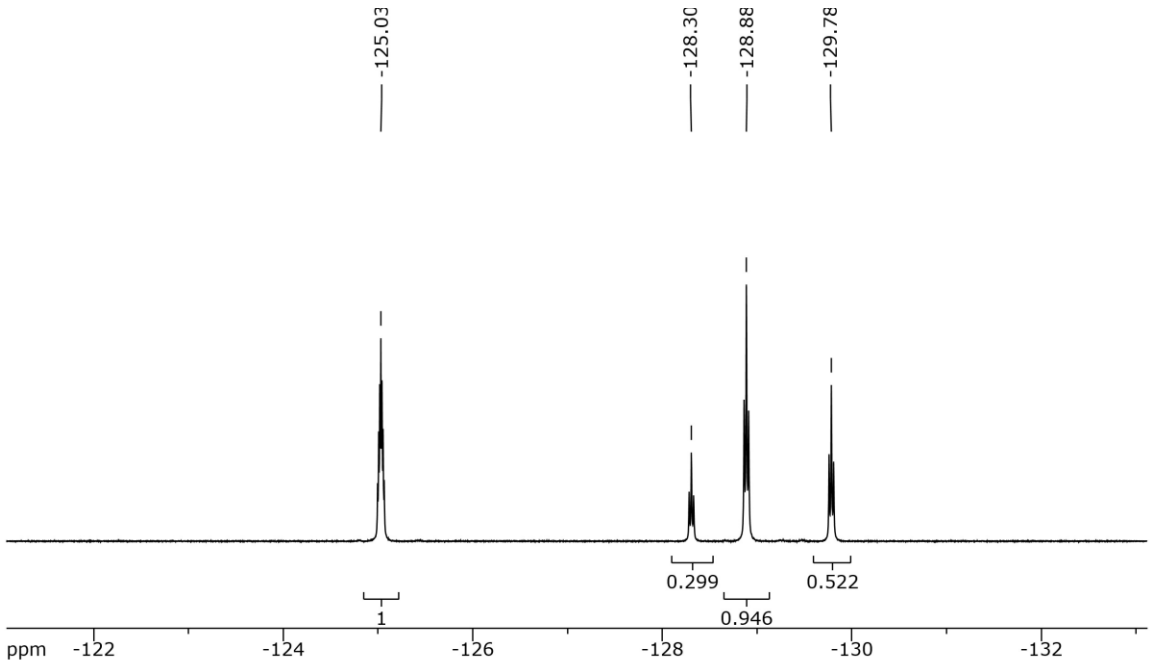

Figure 7: Zn(II)/Mg(II) exchange for entry G in Table 2

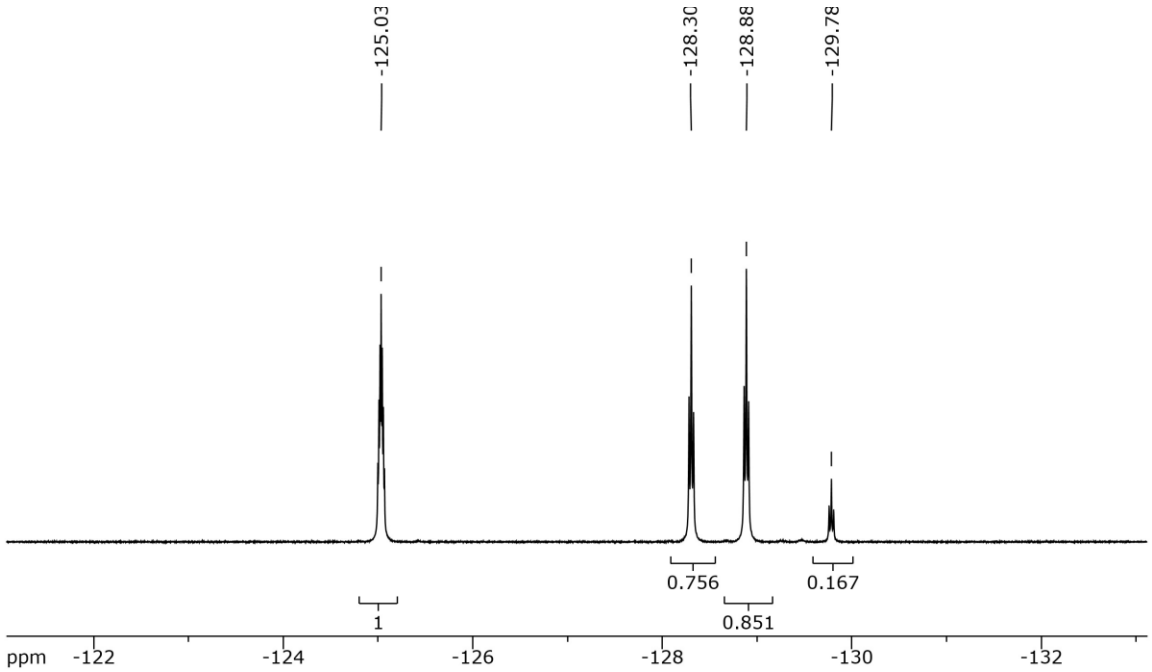

Figure 8:Zn(II)/Mg(II) exchange for entry H in Table 2

Zn^{II} and Fe^{II} Exchange Experiments

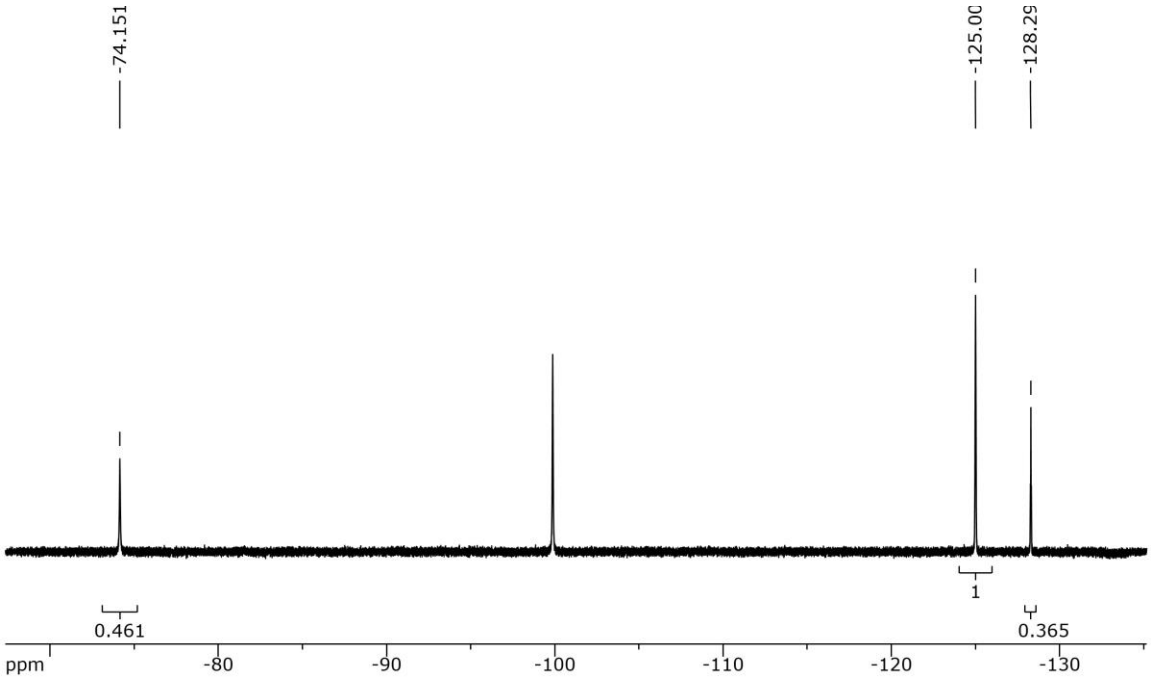

Figure 9: Zn(II)/Fe(II) for entry A in Table 10. First spectrum including FeZnHXTA and Zn_2HXTA integrations.

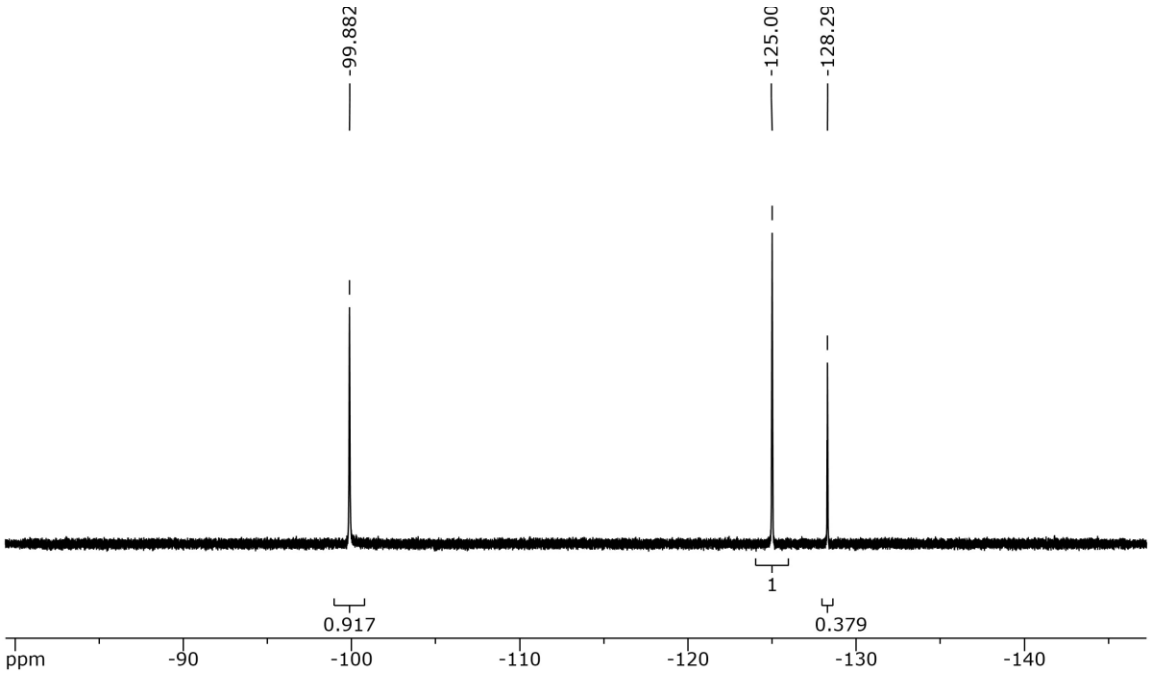

Figure 10: Zn(II)/Fe(II) for entry A in Table 10. Second spectrum including Fe_2HXTA and Zn_2HXTA integrations.

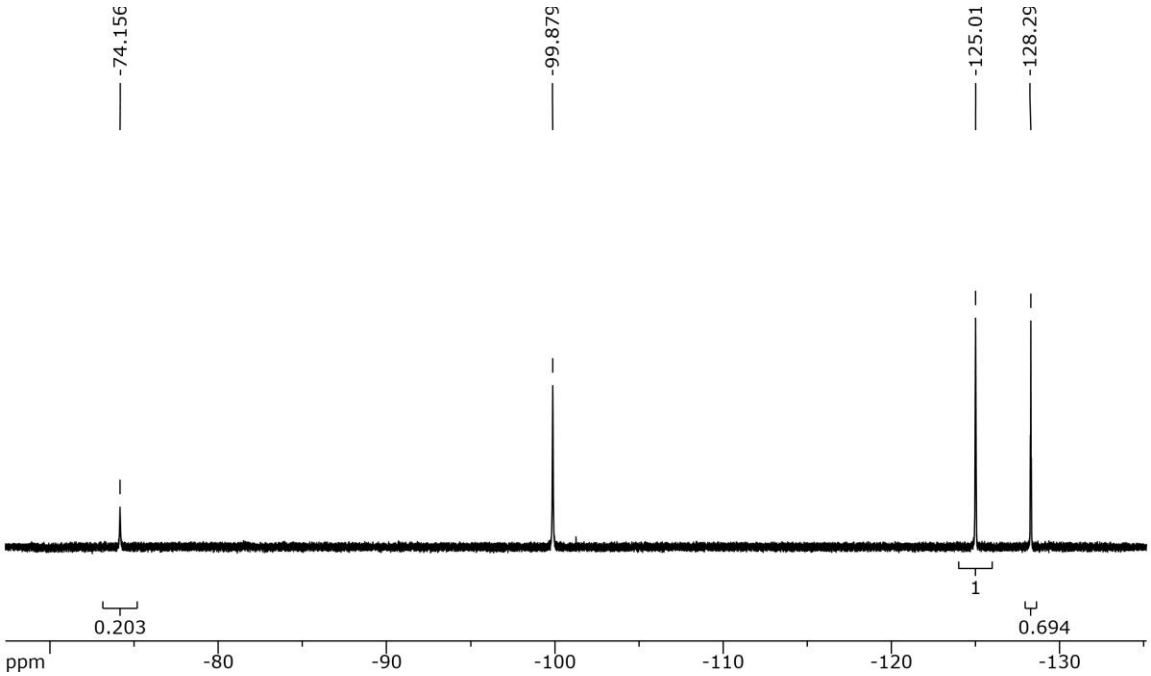

Figure 11: Zn(II)/Fe(II) for entry B in Table 10. First spectrum including FeZnHXTA and Zn_2HXTA integrations.

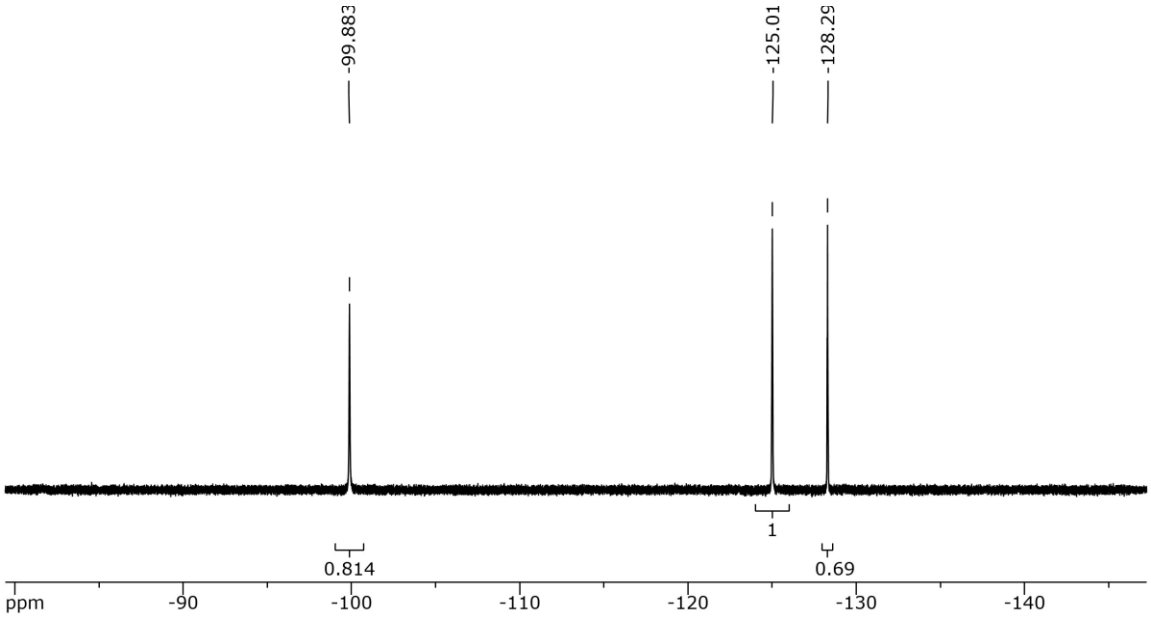

Figure 12: Zn(II)/Fe(II) for entry B in Table 10. Second spectrum including Fe_2HXTA and Zn_2HXTA integrations.

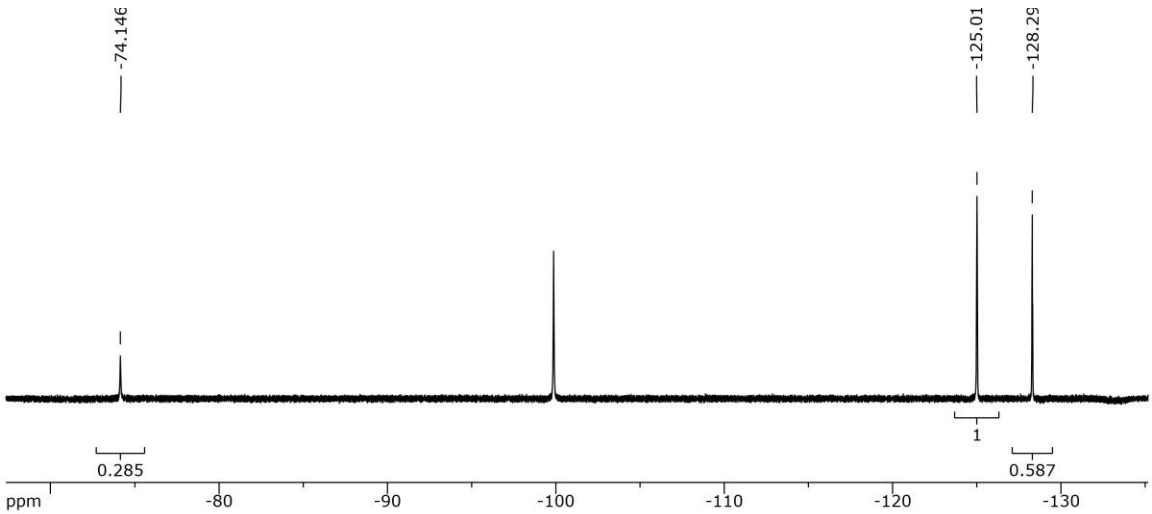

Figure 13: Zn(II)/Fe(II) for entry C in Table 10. First spectrum including FeZnHXTA and Zn_2HXTA integrations.

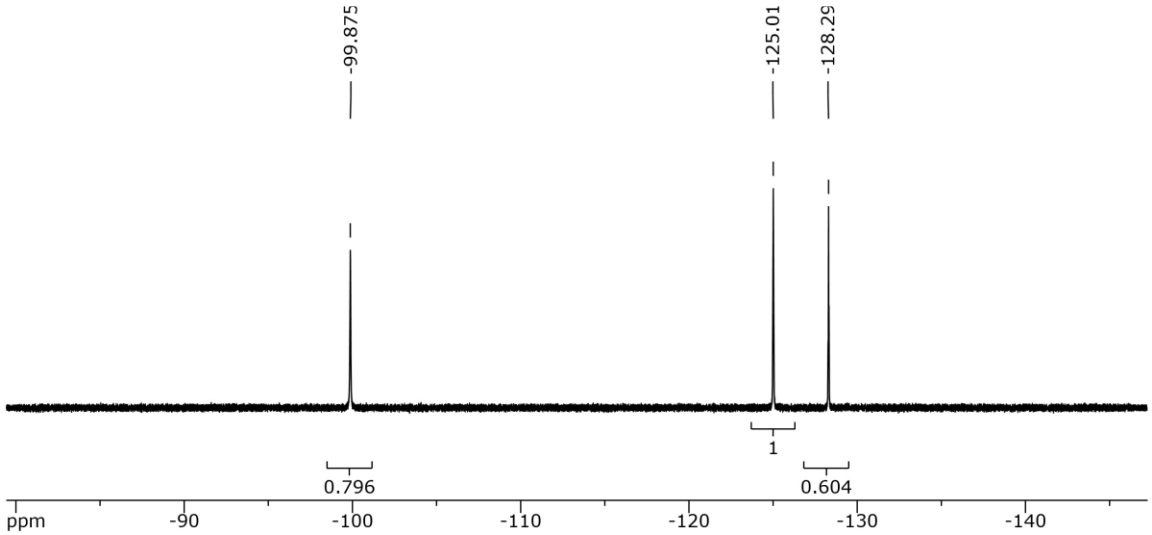

Figure 14: Zn(II)/Fe(II) for entry C in Table 10. Second spectrum including Fe_2HXTA and Zn_2HXTA integrations.

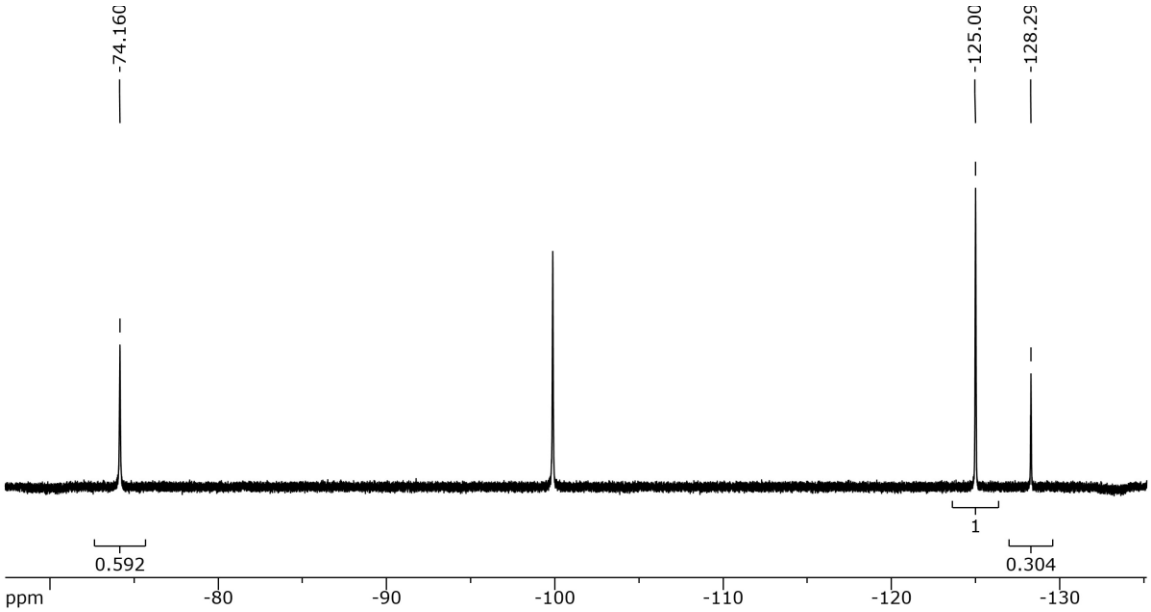

Figure 15: Zn(II)/Fe(II) for entry D in Table 10. First spectrum including FeZnHXTA and Zn_2HXTA integrations.

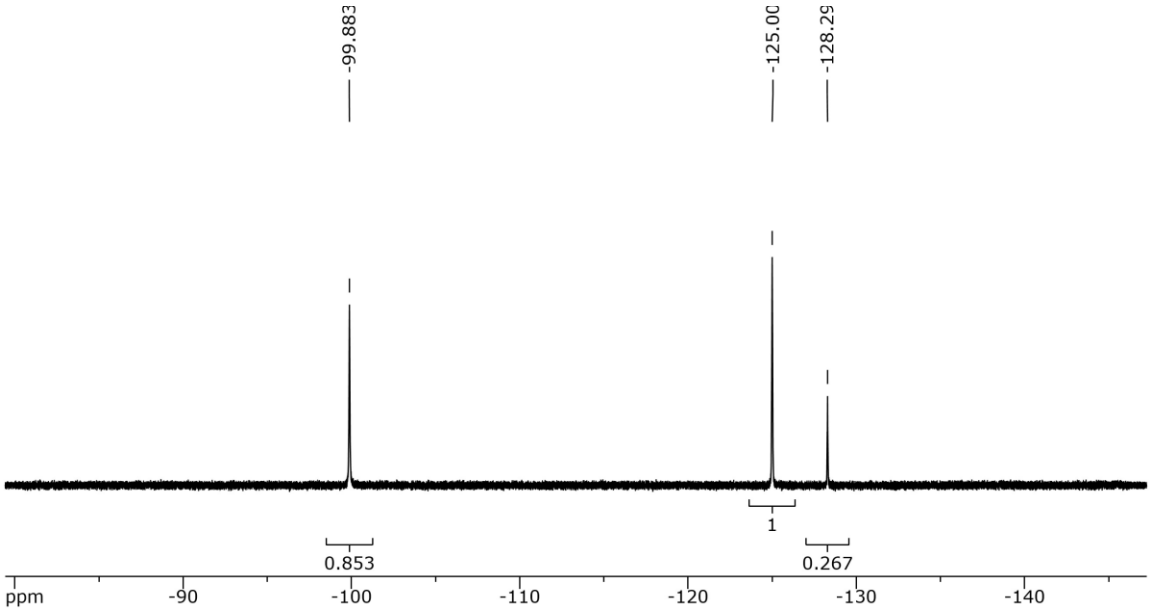

Figure 16: Zn(II)/Fe(II) for entry D in Table 10. Second spectrum including Fe_2HXTA and Zn_2HXTA integrations.

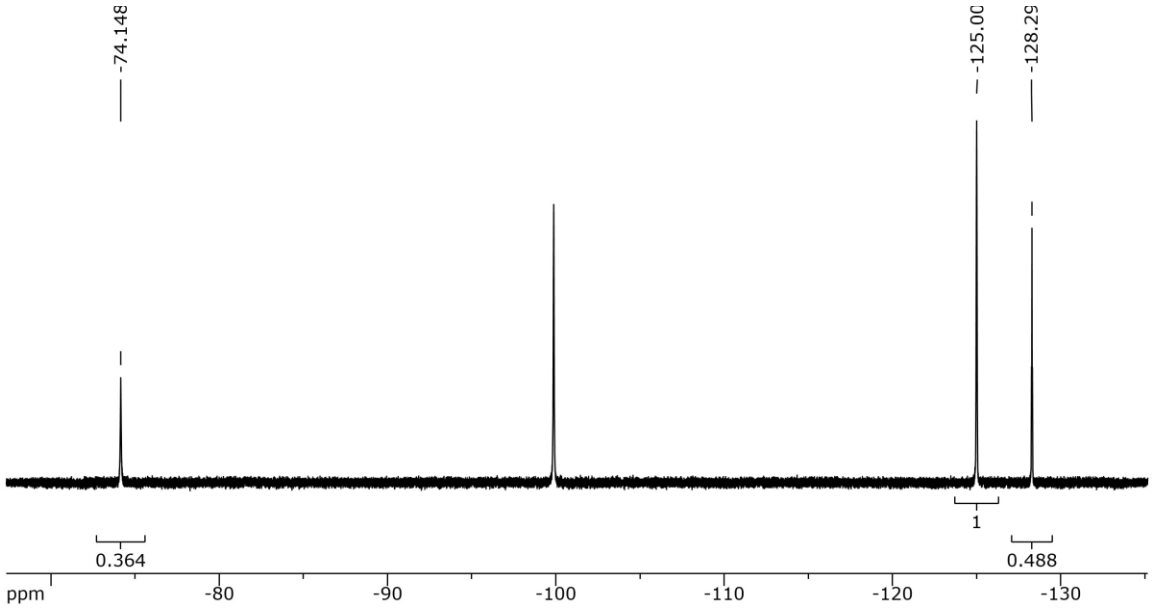

Figure 17: Zn(II)/Fe(II) for entry E in Table 10. First spectrum including FeZnHXTA and Zn_2HXTA integrations.

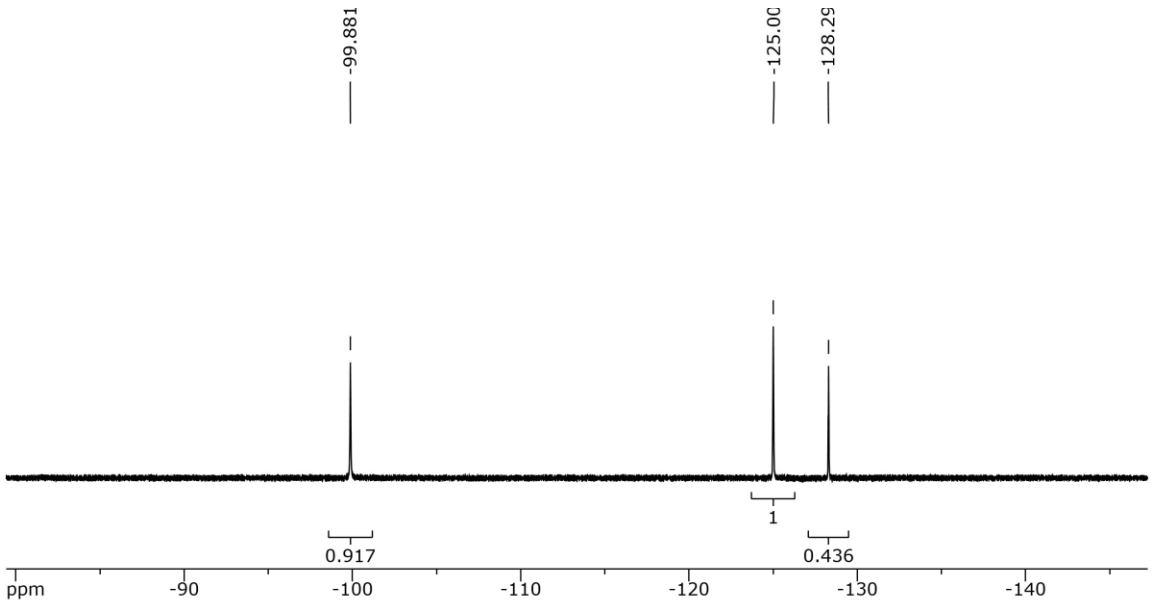

Figure 18: Zn(II)/Fe(II) for entry E in Table 10. Second spectrum including Fe_2HXTA and Zn_2HXTA integrations.

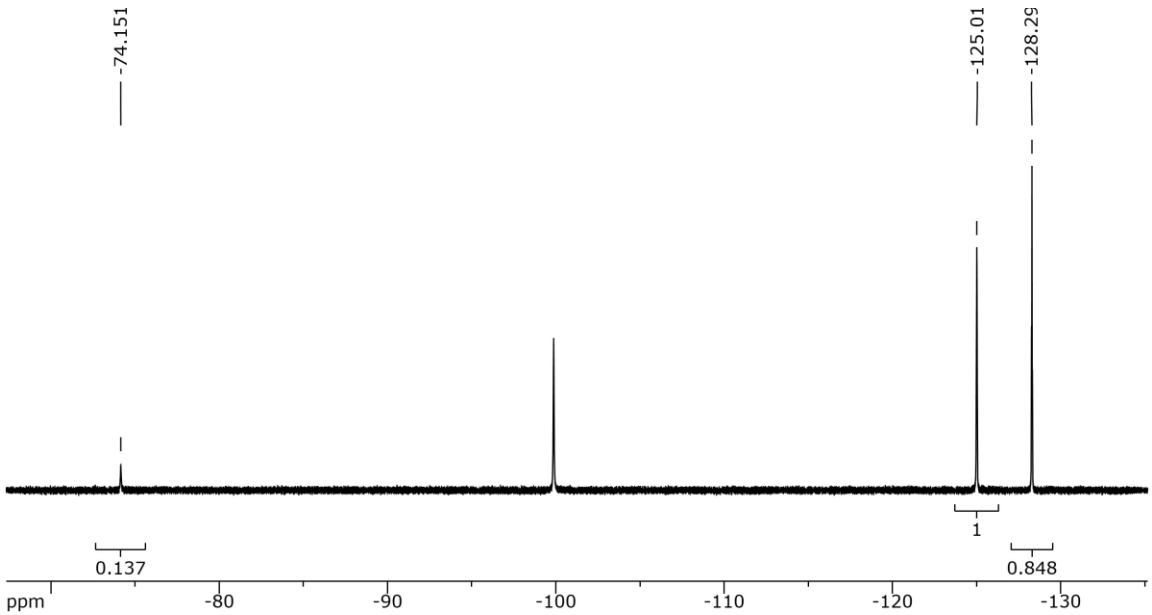

Figure 19: Zn(II)/Fe(II) for entry F in Table 10. First spectrum including FeZnHXTA and Zn_2HXTA integrations.

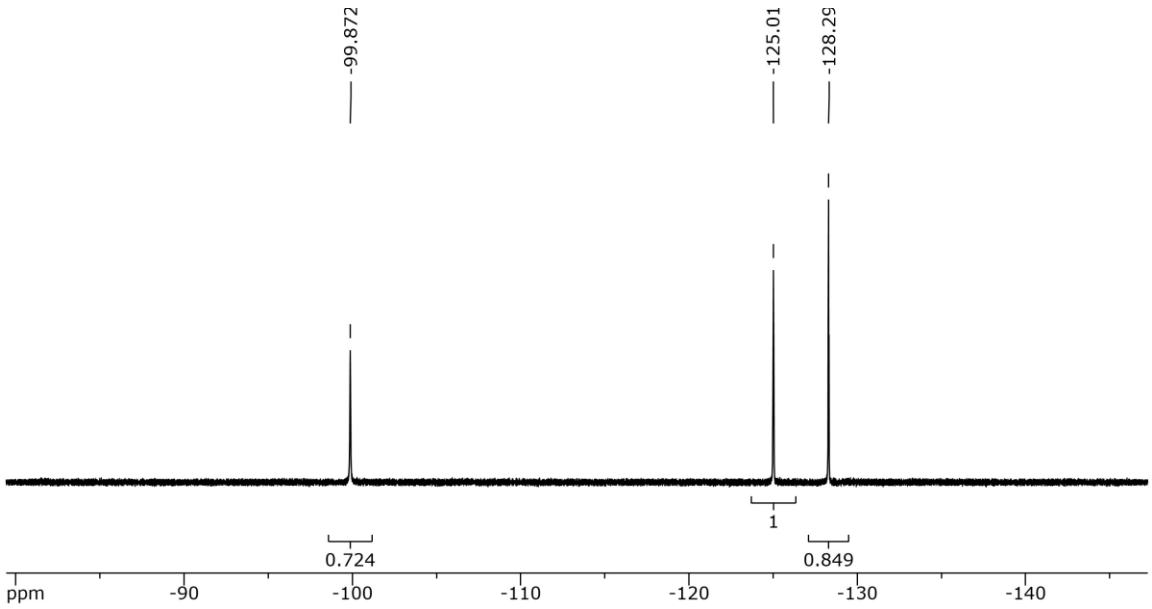

Figure 20: Zn(II)/Fe(II) for entry F in Table 10. Second spectrum including Fe_2HXTA and Zn_2HXTA integrations.

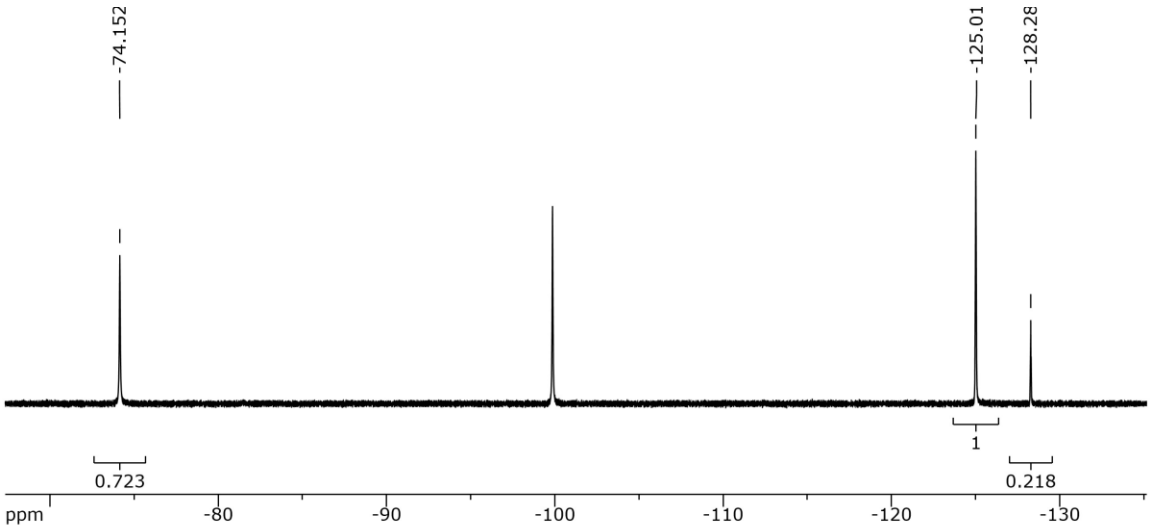

Figure 21: Zn(II)/Fe(II) for entry G in Table 10. First spectrum including FeZnHXTA and Zn_2HXTA integrations.

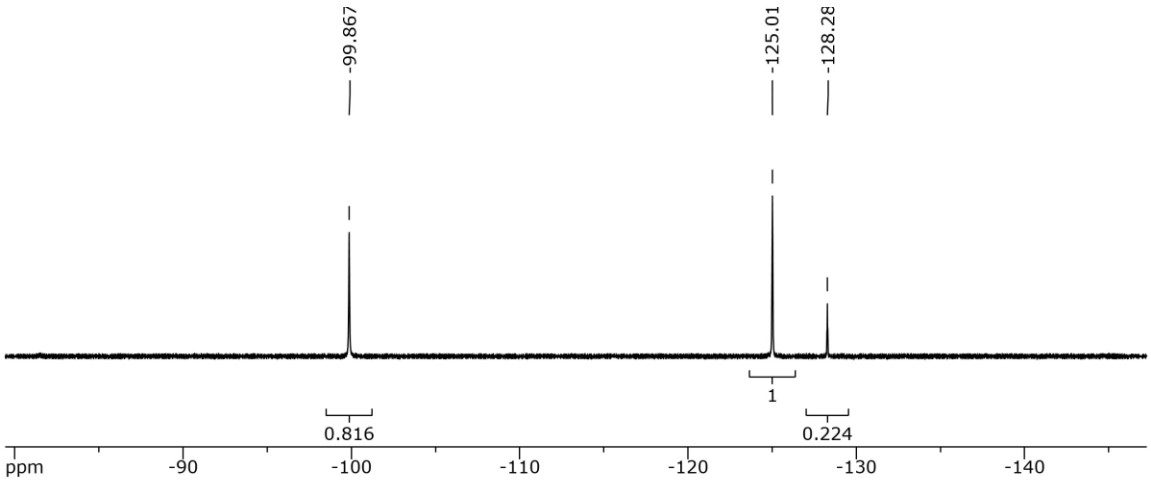

Figure 22: Zn(II)/Fe(II) for entry G in Table 10. Second spectrum including Fe_2HXTA and Zn_2HXTA integrations.

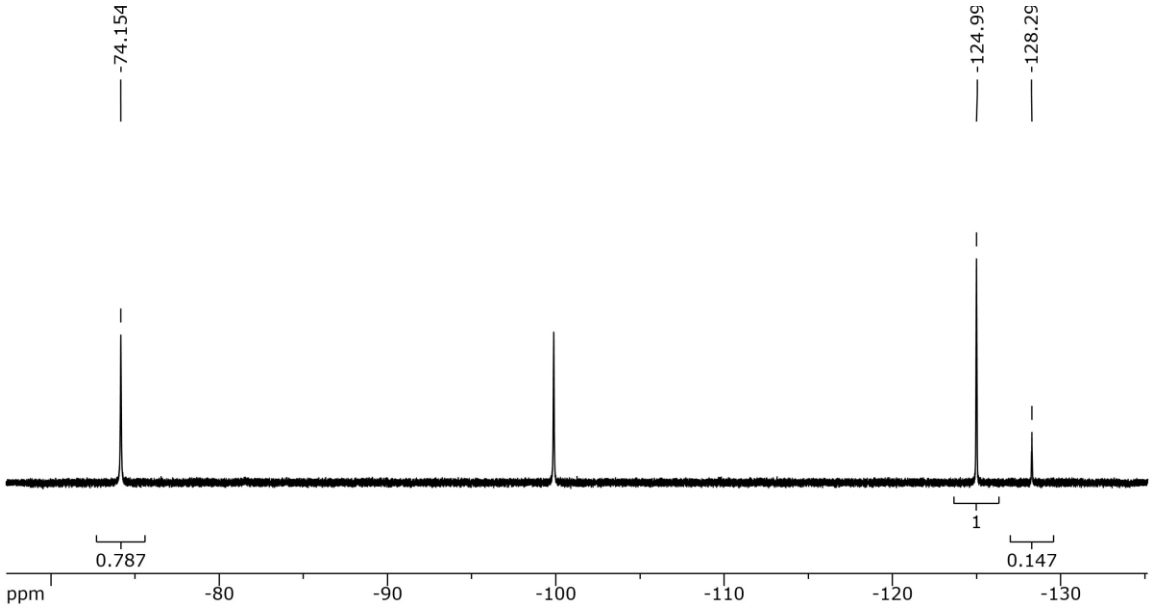

Figure 23: Zn(II)/Fe(II) for entry H in Table 10. First spectrum including FeZnHXTA and Zn_2HXTA integrations.

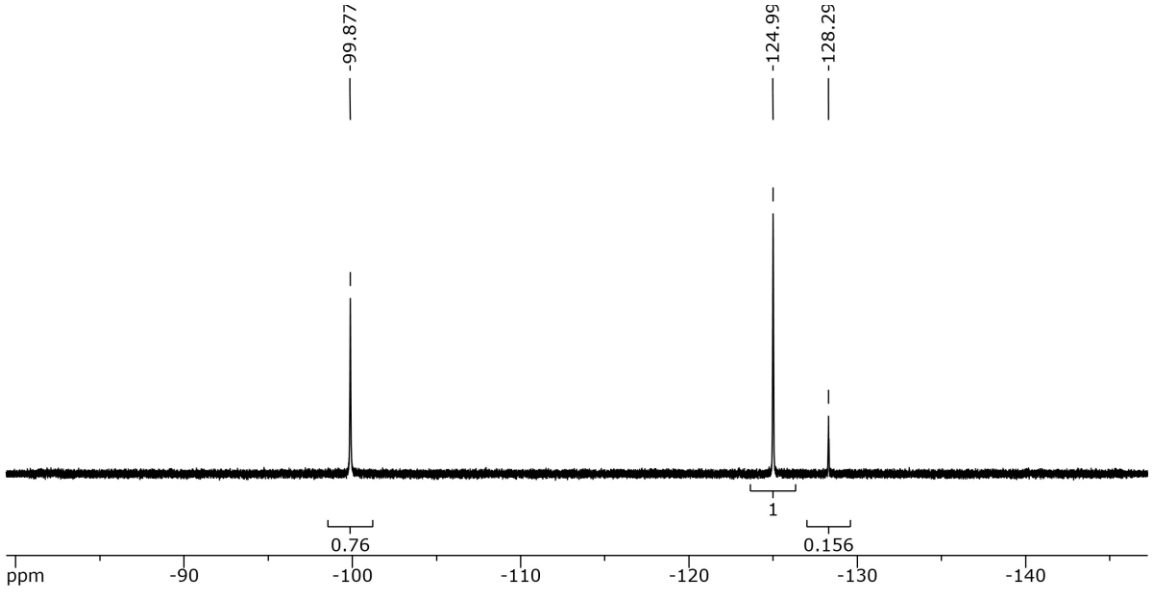

Figure 24: Zn(II)/Fe(II) for entry H in Table 10. Second spectrum including Fe_2HXTA and Zn_2HXTA integrations.

Mg^{II} and Fe^{II} Exchange Experiments

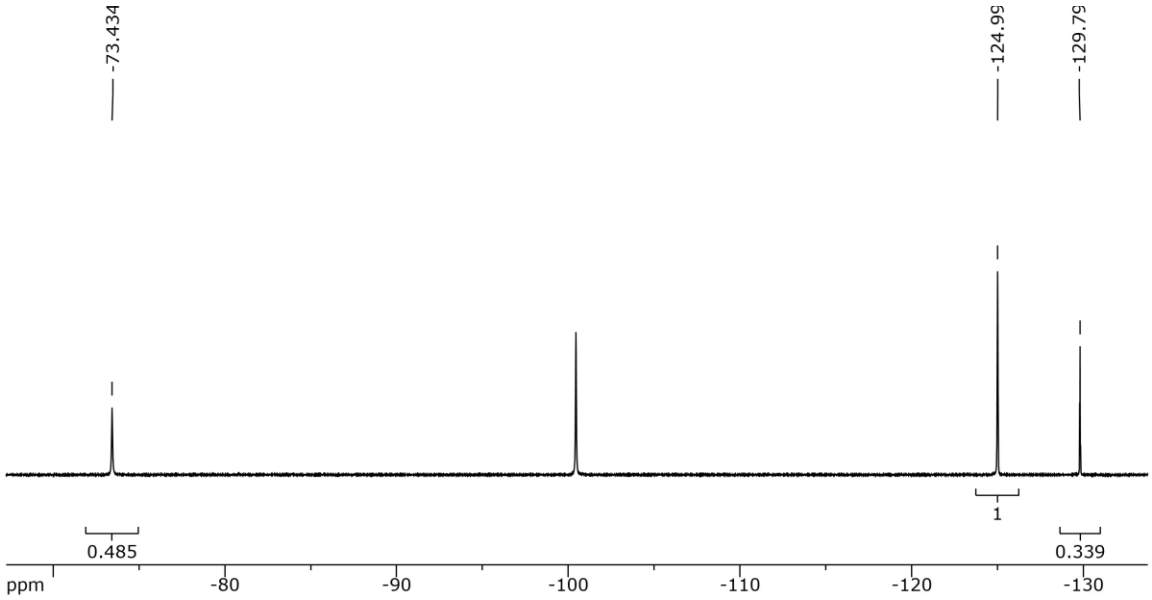

Figure 25: Mg(II)/Fe(II) for entry A in Table 6. First spectrum including FeMgHXTA and Mg_2HXTA integrations.

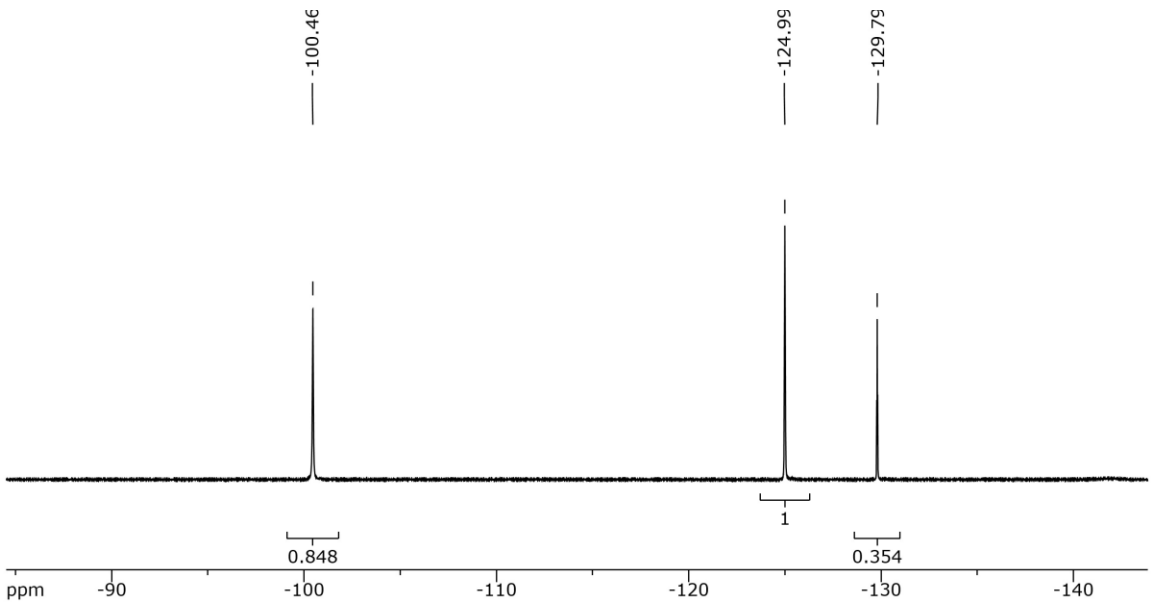

Figure 26: Mg(II)/Fe(II) for entry A in Table 6. Second spectrum including Fe_2HXTA and Mg_2HXTA integrations

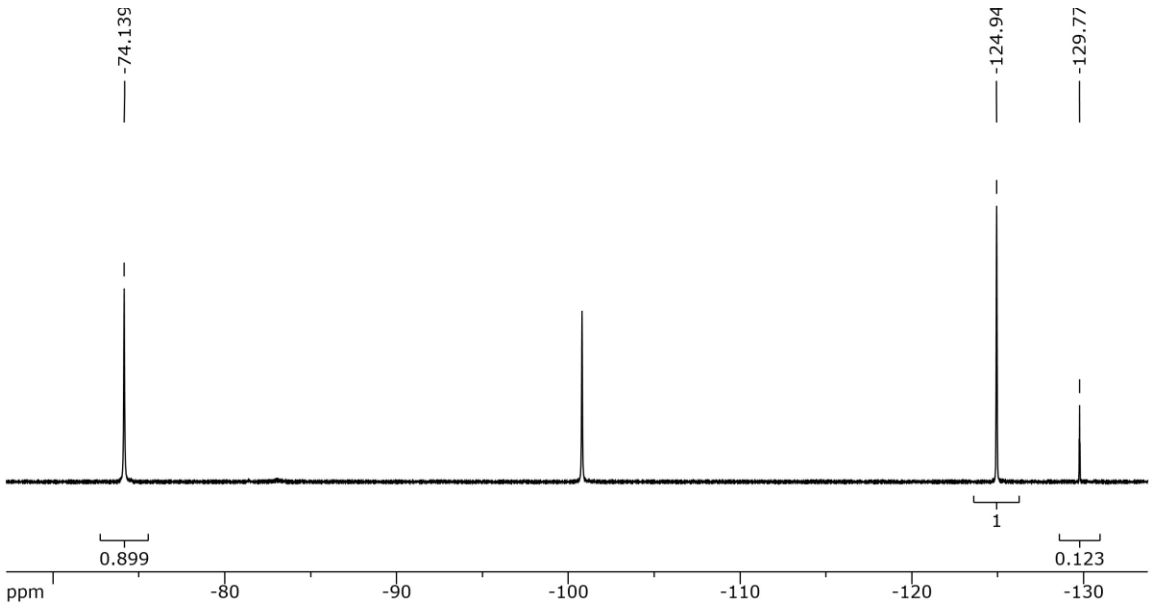

Figure 27: Mg(II)/Fe(II) for entry B in Table 6. First spectrum including FeMgHXTA and Mg_2HXTA integrations.

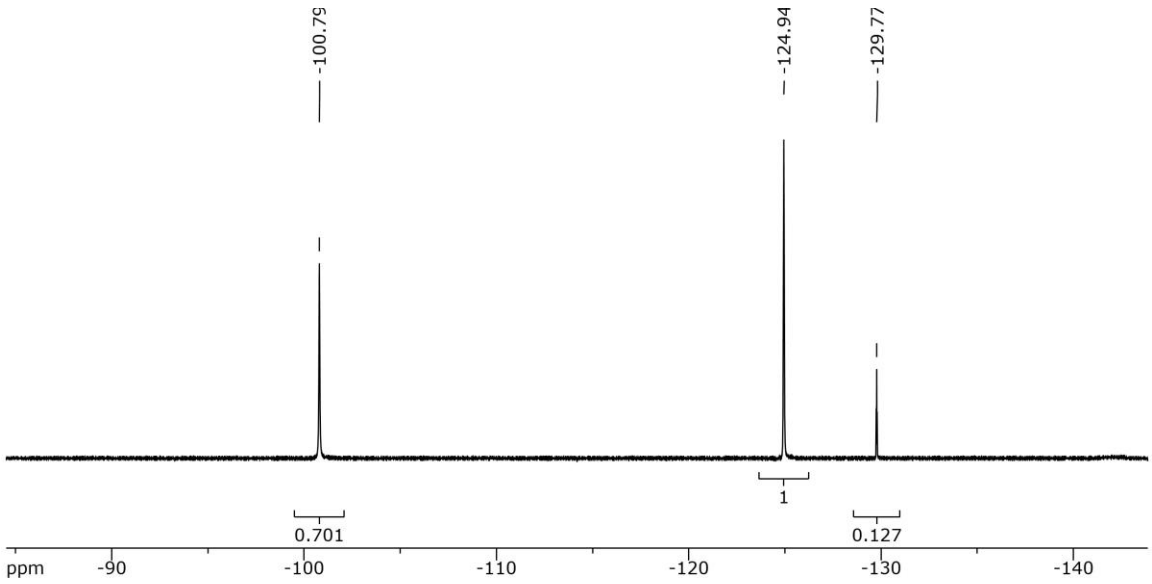

Figure 28: Mg(II)/Fe(II) for entry B in Table 6. Second spectrum including Fe_2HXTA and Mg_2HXTA integrations.

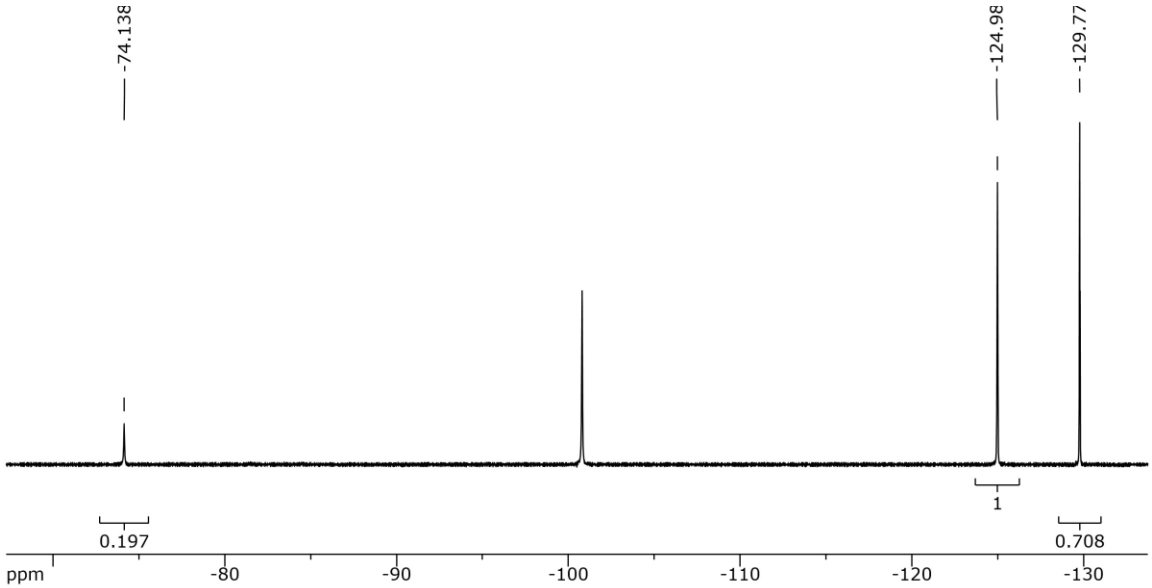

Figure 29: Mg(II)/Fe(II) for entry C in Table 6. First spectrum including FeMgHXTA and Mg_2HXTA integrations.

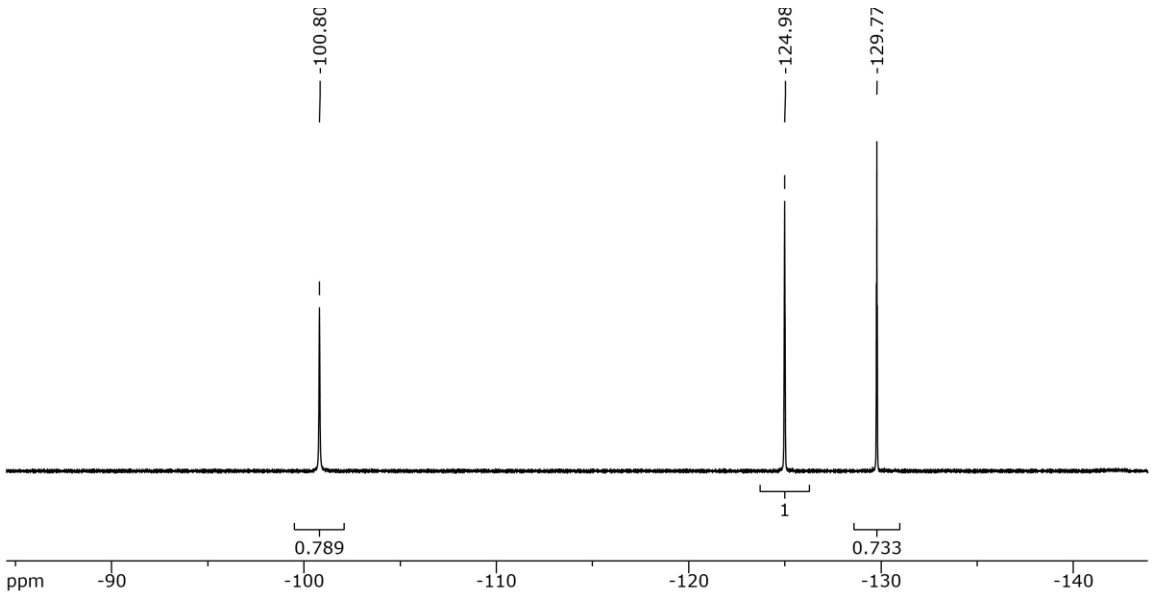

Figure 30: Mg(II)/Fe(II) for entry C in Table 6. Second spectrum including Fe_2HXTA and Mg_2HXTA integrations.

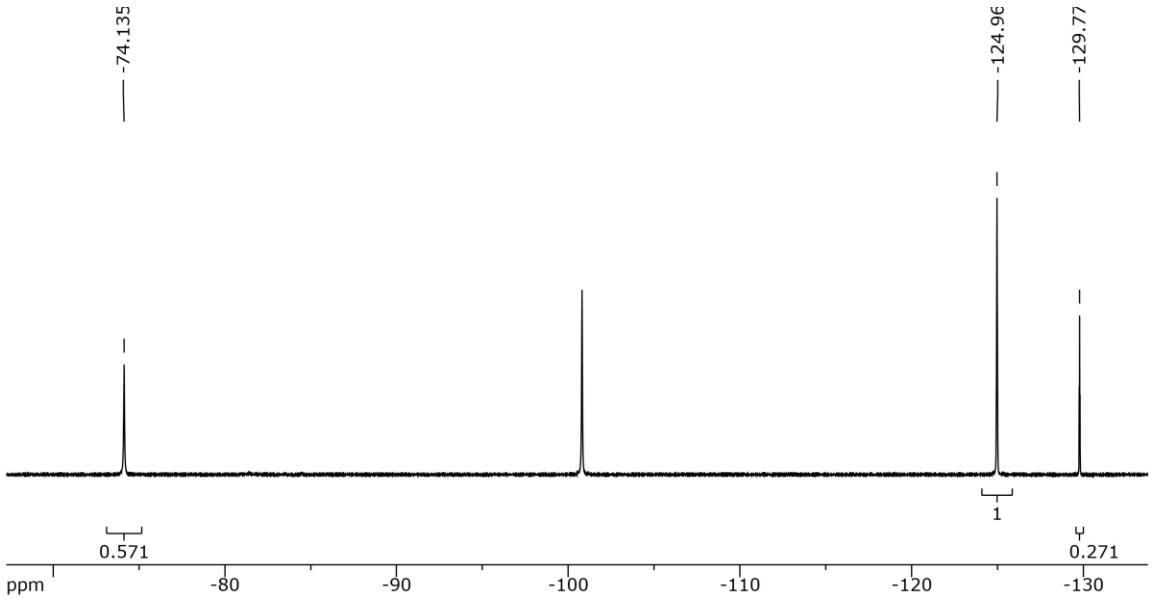

Figure 31: Mg(II)/Fe(II) for entry D in Table 6. First spectrum including FeMgHXTA and Mg_2HXTA integrations.

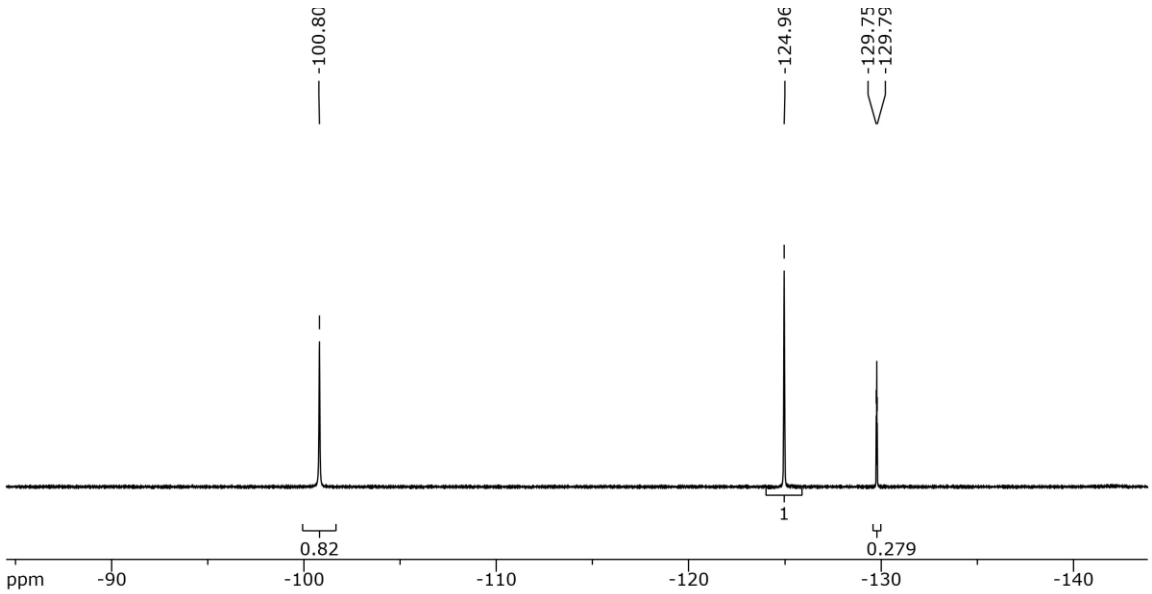

Figure 32: Mg(II)/Fe(II) for entry D in Table 6. Second spectrum including Fe_2HXTA and Mg_2HXTA integrations.

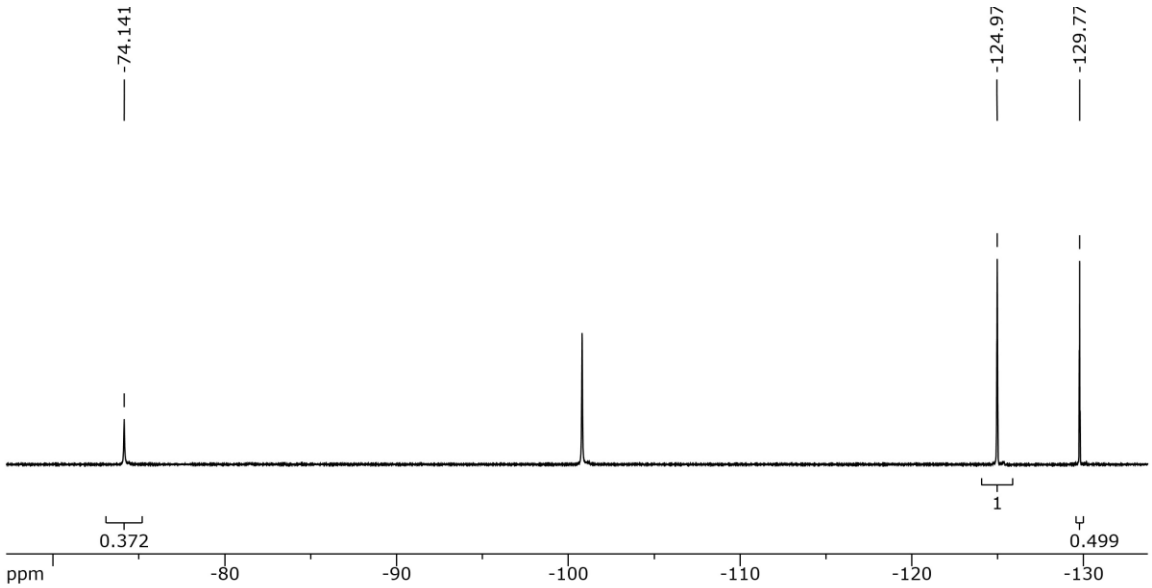

Figure 33: Mg(II)/Fe(II) for entry E in Table 6. First spectrum including FeMgHXTA and Mg_2HXTA integrations.

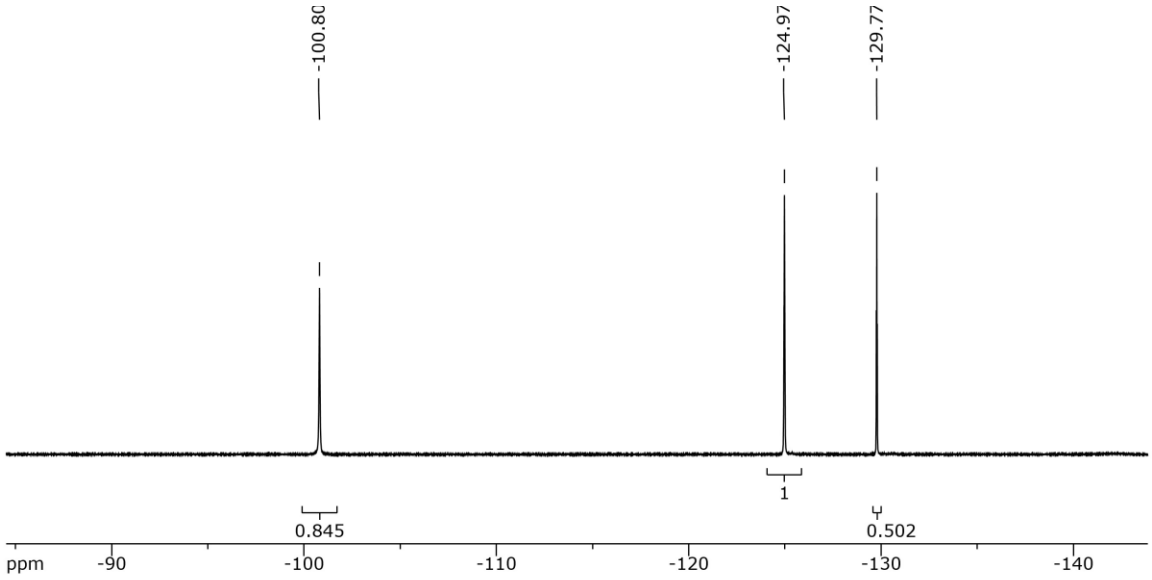

Figure 34: Mg(II)/Fe(II) for entry E in Table 6. Second spectrum including Fe_2HXTA and Mg_2HXTA integrations.

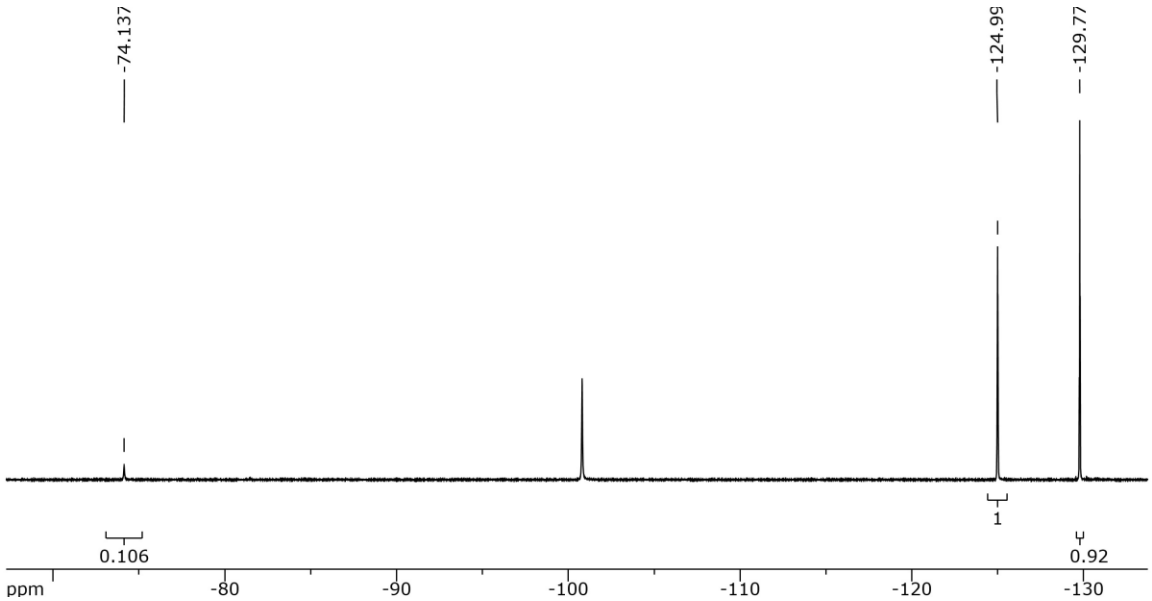

Figure 35: Mg(II)/Fe(II) for entry F in Table 6First spectrum including FeMgHXTA and Mg_2HXTA integrations.

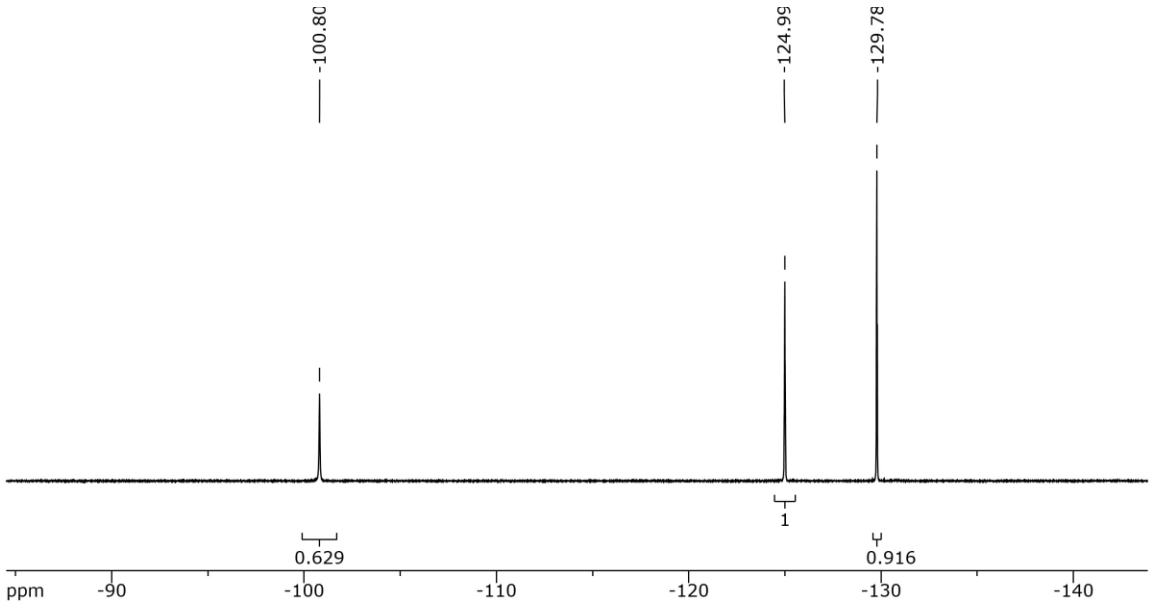

Figure 36: Mg(II)/Fe(II) for entry F in Table 6. Second spectrum including Fe_2HXTA and Mg_2HXTA integrations.